UNIVERSITY OF ZAGREB

FACULTY OF CHEMICAL ENGINEERING AND TECHNOLOGY

Katarina Marušić

PROTECTION OF PATINATED BRONZE
BY NON-TOXIC INHIBITORS

Dissertation

Zagreb, May 2010

Theme of the dissertation was accepted on the meeting of the Faculty Council of the Faculty of Chemical Engineering and Technology in Zagreb, on May 15th 2006 and it was confirmed by the Senat on June 13th 2006.

TABLE OF CONTENTS

PROTECTION OF PATINATED BRONZE BY NON-TOXIC INHIBITORS

Abstract

Bronze is often used for sculptures and building structures. These objects are often covered with patina, a layer of corrosion products, which confers their aesthetic and also protects the substrate bronze. Due to the increasing atmospheric pollution these layers are often dissolving when exposed in urban environment.

This work proposes the use of innoxious imidazole compounds as corrosion inhibitors: 4-methyl-1-phenylimidazole (PMI), 4-methyl-1-*p*-tolylimidazole (TMI) and 1-H benzimidazole (BZI) on the Cu-6Sn (wt-%) bronze, in a diluted Na_2SO_4 + $NaHCO_3$ solution simulating acid rain in urban environment. The results of the electrochemical investigations have shown that PMI protects the bronze without patina layer at pH3, but not at pH5. TMI and BZI protect this alloy in both media.

On the Cu-6Sn bronze, three types of patinas were synthesized by a chemical, thermochemical and electrochemical method. The morphological and structural characterization of these patinas was performed by SEM, EDS and Raman spectroscopy. It was found that the chemical patina is composed essentially of brochantite, the thermochemical patina of atacamite, and the electrochemical patina of malachite. All three patinas have also a smooth part of surface consisting of cuprite. As corrosion inhibitor TMI was used on all patinas, in the Na_2SO_4 + $NaHCO_3$ solution at pH 5. The results have shown that it improves the stability of the patinas. PMI and BZI were used on the electrochemical patina where BZI, unlike PMI showed good protective effect.

Keywords: Adsorption isotherms, Copper-tin bronze patina, EDS, Electrochemical impedance spectroscopy, Imidazole corrosion inhibitors, Raman spectroscopy, SEM, Urban acid rain.

ZAŠTITA PATINIRANE BRONCE NETOKSIČNIM INHIBITORIMA KOROZIJE

Sažetak

Bronca je jedna od najstarijih legura, razvijenih još u antičko doba. Do danas je ostala materijal koji se često koristi za izradu umjetničkih djela, te u arhitekturi za izradu krovova, zvonika itd. Zbog sve većeg zagađenja atmosfere dolazi do propadanja spomenika kulture i ostalih brončanih predmeta izloženih atmosferi, pa ih je potrebno zaštiti.

Uslijed dugotrajnog izlaganja korozivnom djelovanju okoliša bronca korodira stvarajući zaštitni sloj korozijskih produkata patine, obično zelene ili plave boje, koja ovisi o sastavu okoline. Patina na brončanim arheološkim artefaktima kao i na novijim skulpturama ne samo da štiti osnovni metal od korozije nego i poboljšava estetski izgled umjetničkog djela.

U ovom radu ispitivana je mogućnost zaštite patinirane i nepatinirane bronce upotrebom tri različita derivata imidazola kao inhibitora korozije. Ispitivana je djelotvornost: 1-fenil-4-metilimidazola (PMI), 4-metil-1-p-tolilimidazola (TMI) i 1-H benzimidazola (BZI) kao inhibitora korozije Cu-6Sn bronce, u otopini Na_2SO_4 + $NaHCO_3$ zakiseljenoj na pH 3 i pH 5. Ove otopine simuliraju jako kiselu i slabo kiselu kišu u urbanoj atmosferi. Rezultati elektrokemijskih ispitivanja su pokazali da PMI štiti broncu od korozije pri pH 3, ali ne pri pH 5, dok TMI i BZI štite broncu pri pH 3 i pH 5.

Tri vrste patine su sintetizirane na Cu-6Sn bronci: a) kemijskom metodom (u sumpornoj otopini), b) termokemijskom metodom (u klorovodičnoj otopini) te c) elektrokemijskom metodom (u sumporno / ugljičnoj otopini). U sva tri slučaja dobivene su plavo-zelene patine a njihove morfološke i strukturalne karakterizacije provedene su pomoću SEM, EDS i Raman spektroskopije. Rezultati ispitivanja pokazali su da patina dobivena kemijskim putem u sumpornoj otopini ima sastav minerala brohantita, $CuSO_4 \cdot 3Cu(OH)_2$, dok patina dobivena u klorovodičnoj otopini ima sastav minerala atakamita, $Cu_2Cl(OH)_3$, a patina

dobivena elektrokemijskom metodom ima sastav minerala malahita, $CuCO_3 \cdot Cu(OH)_2$. Sve tri patine imaju još i glatki dio površine koja ima sastav minerala kuprita, Cu_2O.

Derivat imidazola TMI je ispitivan kao korozijski inhibitor na sintetiziranim patinama, u otopini Na_2SO_4 + $NaHCO_3$ zakiseljenoj na pH 5 koja simulira umjereno kiselu kišu u zagađenoj atmosferi. Rezultati ispitivanja su pokazali da ovaj inhibitor stabilizira sve tri vrste patine. PMI i BZI su primijenjeni na elektrokemijskoj patini. BZI je pokazao dobra zaštitna svojstva, za razliku od PMI koji u ovim uvjetima ne štiti brončanu patinu.

Ključne riječi: Adsorpcijska izoterma, bronca, EDS, Elektrokemijska impedancijska spektroskopija, imidazoli, korozijski inhibitori, patina, Ramanova spektroskopija, SEM, urbana kisela kiša.

1. INTRODUCTION

Corrosion is a damaging process of a material, especially metal, which results from a reaction with its environment. Many structural alloys corrode merely from exposure to moisture in air, but this process can be strongly affected by presence of certain substances, such as CO_2, SO_2, NO_x, O_2, seawater, etc.

Bronze is one of the first metallic materials employed by human beings, thus numerous objects are currently excavated out every day. During the period when these artefacts have been exposed to atmosphere or sea water, or buried in soil, a layer of corrosion products called patina will be formed spontaneously. A patina on a bronze sculpture not only protects the substrate metal, but also enhances the aesthetic of art objects.

It is possible to distinguish two kinds of patina. The first one is natural patina formed spontaneously during long time exposure to environment. The structure and composition of a bronze patina are specific to each case and depend on the environment to which the bronze is exposed. The second type is synthetic or artificial patina with a defined chemical composition that can be formed in laboratory or workshop, allowing appropriate accelerated surface treatment of bronze. The main interests for application of an artificial patina are; reconstruction of historic objects and works of art, gaining an antique visual effect; and for the purpose of scientific research. Accelerated surface treatment of bronze for obtaining artificial patina can be divided in chemical treatment, mostly used, and electrochemical treatment, used essentially for research purposes.

Because of the markedly increasing air pollution, additional protection for bronze and its patina exposed in urban environment is needed. The use of corrosion inhibitors is one of the interesting methods for protection of metals. Inhibitors are chemical compounds that,

when added in small amounts to a corrosion system decrease greatly the corrosion rate of a metal or alloy. In the field of corrosion protection, inhibitors occupy a special place because of their specific protection and widespread application. Because the corrosion process involves in most cases water molecules, most inhibitor applications are in water and partially water systems (natural water, acid solutions for pickling, primary and secondary processing of petroleum and refining processes), and protection from atmospheric corrosion.

Until recently very efficient, but toxic, inhibitors have been used, e.g. chromates, sodium-nitrite, benzotriazol etc. Nowadays, many regulations and recommendations forbid or restrict the use of these inhibitors, so new non-toxic inhibitors are being developed, e.g. inhibitors of plant origin (green inhibitors), as well as synthetic non-toxic and self-degradable compounds. Imidazole derivatives are corrosion inhibitors, which satisfy these requirements.

Present studies were performed on bare Cu-6Sn binary bronze, as well as on the Cu-6Sn bronze covered with three types of artificial patinas: chemical patinas formed in a sulphate solution, thermochemical patina formed in an ammonium chloride solution, and an electrochemical patina synthesized in a sulphate / carbonate solution.

The aim of this work is to investigate the morphology and structure of different patinas and to examine the possibility of their protection, as well as the protection of bare bronze by new non-toxic imidazole derivatives as corrosion inhibitors.

2. THEORY

In this chapter, we will present first some properties of copper and copper alloys, especially the bronze of cultural heritage in Croatia. The statues of bronze are generally covered with patina, thus the minerals relative to bronze patinas will be described. Bronze as well as patina are considered to be corrosion resistant, however, in the last decades an increase of pollution of urban atmosphere significantly enhances the degradation of bronze statues exposed in urban environment. Some basic concepts of corrosion and corrosion inhibitors will be described at the end of this chapter.

2.1. SEVERAL PROPERTIES OF COPPER AND ITS ALLOYS

Copper is, after iron, probably technically the most important metal. The earth's crest has only 10^{-4} wt-% copper. Though the content of copper is small, copper-bearing mines are well located, so it is relatively easy to extract them. [1]

The world copper production was almost 18.5 million tons in 2008. Chile and Peru are the first and second largest producers of copper in the world. According to Peru's National Association of Mining, Oil and Energy, the country became world's second largest copper producer with a total production of 1.273 million metric tons in 2009. Peru followed Chile whose copper output soared to 5.41 million tons in 2009 and displaced the United States as the second largest copper producer. The U.S. produced 1.19 million tons in 2009. [2, 3]

Copper is found in nature with elements such as lead, nickel, silver, and zinc. [4] It is widely used in industry both as a pure metal and as an alloying element. It is a metal with characteristic light reddish colour, ductile and well recyclable. [1] This metal exhibits excellent electrical and heat conductivities, high resistance towards corrosion and good mechanical properties. Copper has, after silver, the best electrical conductivity. This is the reason why electrical and electronic industries are probably the main field of its application. The second

important field of its use is metallurgy, to yield different alloys. Because of their resistance towards corrosion, copper alloys, namely cuprous nickel is largely used for ship equipments.

2.1.1. NOMENCLATURE OF COPPER AND COPPER ALLOYS

Table 2.1. Advantages and Limitations of Copper and Its Alloys. [4]

Advantages	Drawbacks
High conductivity of electrical grades superior to all other metals except silver on a volume basis and aluminum on weight basis.	High cost relative to other common metals.
High thermal conductivity.	Conductivity reduced by small quantities of other elements.
Excellent ductility permits easy working.	High casting temperatures of the metal and its alloys.
Wide range of copper-base alloys, most types having good ductility and malleability in the annealed condition and being particularly appropriate for tube forming, hot forming, spinning, deep drawing, etc.	High-temperature properties of the metal impose limitations on its use.
Mechanical properties of copper strength, creep resistance, and fatigue performance are improved by alloying (but conductivity is impaired)	The "gasing" reaction of copper with oxygen requires precautions when temperatures exceed 700°C.
Good corrosion resistance to potable water and to atmospheric and marine environments; can be further improved by alloying.	Toxic; therefore must not be used in contact with foodstuff (e. g., food processing plant).
Useful biocide properties of the metal and salts.	Some alloys are prone to stress corrosion and other forms of attack (e. g., dezincification of brasses).
Wide range of alloys with special properties (e. g., very high damping capacity).	
Mechanical and electrical properties retained at cryogenic temperatures.	
Weldability of alloys good by appropriate process.	
Nonmagnetic, except some Cu-Ni alloys.	

Table 2.1 summarizes briefly some of the advantages and limitations of copper and its alloys.

Copper-based alloys are usually classified in terms of one of the main alloying elements. Two main categories of copper alloys are brass and bronze. Brasses are essentially copper-zinc alloys to which other elements may be added. True bronzes are copper-tin binary alloys, but other elements such as Al, Be, Pb, Mn, W… are also added, namely for industrial applications.

In the nomenclature of copper and copper alloys, numbers from C10000 through C79999 denote wrought alloys. Cast alloys are numbered from C80000 through C99999. Within these two categories, the compositions are grouped into the following coppers and copper alloys. More detailed families are described in Table 2.2 for wrought and cast alloys. [4]

Table 2.2. Generic Classification of Wrought Copper Alloys. [4]

	UNS Number	Composition
Coppers		
Coppers	C10100-C15760	> 99% Cu
High-copper alloys	C16200-C19600	> 96% Cu
Brasses		
Brasses	C20500-28580	Cu-Zn
Tin brasses	C31200-C38590	Cu-Zn-Sn
Leaded brasses	C40400-C49080	Cu-Zn-Sn-Pb
Bronzes		
Phosphor bronzes	C50100-C52400	Cu-Sn-P
Leaded phosphor bronzes	C53200-C54800	Cu-Sn-Pb-P
Copper-phosphorus and copper- Silver-phosphorus alloys	C55180-CS5284	Cu-P-Ag
Aluminium bronzes	C60600-C64400	Cu-Al-Ni-Fe-Si-Sn
Silicon bronzes	C64700-C66100	Cu-Si-Sn
Others		
Other copper-zinc alloys	C66400-C69900	
Copper-nickels	C70000-C72950	Cu-Ni-Fe
Nickel silvers	C73200-C79900	Cu-Ni-Zn

Detailed compositions of individual alloys can be found in literature: [4]

- *Coppers.* Metals with a designated minimum copper content of 99.3%.

- *Brasses.* These alloys contain zinc as the main alloying element with or without other designated alloying elements such as iron, aluminium, nickel, and silicon. The wrought alloys comprise three main families of brasses. The cast alloys comprise five main

families of brasses. Ingot for remelting for the casting manufacture may vary slightly from the ranges shown.

▪ *Bronzes*. Roughly speaking, bronzes are copper alloys in which the major alloying element is not zinc or nickel. Archaeological bronzes are essentially binary alloys with tin as the only or principal alloying element. Nowadays, the term bronze is used with other alloying elements. Bronzes are unquestionably one of the most versatile classes of corrosion- and wear-resistant materials, offering a broad range of properties from a wide selection of alloys and compositions. Tin bronzes can contain between 1 and 10% tin. Though depending on the preparation method, within this content, bronze is a single phased bronze. Above 10 to 15 %, bronze may constitute of two phases, modifying significantly its physical and chemical properties. Phosphor bronze contains up to 0.4% phosphorus. Gunmetal is essentially a tin bronze with up to 5% zinc and may additionally have up to 5% lead. Silicon bronze typically contains 3% silicon and 1% manganese and is probably the easiest of the bronzes to weld.

▪ *Copper-nickels*. They are alloys with nickel as the principal alloying element, with or without other elements, namely Zn designated commonly, because of its aspect, as "nickel silvers".

▪ *Leaded coppers*. This term comprises a series of cast alloys of copper with 20% or more lead, sometimes with a small amount of silver but without tin or zinc.

▪ *Special alloys*. Alloys whose chemical compositions do not fall into any of the above categories are classified as "special alloys."

2.1.2. WELDING OF BRONZES

Because of the increasing application of bronze, for instance, to artwork, the welding of different parts is necessary. Bronzes are generally considered to be weldable, apart from

phosphor bronze and leaded gunmetal, and a matching filler composition is normally employed.

Rigorous cleaning of the material surface is essential, both before and after each run, to avoid porosity. Single-phase alloys can be susceptible to weld metal cracking, and heat-affected zone (HAZ) cracking can occur under highly restrained conditions. It is often necessary to use matching filler metals to maintain corrosion resistance, but non-matching, two-phase filler will reduce the cracking risk. Two-phase alloys are more easily welded. For both types, preheating and interpass temperatures should be restricted to prevent cracking. [5]

2.2. BRONZE STATUES OF CULTURAL HERITAGE IN CROATIA

Bronze is the ancient name for a broad range of copper alloys, but as stated before, usually with tin as the main additive. First occurred in the Bronze Age, it was used to make tools and weapons. Some ritual artefacts survived until today. The date of arrival of the "Bronze Age" varies from culture to culture. Some areas had their Bronze Age early, others had it later. The earliest bronze occurred in Sumer in Mesopotamia (Iraq), about 3500 BC, and also on some ancient sites in Susa (Iran). The Chinese had begun to use bronze by 2000 BC. In Europe (namely Greece), by 2000 BC, Early Helladic civilization used bronze, and by 1600 BC, Mycenaean begins to develop bronze artwork. The Bronze Age is a period in the civilization's development when the most advanced metalworking has developed techniques of smelting copper from natural outcroppings and alloying it to cast bronze. [6]

Bronze is one of the first metallic materials employed by human beings, thus numerous object are currently excavated out every day. Therefore, bronze objects attract particular attention of archaeologists. [7] In presence of oxygen and humidity, copper and its alloys form a thin layer of corrosion products, called patina.

2.2.1. STATUE OF APOXYOMENOS

Bronzes are widely used in sculpturing. There are many examples of bronze sculptures, ancient and new. Fig. 2.1 presents a 1.92 m high sculpture of Apoxyomenos before and after restoration. This is, a bronze sculpture of an athlete that scrapes oil and dust of himself after competition. It was found in 1999 on the bottom of the sea near the Lošinj Island, in Croatia. It is assumed that this statue was created during the transition of Greek classics to Hellenism in the 4th century BC.

Before restoration	After restoration
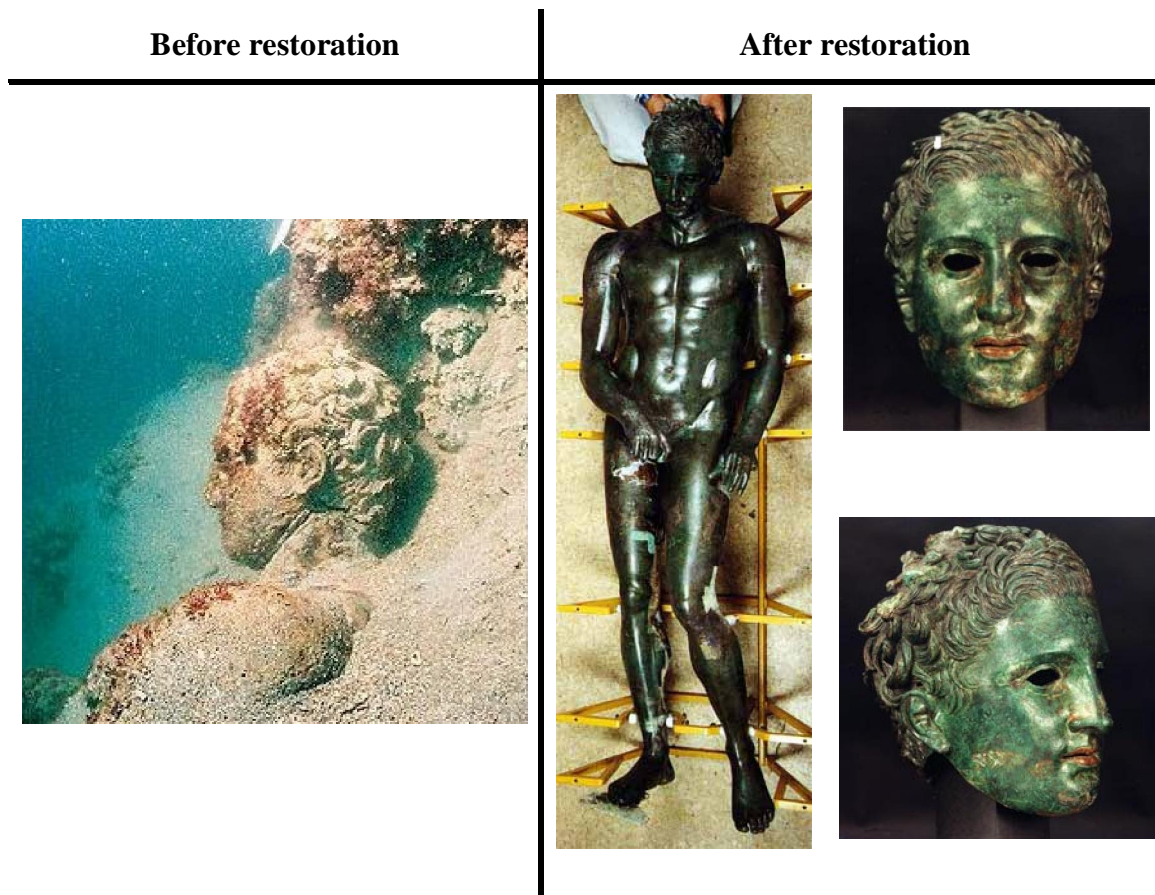
Figure 2.1. The sculpture of Apoxyomenos before and after restoration.

2.2.2. SCULPTURES IN ZAGREB

Many modern bronze sculptures (19th to 20th centuries) can be seen in many Croatian cities. Fig. 2.2 shows some of them in the city of Zagreb.
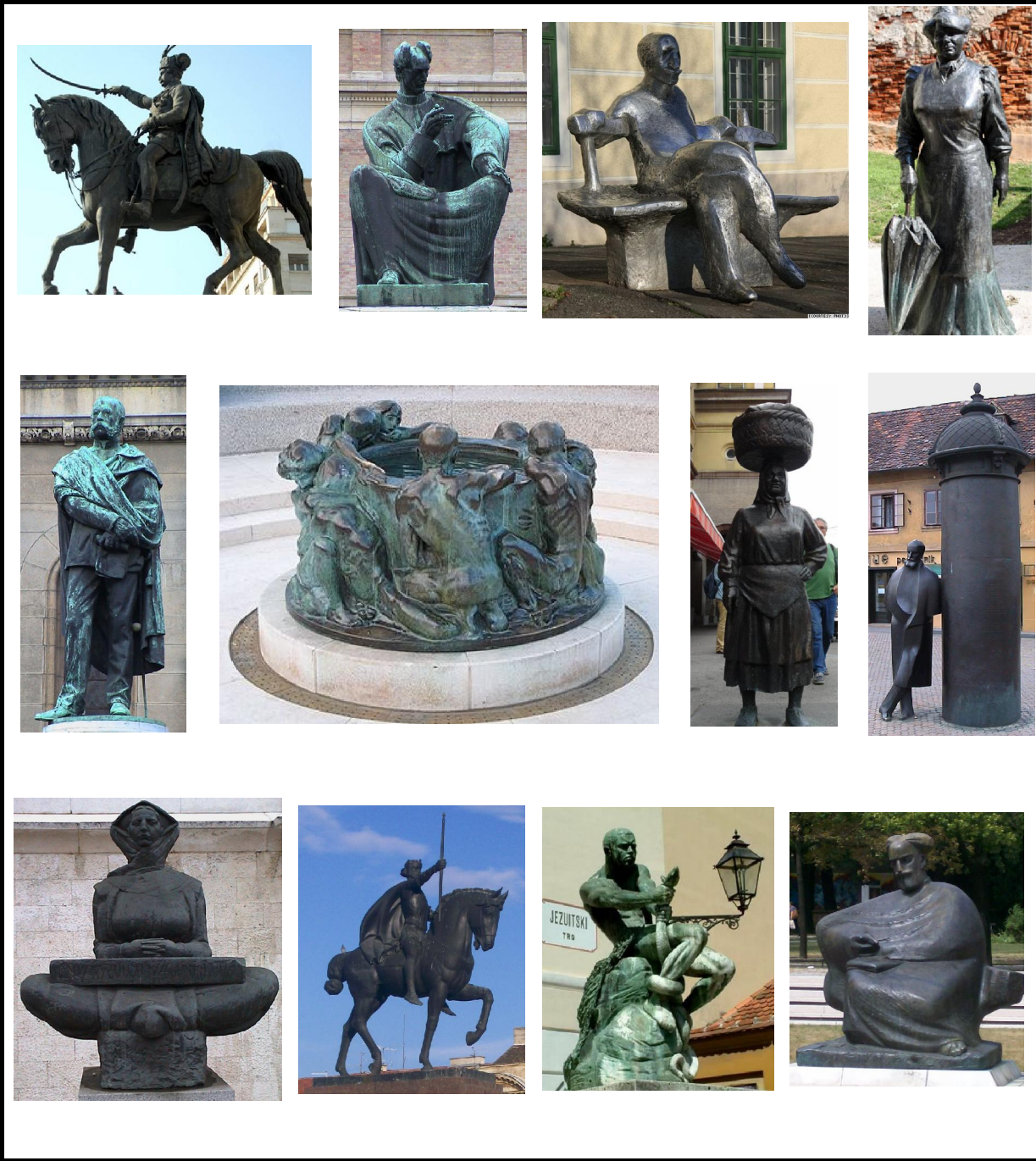
Figure 2.2. Some of the patinated and non-patinated bronze statues in Zagreb.

From left to right:

First line:

- Statue of the Count Josip Jela i by Anton Fernkorn (1866),

- Statue of Bishop Josip Juraj Strossmayer by Ivan Meštrovi (1926),

- Statue of the poet Antun Gustav Matoš by Ivan Kožari (1978),

- Statue of the writer Marija Juri Zagorka by Stjepan Gra an (1991),

Second line:

- Statue of the poet General Petar Preradovi by Ivan Rendi (1895),

- The "Well of Life" by Ivan Meštrovi (1912),

- Statue of "an old lady Barica with a basket on her head" on the farmer's market Dolac by Stjepan Gra an (2006),

- Statue of the novelist August Šenoa by Marija Ujevi (1987),

Third line:

- Statue "History of Croats" by Ivan Meštrovi (1932),

- Statue of the first Croatian king Tomislav by Robert Frangeš Mihanovi (1938),

- Statue of a fisherman by Simeon Roksandi (1911),

- Statue of the poet Marko Maruli by Vlado Radas (1999).

From these pictures, one can notice readily that these sculptures are covered with patina of various colours. Some of them are pale green especially where the rain fall will wet the surface, reddish where the people may touch frequently its surface, the others are dark green and some of them are dark brown or blackish.

2.2.3 THE STATUE OF LIBERTY IN NEW YORK

As stated above, the structure and composition of patina and bronzes are specific to each case. A patina that has developed spontaneously over many years contains a number of

compounds that together provide an overall appearance. For example, the Statue of Liberty (*Liberty Enlightening the World*) or "Lady Liberty" (Fig. 2.3) is a large statue in the harbor of New York City. It was built in 1886 and given as a gift from France to the United States of America for the 100th anniversary of their independence. The statue is one of the best known landmarks in America. It serves to greet visitors and immigrants. The French sculptor Frédéric Auguste Bartholdi designed the statue and Gustave Eiffel, the designer of the Eiffel Tower, helped design it.

Figure 2.3. The statue of Liberty in New York.

It was deeply restored on the 200th anniversary of the independence. The restorers, curator, and scientists have had therefore a particularly interesting opportunity to examine exhaustively various aspects of patina formed naturally in urban – marine environment. These analyses showed that the patina on the Statue of Liberty contains, in addition to cuprite, Cu_2O, brochantite, $CuSO_4 \cdot 3Cu(OH)_2$, antlerite, $CuSO_4 \cdot 2Cu(OH)_2$, and atacamite, $Cu_2Cl(OH)_3$. Traces of posnjakite, $CuSO_4 \cdot 3Cu(OH)_2 \cdot 2H_2O$, a hydrated form of brochantite, were only found in the younger patinas and were considered to be a precursor phase. The presence of antlerite, which is more stable than brochantite at a lower pH, was attributed to the acidic precipitation in the New York Harbour. The identified sulphate and chloride patina are due to location of this statue, an urban atmosphere at the seacoast. [8]

2.3. PATINA

When exposed to atmosphere, copper and its alloys form a thin layer of corrosion products, called patina, as illustrated on several statues in Zagreb (Fig. 2.2) and the Statue of Liberty (Fig. 2.3). A patina on a bronze sculpture, as stated in the "Introduction" section, not only protects the substrate metal, but also enhances the aesthetic of art objects. [9]

Because of its aesthetic aspect and also due to the subjective association to antique artefacts, patinas are often deliberately added by artists and metalworkers. Scientists are interested in the mechanism of patina formation and the protection of cultural heritage for future generations, thus they have recourse to synthetic patina. Patinas may be used to 'antique' objects, as a part of the design or decoration of art and furniture during restorations (cf. Statues of Apoxyomenos: Fig. 2.1).

In other terms, it is possible to distinguish two kinds of patina:

- The first one is natural patina formed spontaneously during a long time exposure to environment. The structure and composition of patina and bronzes are specific to each case due to the metallurgy of bronze itself and also to the environment surrounding the bronze artefact.

- The second type is synthetic or artificial patina with a defined chemical composition that can be formed in laboratory or foundry workshop allowing appropriate accelerated surface treatment of bronze. [10, 11]

2.3.1. NATURAL PATINAS

Coloured natural patinas form spontaneously on copper alloys by very slow corrosion process. They are a result of a chemical interaction with the main composition of air, humidity, oxygen and carbonate, and also with trace amounts of pollutants in the atmosphere, particularly, sulphates, and chlorides, although other elements such as NO_2, O_3, H_2S play a

role. [12] The colour depends on the corrosion products formed, which depend partly on the alloy and partly on the environment. Particularly, copper or bronzes exposed to urban atmospheres for many decades exhibit a greenish patina, because of the copper carbonate or sulphate crystals, containing several constituents that had been largely studied. [7, 10, 12-22]

2.3.2. ARTIFICIAL PATINAS

As for artificial or synthetic patinas, a wide range of chemicals, both household and commercial, can give a variety of patinas [23] and hundreds of recipes for patina formation are known. [24] Artists often use patination as a creative act (which joins skill and spirit) on surface improvement either for colour, texture, or both, but also aesthetic dimension and artistic expression. Patina composition varies with the reacted elements and these will determine the colour of the patina. Exposure to chlorides leads to green, while sulphur compounds tend to brown. For artworks, patination is deliberately accelerated by heat. Colours range from matt sandstone yellow to deep blues, reds and various blacks, sometimes with the surface sheen enhanced by waxing for artwork displayed indoors. [23] There are two kinds of patina synthesis: chemical synthesis, mostly used, and electrochemical synthesis used nowadays only for scientific purpose.

The patina electrochemically formed in earlier work was synthesized under current regulation. [11, 25, 26] However, this method produces a patina which does not cover uniformly the surface of bronze and goes deep in the core of the metal. For this reason a new method of electrochemical synthesis under potential regulation was developed for this work. [26-28] Patina obtained according to this method mimics much better naturally formed patina in an urban atmosphere.

2.3.3. MINERALS IDENTIFIED IN THE BRONZE PATINA

Patina is composed of a variety of fine crystalline particles covering copper or bronze surface. Some of them adhere well to the surface, the others not. Each particle, however, can be identified as its homologous well defined mineral of a larger crystal.

A basic green colouration is given by emerald / dark-green malachite, basic copper(II) carbonate, $CuCO_3 \cdot Cu(OH)_2$, whilst, less commonly in very slightly humid environments, a blue colour develops from another basic copper(II) carbonate, azurite, $2\ CuCO_3 \cdot Cu(OH)_2$. Carbonate patinas form in clean atmospheres. On some high-tin contained bronzes, white to grey turquoise patinas called 'water' patinas are found, and consist mainly of tin oxide, SnO_2. The hue of a patina can be reddened by an underlying layer of copper(I) oxide, cuprite, Cu_2O. [12, 27, 29]

In sulphate environments (urban atmosphere), the initial corrosion product is cuprite, Cu_2O, with posnjakite, $Cu_4(SO_4)(OH)_6 \cdot H_2O$. [30] Posnjakite is either 'washed away' or converted to brochantite, $CuSO_4 \cdot 3\ Cu(OH)_2$, after longer exposure. The amount of brochantite increases with exposure time and forms a green-blue patina layer. [31] Even before industrialization, there was enough hydrogen sulphide and sulphur dioxide in air to induce its formation. [29]

In chloride containing environments (marine), the initial phase of corrosion product to be formed is cuprite, with paratacamite, $Cu_2Cl(OH)_3$, an isomorphic compound of atacamite, which appears as a secondary phase growing on the cuprite. Atacamite also appears after longer exposures. Both atacamite and paratacamite present a green-blue colouring, characteristic of the copper patinas formed in marine atmospheres. [12] The phases commonly found on copper specimens weathered in the atmosphere are summarized below: [32]

- *Cuprite* [Cu_2O]: Purple red. It is insoluble in water and slightly soluble in acid.

- *Brochantite* [$Cu_4(SO_4) \cdot Cu(OH)_2$]: Green-bleu. It is nearly always the most common component of the green patina formed on copper after long atmospheric exposures.

- *Antlerite* [$Cu_3(SO_4)(OH)_4$]: Deep green. This crystal form may be found in more acidic conditions than brochantite. [12] There is some evidence that antlerite may form at earlier stages of the patination process than brochantite. It is suggested that acid rain is converting brochantite to less protective antlerite, which is more susceptible to erosion.

- *Posnjakite* [$Cu_4(SO_4)(OH)_6 \, H_2O$]: Blue to dark blue. It is a precursor of brochantite and has a similar structure (hydrated form of brochantite).

- *Atacamite* [$Cu_2Cl(OH)_3$]: Green to yellow-green. It is soluble in weak acid. It was found to be as or more abundant than brochantite in patinas formed near seaside due to the influence of sea-salt aerosols. It is not found on specimens exposed for short periods.

- *Paratacamite* [$Cu_2Cl(OH)_3$]: Dark green to greenish black. Its presence is temporary and it eventually converts to atacamite. It is not found in patinas corresponding to long exposures.

- *Malachite* [$Cu_2(CO_3) \cdot Cu(OH)_2$]: Green to dark green. Atmospheric conditions do not favour the formation of this type of patina, but this basic carbonate is sometimes unexpectedly found in practice.

- *Azurite* [$2CuCO_3 \cdot Cu(OH)_2$]: Azure blue to blue. Azurite is unstable in open air, when compared with malachite, and therefore is often pseudomorphically replaced by it.

- *Gerhardtite* [$Cu_2NO_3(OH)_3$]: Green – dark green. It is also found in some locations.

Fig. 2.4 illustrates the minerals presented above.
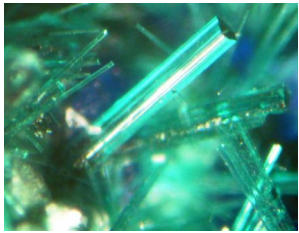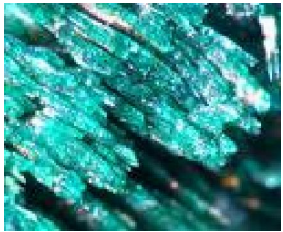
	$CuSO_4 \cdot 3Cu(OH)_2$	$Cu_3(SO_4)(OH)_4$	$Cu_4(SO_4)(OH)_6 \cdot H_2O$
Sulphate patina	Brochantite	Antlerite	Posnjakite
	$Cu_2Cl(OH)_3$	$Cu_2Cl(OH)_3$	
Chloride patina	Paratacamite	Atacamite	
	$CuCO_3 \cdot Cu(OH)_2$	$2CuCO_3 \cdot Cu(OH)_2$	
Carbonate patina	Malachite	Azurite	
	$Cu_2NO_3(OH)_3$		
Nitric patina	Gerhardtite		

Figure 2.4. Minerals found in bronze patinas as fine particles. [33-36]

2.4. CORROSION OF COPPER

The concentrations of air pollutants and the chemistry of precipitation have changed markedly during the last century as a result of anthropogenic activity. Alterations in the appearance of aged outdoor objects were observed. [11, 13, 21] Because of an increase of air

pollution and acid rainfall, the bronze as well as patina presented in urban environment suffer an acceleration of corrosion and the alteration of this aspect. The main corrosion reactions of copper will be examined thermodynamically by so called potential – pH diagram.

2.4.1. POTENTIAL-PH DIAGRAM OF CU – WATER SYSTEM

The main constituent of bronze is copper. Corrosion of this alloy is a rather complex task, thus the corrosion behaviour is generally studied by that of copper without the alloying elements. The most common approach to study the possible chemical and electrochemical reactions undergoing on copper surface is the use of potential – pH diagram, named also Pourbaix diagram. [37]
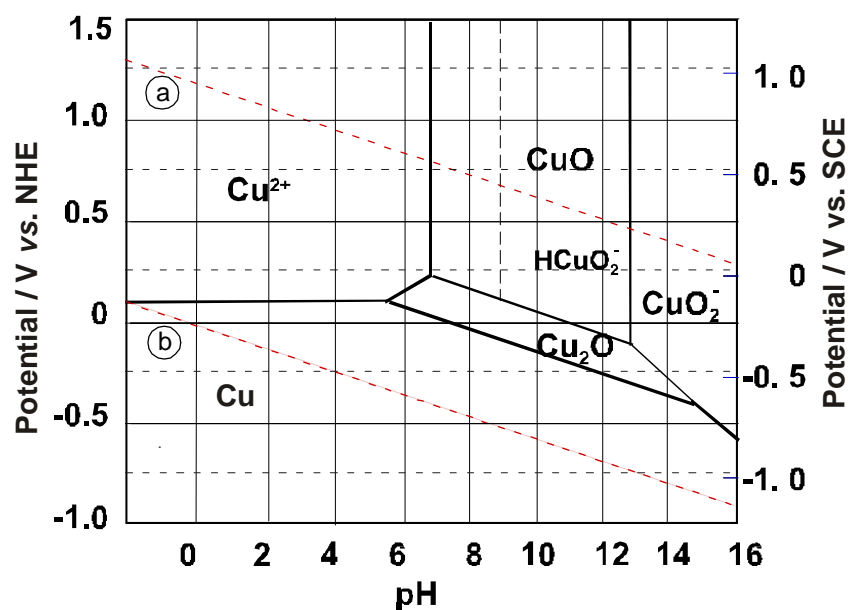
Figure 2.5. Potential – pH diagram of Cu in aqueous medium (10^{-6} mol·dm^{-3}).

In this diagram, different thermodynamically stable states of Cu species are shown with respect to potential and pH. The frontier is determined by the thermodynamic, Nernst potential. For instance, the horizontal line separating Cu and Cu^{2+} are determined by:

$$Cu_{(s)} \Leftrightarrow Cu^{2+}_{(aq)} + 2\ e^- \tag{2.1}$$

$$E^{\otimes} = E_0 + \frac{R \cdot T}{n \cdot F} \cdot \ln\left[c(Cu^{2+})\right], \qquad E_0 = 0.34\ V_{NHE} \tag{2.2}$$

where:

$E^{\otimes}$ – Thermodynamic equilibrium potential (V),

E_0 – Standard redox potential (V),

$c(Cu^{2+})$ – Concentration of cuprous ions (mol·dm^{-3}),

R – Gas constant (8.315 J·mol^{-1}·K^{-1}),

F – Faraday constant (96485 A·s·mol^{-1}),

n – Number of electrons involved in a single reaction (here 2),

NHE (subscript) – Normal hydrogen electrode scale.

It can be seen, thus the frontier between Cu and Cu^{2+} depends on the concentration of the latter, and the figure presented here is drawn for $c(Cu^{2+}) = 10^{-6}$ mol·dm^{-3}. Below this line (more negative potential) Cu is stable in its metallic form, thus no corrosion will take place. The line (a) is the electrolysis of water:

$$\tfrac{1}{2}\ H_2 \Leftrightarrow H^+ + e^- \tag{2.3}$$

Since this line is located in the domain where Cu is stable in its metallic state, no corrosion can take place in aqueous medium. However, in presence of oxygen, the reduction of dissolved oxygen delimited by the line (b) will take place:

$$4\ OH^- \Leftrightarrow O_2 + 2\ H_2O + 4\ e^- \tag{2.4}$$

Consequently, Cu dissolves in acidic medium with the reduction of the dissolved oxygen. However, no external current may be observed when the copper specimen is left alone at the abandoned state; the electrons formed by the reaction (2.1) are consumed by the reaction (2.4).

$$2\ Cu_{(s)} + O_2 + 2\ H_2O \rightarrow 2\ Cu^{2+}_{(aq)} + 4\ OH^- \tag{2.5}$$

As materialized by "→" this reaction is no longer in thermodynamic equilibrium, but the overall charge balance is zero.

In neutral to weakly alkaline medium, as can be seen in Fig. 2.5, cuprite, Cu_2O, can be formed upon the Cu electrode in presence of dissolved oxygen. The neat reaction is thus:

$$4\ Cu_{(s)} + O_2 + 2\ H_2O \rightarrow 4\ Cu(OH) \hspace{4cm} (2.6)$$

Then, cuprous hydroxide Cu(OH) will transform into cuprite Cu_2O:

$$4\ Cu(OH) \Leftrightarrow 2\ Cu_2O + 2\ H_2O \hspace{4cm} (2.7)$$

The further oxidation of Cu into Cu_2O needs the diffusion of Cu^+ through the Cu_2O thus formed, and therefore, this reaction is extremely slow. Nonetheless, Eqs. (2.6) and (2.7) indicate that the first step of the patina formation reaction is the transformation of copper into cuprite. As stated above, this compound is purple red.

In absence of other reacting agents, but only in the presence of humidity and air (oxygen), cuprite will transform then into CuO, tenorite.

$$2\ Cu_2O + O_2 + 4\ H_2O \rightarrow 4\ Cu(OH)_2 \hspace{3.5cm} (2.8)$$
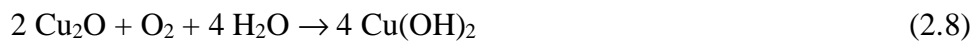
Cupric hydroxide thus formed in wet air will then be transformed into the black tenorite:

$$4\ Cu(OH)_2 \Leftrightarrow 4\ CuO + 4\ H_2O \hspace{4cm} (2.9)$$

Tenorite is stable, and no further transformation will take place in neutral to weakly alkaline water. Since the first stage of the copper oxidation is a slow process, as stated above, copper and its alloys exhibit consequently a low corrosion rate when exposed to atmospheric conditions. Because of this interesting property, they have long been used for building structures such as roofs, facades, and gutters. Many copper roofs have lasted for centuries on castles and other monumental buildings. [38]

The potential – pH diagram indicates also that in very alkaline medium, copper will form soluble cuprate, CuO_2^-, but in a natural system, this reaction is unrealistic.

2.4.2 PATINA FORMATION REACTIONS

In presence of anions (except OH^-), the potential – pH diagram of Cu – water system will be deeply changed. For instance, in presence of halide ions, namely chloride, cuprous ions form a stable complex, whereas this cation is not stable in Cu-water system. Indeed, the standard equilibrium potential of Cu / Cu^+ is:

$$E_0 (Cu/Cu^+) = 0.52\ V_{NHE} \qquad (2.10)$$

This potential is more positive, for a less oxidized state, than the cupric ions. Thus, the following disproportion reaction will occur:

$$2\ Cu^+_{(aq)} \Leftrightarrow Cu_{(s)} + Cu^{2+}_{(aq)}$$
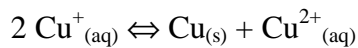
The standard equilibrium potential between cuprous and cupric ions is as follows:

$$E_0 (Cu^+/Cu^{2+}) = 0.17\ V_{NHE} \qquad (2.11)$$

By applying the Nernst equilibrium potential, one gets readily:

$$pK = -\log(K) = \frac{0.52 + 0.17}{0.06} = 11.50 \qquad (2.12)$$

Therefore, the mole ratio of Cu^+/Cu^{2+} = $3.2 \cdot 10^{-12}$. When the complex, with Cl^- for instance, is formed, Eq. (2.12) is completely changed, and Cu^+ becomes stable.

As indicated above, cuprite is generally the first corrosion product formed regardless of the exposure conditions, and so it is always present on the copper surface. When SO_2 is present in atmosphere, as an urban or industrial pollutant, this species will be oxidized into sulphate anions according to:

$$SO_2 + H_2O + 1/2\ O_2 \quad H_2SO_4 \qquad (2.13)$$

And then, the cuprite will react with sulphate ions.

$$\frac{x}{2}Cu_2O + SO_4^{2-} + yH^+ + nH_2O \rightarrow Cu_x(SO_4)(OH)_y \cdot nH_2O \qquad (2.14)$$
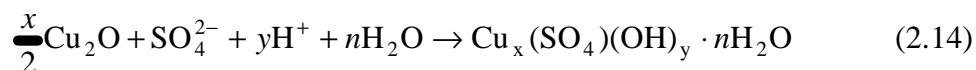
Posnjakite, Brochantite, Antlerite

Copper ions react slowly with pollutants, such as Cl^- and SO_4^{2-}, to form basic copper salts, provided that the pH value of the surface moisture is sufficiently high. In urban, industrial and rural atmospheres basic sulphates are the predominant components, while in marine atmospheres basic chlorides are predominant: [39]

$$Cu_2O + Cl^- + 2H_2O \rightarrow Cu_2Cl(OH)_3 + H^+ \qquad (2.15)$$

Paratacamite, Atacamite

$$2\,CuO + Cl^- + 2\,H_2O \rightarrow Cu_2Cl(OH)_3 + OH^- \qquad (2.16)$$
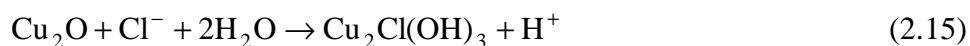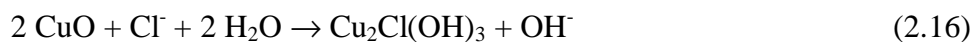
Patinas, in addition to their aesthetic dimension, also have a precious protective role, but they can also be vile and induce destructive phenomena. For example, on a bronze surface, a copper chloride corrosion product can rest until moisture, which provokes the well-known "bronze cancer", occurs. [40, 41] The main reaction responsible for "bronze cancer" is the hydrolysis of copper (I) chloride which results with the formation of cuprite:

$$2\,CuCl + H_2O \rightarrow 2\,HCl + Cu_2O \qquad (2.17)$$

The hydrochloric acid produced this way produces even more copper chloride:

$$2\,HCl + 2Cu \rightarrow 2\,CuCl + H_2 \qquad (2.18)$$

These processes repeat themselves again and again turning in extreme situations a solid object in a pale green mass.

2.5. CORROSION OF COPPER AND BRONZE

One of the key factors in any corrosion situation is the environment. The definition and characteristics of this parameter can be quite complex. It is important to realize that the environment is a variable that can change with time and atmospheric conditions. It is also important to realize that the environment that actually affects a metal corresponds to the micro-environmental conditions that this metallic material really "sees", i.e., the local environment at the surface of the metal. It is indeed the reactivity of this local environment that will determine the real corrosion damage. Thus, an experiment that investigates only the nominal environmental condition without consideration of local effects such as flow, pH cells, deposits, and galvanic effects is useless for lifetime prediction. [4]

2.5.1. CORROSION MECHANISM

With acid rain in urban atmosphere, the following reaction may take place leading to the corrosion of copper and copper alloy:

$$Cu_{(s)} + H^+ + HSO_4^- + 1/2 O_{2\,(g)} \rightarrow Cu^{2+} + SO_4^{2-} + H_2O \qquad (2.19)$$
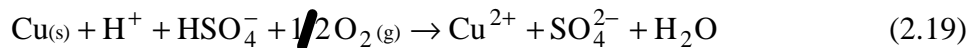
This reaction leads to corrosion of copper and copper alloy since $Cu^{2+}_{(aq)}$ is stable in acid medium as illustrated in Fig. 2.5. It is important to notice that in a mildly acidic medium (pH > 2), HSO_4^- is the major sulphate cation, where SO_4^{2-} is major only at very acid media.

Eq. (2.19) does not show explicitly the current exchange at the electrode surface, but as it is explained in Eqs. (2.1) through (2.4), individual reactions involve the charge transfer, the electron exchange with chemical entities. The partial anodic reaction is thus expressed as follows:

$$Cu_{(s)} \rightarrow Cu^{2+}_{(aq)} + 2\ e^- \qquad (2.20)$$

The rate of this reaction can be expressed as the anodic current flow I_a. Simultaneously, as stated above, the reduction of dissolved oxygen is taking place:

$$O_2 + 2\,H_2O + 4\,e^- \rightarrow 4\,OH^- \tag{2.21}$$

The reaction rate will be thus expressed by the cathodic current I_c.

Since no overall current is observed externally, the sum of these two currents is zero:

$$I_a + I_c \equiv 0 \tag{2.22}$$

It is important to emphasize that, though there is no external current, Eq. (2.22) is not describing the equilibrium, since the anodic and cathodic processes involve different species, and do not present the reversible reaction. For the characterization of electrochemical processes, it is always preferable to normalize the value of the current by the geometrical surface area of the electrode and use the current density, often expressed by a low case j (expressed in terms of A·cm^{-2}): [4]

$$j = \frac{I}{A} \tag{2.23}$$

where:

I – Current (A),

A – Surface area (cm^2).

When an external current source (or potential) is applied to the electrode at the open circuit conditions, Eq. (2.22) is no longer applicable, and the overall current ,I, or current density, j, will pass through the electrode interface. The potential difference from the equilibrium or more generally from the open circuit potential, E_{OC}, is called the overpotential, η. There are three distinct types of polarization in any electrochemical cell. The total polarization across an electrochemical cell η_{total} is the sum of the individual elements as expressed in Eq. (2.24):

$$\eta_{total} = \eta_{act} + \eta_{conc} + j \cdot R \tag{2.24}$$

where:

$_{act}$ – Activation overpotential. A complex function describing the charge transfer kinetics of the electrochemical processes. $_{act}$ is generally predominant at small polarization currents or potentials.

$_{conc}$ – Concentration overpotential. A function describing the effect of mass transport associated with electrochemical processes. $_{conc}$ is predominant at large polarization currents or potentials.

$j \cdot R$ – Ohmic drop. $j \cdot R$ follows Ohm's law and describes the polarization that occurs when a current flows through an electrolyte or through any other interface, such as the surface film, connectors, etc. exhibiting the resistance R (expressed in terms of $\Omega \cdot cm^2$). [4]

When the reaction rate is controlled by the charge transfer (transfer of electrons into chemical entity), the reaction is said to be under activation or charge-transfer control.

The kinetics associated with apparently simple processes rarely occur in a single step. The overall anodic reaction expressed in Eq. (2.1) would indicate that metal atoms at the outermost metal lattice are in equilibrium with an aqueous solution containing Cu^{2+} cations. The reality is much more complex, and one would need to use at least two intermediate species to describe this process, i. e.

$$Cu_{(lattice)} \Leftrightarrow Cu^{+}_{(surf)} \tag{2.25}$$

$$Cu^{+}_{(surf)} \Leftrightarrow Cu^{2+}_{(surf)} \tag{2.26}$$

$$Cu^{2+}_{(surf)} \Leftrightarrow Cu^{2+}_{(aq)} \tag{2.27}$$

In addition, one should consider other parallel processes, such the hydrolysis of the Cu^{2+} cations to produce a precipitate or some other complex form of copper cations.

$$Cu_{(aq)}^{2+} + 2H_2O \Leftrightarrow Cu(OH)_2 + 2H^+ \qquad\qquad (2.28)$$

The electrolyte medium at the vicinity of the electrode surface thus becomes more acid.

2.5.2. ACID RAIN

Acid rain is one of the major effects that damage bronze artefacts exposed to atmospheres. The term "acid rain" is used to characterize air pollution that travels long distances and harms valued environmental assets as a result of direct acidic or corrosive effects or through combinations of harmful chemical reactions. [42] Acidification of rain and snow may seem to be a recent environmental pollution problem. However, the phenomenon has been known for over a century since it was first noticed that buildings, trees and plants were damaged if they were downwind of chemical factories discharging acid fumes. The damage was mostly confined to periods of rainfall because of the removal of air-borne pollutants by rain droplets. At that time, the problem was a local one, confined to an area close to the factories. This was because the factory chimneys were relatively short and there was no widespread dispersion of the pollutants. The air was also polluted with the smoke from the individual coal fires in all the houses, as well as from small power stations adjacent to the towns and cities that burned coal to produce electricity. [43]

Nowadays, heavy industry is more centralized, and electricity production takes place at fewer larger power stations which use a greater variety of fuels than, say, 50 years ago. The waste gases from these industries and power stations are usually discharged into the atmosphere from high stacks, so the gases are dispersed much more widely.

The main acidifying gases are sulphur dioxide, SO_2, and various oxides of nitrogen such as nitrous oxide, N_2O, nitric oxide, NO, and nitrogen dioxide, NO_2. These are collectively referred to as NO_x. The SO_2 originates mostly from power stations, especially the

ones using coal as combustible, whilst road traffic is the main source of NO_x. These gases undergo a series of chemical reactions with cloud water and sunlight to form sulphuric (cf. Eq. (2.13)) and nitric acids with similar reactions.

As a result of using high chimneys to prevent the fumes from factories and power stations to affect the local population, the polluting gases can sometimes cross even national boundaries and get washed down by rain into a different country from that in which they originated.

For example, the Norwegians and Swedes have shown that they receive ten times more acidity in rainfall from other countries than they produce themselves. [44] Much of this acidity originates from industrial areas in the UK. Similarly, Canada is a net importer of polluted air from the Middle-West states of the USA and Japan receives acid rain from China. In Croatia examples are the city Ogulin which has no industry, yet very often acid rain (Fig. 2.6), as well as Zavižan on Velebit, a nature park. They are a result of the work of the electric power plant Plomin 2 in Istria. Rainfall is naturally slightly acidic (about pH 6.0) because it dissolves carbon dioxide from the air to form carbonic acid. If rainfall has a pH of less than 5.6 it is regarded as being polluted with acid gases. Very polluted rain has a pH value down to 3.0. Fig. 2.6 illustrates the percentage of acid rain over rainfalls for some Croatian cities in 2004 to 2006.
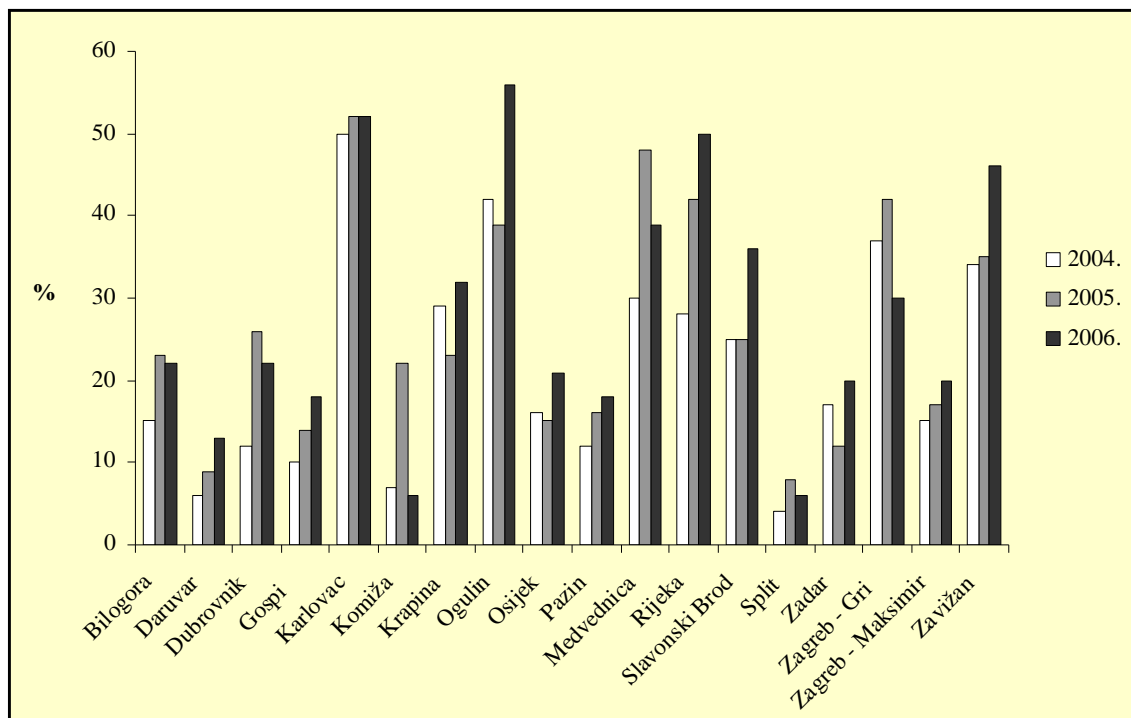
Figure 2.6. Acid rainfall frequency at measuring stations

in the period of 2004 – 2006 in Croatia. [45]

Table 2.3 presents acid rainfall frequency at measuring stations in Croatia in 2007, where:

RR_A – Analysed amount of precipitation in %,

N_A – Number of analysed samples,

N – Number of acid rainfalls.

Table 2.3. Acid rainfall frequency at measuring stations in Croatia, in 2007. [45]

Measuring station	RR_A, %	N_A	N - high acidity rainfalls 3.0 pH<4.0	N - medium acidity rainfalls 4.0 pH<5.0	N - low acidity rainfalls 5.0 pH<5.6
Bilogora	94	134	2	15	23
Daruvar	98	139	0	6	10
Dubrovnik	99	85	0	5	10
Gospi	99	104	1	10	16
Karlovac	100	122	2	29	27
Komiža-Vis	99	73	0	8	10
Krapina	99	110	2	10	28
Ogulin	100	152	3	32	36
Osijek- epin	93	98	0	4	13
Pazin	100	91	0	5	15
Puntijarka (Medvednica)	99	125	0	15	33
Rijeka	100	109	1	28	15
Slavonski Brod	99	117	0	15	23
Split-Marjan	98	92	0	0	3
Zadar	100	78	0	6	13
Zavižan	100	125	0	13	26
Zagreb-Maksimir	99	104	0	0	3
Zagreb-Gri	99	112	2	10	15

2.5.3. AIR POLLUTION

Problems with air pollution have existed ever since the human beings started to use fire. Anyone who has lit a wood fire or who has a coal fire at home will be well aware of the amount of smoke that is generated when they are first alight. Multiply the individual fires by the number of homes using them, and it is easy to see why towns and cities were such unhealthy places in the past. [44]

The first documented complaints about air pollution can be traced back to 1257 when the wife of Henry III, Queen Eleanor, refused to stay in Nottingham Castle because of the choking air sent up to the royal chambers from the coal fires in the surrounding houses below the castle.

The emissions from vehicles contain a complex mixture of pollutants and these vary according to the type of fuel. There is a significant increase in the proportion of cars that have diesel engines. Although these are 'cleaner' because they have a better fuel consumption (more kilometres per litre) and don't use petrol with lead in it, they emit more particles into air. It is more likely to see black smoke coming from a diesel vehicle than from ones with a petrol engine. Between 1980 and 1990, there was a 75 % increase in the amount of black smoke emitted from road traffic whilst other pollutants, such as carbon monoxide, nitrogen oxides and carbon dioxide, also increased substantially.

It has been known for several centuries that air pollutants emitted by burning of fossil fuels have a serious impact on buildings. The effects include loss of mechanical strength and leakage, and failure of protective coatings due to degradation of materials. Also, the unsightly appearance in all larger towns of soiled but otherwise beautiful buildings is caused by deposition of particulate matter arising from atmospheric pollution. On the other hand, there are many parameters that can influence the materials damage; it is interplay between chemical, physical and biological parameters. Systematic laboratory exposures in the 1930s

demonstrated the corrosive effect of SO_2 on metals, which was later also proved by field exposures, and SO_2 has for a long time been regarded as the main corrosive pollutant. Thanks to powerful international efforts, SO_2 concentration in air has decreased substantially and is no longer the only important corrosion stimulator. Now, the effect of SO_2 needs to be considered in a multi-pollutant situation in combination with other gaseous pollutants such as NO_2, O_3, and their reaction products, including particles. [46]

The main air pollutants in urban areas are: carbon monoxide, CO, nitrogen oxides, NO_x, hydrocarbons, HC_s, sulphur dioxide, SO_2, and particulate matter – especially small particles which are sometimes called PM10s because they are smaller than 10 µm. On sunny days, especially in summer, these gases interact with one another, particularly the nitrogen oxides and the hydrocarbons, to form ozone. This gas is harmful to human health and damages plants. High levels of ozone can cause breathing difficulties and are alleged to set off asthmatic attacks to vulnerable people.

In the past ten years, there has been a fourfold increase in the number of people suffering from asthmatic attacks in cities. The Department of Health also estimates that air pollutants account many hospital admissions and premature deaths each year. [44]

There are differing trends in air quality in towns, cities and countryside: some pollutants have increased whilst others have declined. For example, the amount of black smoke emitted from houses in urban areas is much less than 40 years ago because fewer people heat their homes with coal fires. However, as mentioned earlier, the amount of black smoke from vehicles has increased greatly. The amount of lead in the atmosphere has declined in recent years because many more vehicles use lead-free petrol and diesel for fuel, mainly because it's cheaper. This is a very good example of how the pricing of goods can influence people's buying habits with a benefit to the environment.

It was realized a few years ago that the lead in atmosphere was increasing as a result of the rising number of vehicles on the roads. At that time, in order to make engines burn petrol more efficiently, a substance called tetraethyl lead (TEL) was added to petrol. TEL was an 'anti-knock' agent; in other words, it stopped the premature igniting of petrol in the compression stage of the engine cycle. The lead from all the emissions from vehicles stayed in atmosphere for a long time and spread slowly around the globe.

2.6. INHIBITORS

One of the most employed methods to mitigate corrosion is the use of inhibitors. Inhibitors are substances which, when added in small amounts to an aggressive media, reduce markedly the corrosion rate.

In terms of corrosion, inhibitors occupy a special place because of their specific protection and widespread application. Most inhibitor applications are in aqueous medium (natural water, acid solutions for pickling) and partially water systems (primary and secondary processing of petroleum and refining plants), and protection from atmospheric corrosion.

When selecting inhibitors, it should be taken into account what metal is to be protected, the environment in which the metal is exposed, the conditions (temperature, pressure, flow, etc.) in which the metal is submitted, and also their efficiency, availability, toxicity and cost-effectiveness.

2.6.1. MECHANISM OF CORROSION INHIBITION

An accurate analysis of the different modes of inhibiting electrode reactions, including corrosion, was carried out by Fischer. [47] He distinguished various mechanisms of action, such as:

- Interface inhibition,
- Electrolyte layer inhibition,
- Membrane inhibition,
- Passivation. [48]

Subsequently, Lorenz and Mansfield [49] proposed a clear distinction between two-dimensional and three-dimensional film forming inhibitors, representing two different types of retardation mechanisms of electrode reactions including corrosion. More detailed

describing of this classification will be presented later on (cf. §2.6.3-b – According to the thickness of the protective layer).

The first step of the corrosion protection effect of inhibitor is its adsorption on the corroding metal.

2.6.2. ADSORPTION OF INHIBITORS ON THE METAL SURFACE

The adsorption process of inhibitors is influenced by the nature and surface charge of metal, its chemical structure, and type of aggressive electrolyte. Physical (or electrostatic) adsorption and establishment of chemical linking are the main types of interaction between the organic inhibitor and metal surface. The interaction between adsorbed molecules shall be also taken into consideration to evaluate inhibitor effectiveness.

a. Physical adsorption (physisorption)

Physical adsorption is the result of electrostatic attractive force between inhibiting organic ions or dipoles and electrically charged metal surface, known as Van der Waals force. Surface charge of metal is located at the electrochemical double layer. Its polarity can be defined by the potential of metal (E_{corr}) to zero charge potential (ZCP) ($E_{q=0}$). When the difference E_{corr} - $E_{q=0}$ (= ϕ) is negative, cation adsorption is favoured. Adsorption of anions is enhanced when ϕ becomes positive. This behaviour applies not only to compounds with a formal positive or negative charge, but also to dipoles, whose orientation is determined by the electrode potential.

According to Antropov [50] for the same values of ϕ for different metals, similar behaviour of a given inhibitor should be expected in the same environment. This was confirmed by the adsorption of charged organic molecules on mercury and iron electrodes at the same ϕ potential for both metals. It is important to recall that the experimental determination of $E_{q=0}$ of the mercury electrode is rather easy by using a dropping mercury

electrode. The period during which one mercury drop is hanging at the capillary tip is longest at this potential. In contrast, its determination of a solid electrode is a rather complicated task.

With regard to the concepts explained above in relation to the inhibition of corrosion, when the inhibited solution contains anions, they adsorb on the metal surface creating oriented dipoles and, consequently, increase the adsorption of organic cations on the dipole. In these cases, the result is the positive synergistic effect; therefore, the degree of inhibition in the presence of both adsorbing anions and cations of the inhibitor is greater than the sum of their individual effects.

In the study of ion adsorption at the metal / solution interface, it was first assumed that the ions retain their total charge during the adsorption giving in this way a pure electrostatic connection to arise. Lorenz [48] suggested that partial charge is present at the adsorption of ions. In this case, a certain amount of covalent connections with the process of adsorption must be taken into account. The concept of partial charge was studied by Vetter and Schulze [48] who defined electro-sorption valence as the coefficient for the dependence of the flow potential and the charge electro-sorption process. The term valence was chosen because of its analogy with the valence of electrode reactions, which enters the Faraday's law as well as Nernst equation.

b. Chemical adsorption (Chemisorption)

Another type of interaction between metal and inhibitor is chemisorption. This process involves exchange or transfer of charge from inhibitor molecules to the surface of metal to form a coordinated relationship. Therefore, the covalent bonding between the metal surface and the inhibitor molecules is established.

The process of chemisorption takes place more slowly than electrostatic adsorption, and with higher activation energy. It depends on the temperature, and at high temperatures a

higher degree of inhibition can be expected. Chemisorption is specific for each particular metal and is not fully reversible. [51] Coupling that occurs with electron transfer depends on the type of metal and nature of the organic inhibitor. In fact, electron transfer is characteristic for metals with free electron orbitals with low energy. Electronic transfer of the inhibitor can be expected with compounds which have relatively loosely associated electrons. Such a situation may arise due to the presence of multiple bands or aromatic rings on adsorbed inhibitors, whose electrons have the   character. Clearly, the presence of heteroatoms with unpaired electron pairs in the adsorbed molecules will favour electron transfer. Most organic inhibitors are compounds with at least one functional group that is the centre of the chemisorption reaction process. In this case, the strength of the adsorption bonding depends on the electron density of the heteroatoms and polarizability of functional groups. For example, the inhibitor efficiency of homologous series of organic matter, which relates only to the heteroatom is usually in the following order: [52]

$$P > Se > S > N > O$$

The interpretation is: easier polarizability and lower electro-negativity of elements on the left side of the upper sequence. The surface connection of the Lewis acid-base type, usually with the inhibitor as an electron donor and metal as acceptor, is based on this concept.

c. Interaction between adsorbed molecules

When the coverage of a metal surface by an adsorbed inhibitor is increased, interactions between inhibitor molecules affect its efficiency.

Attractive interaction between inhibitor molecules usually leads to stronger adsorption and greater inhibiting efficiency - synergistic effect. This effect is observed in the case of compounds containing long chains of hydrocarbons, due to the Van der Waals attractive forces. [51] In presence of ions or molecules that contain dipoles, repulsive interactions can

occur, and therefore, weaken and reduce adsorption, which reduces consequently the inhibitors efficiency.

2.6.3. CLASSIFICATION OF INHIBITORS

Inhibiting action to the corrosion can be classified in different ways. [39, 47, 49, 50, 53-57]

- According to reaction concerned: anodic, cathodic, or mixed inhibitors.

- According to thickness of the inhibitor layer.

- According to chemical nature: organic and inorganic inhibitors.

- According to oxidizing and reducing properties.

- According to the risk in the failure of protective effect and hazards.

- According to the corrosive medium: acid, neutral or alkaline solution.

- According to the technological application: pickling (industrial cleaning), cooling water systems, etc.

Following, these classifications are explained in more detail. The same inhibitors will be considered in different classifications.

a. According to the impact on the partial corrosion reaction

As shown above, one of the classifications is based on the impact of inhibitor addition towards the partial electrochemical processes involved in the corrosion reaction. [47, 49, 50, 53-56] As can be deduced readily from Eq. (2.22), the decrease of one of the partial currents I_a or I_c (in absolute value) will result directly with a decrease of the corrosion current I_{corr} (= I_a = -I_c). The open circuit corrosion potential changes in presence of inhibitors to satisfy the conditions of zero overall current.

Anodic inhibitors

With this type of inhibitor, generally a thin film composed of oxide or poorly soluble salts will be formed on the metal surface. The thin layer constitutes a barrier that isolates the

underlying metal from aggressive environment. The function of anodic inhibitors is also the maintenance, restoration or reinforcement of the natural oxide film which already exists on metals and alloys before the application of an inhibitor. [57]

When an inhibitor prevents only the anodic reaction, the rate of corrosion can be reduced due to slower transfer of metal ions into the solution by barrier effect, to the slow chemical dissolution of the surface film, or to the reduction of insoluble anode surface. [58]

Anodic inhibitors are mainly used in neutral solutions. When the concentration of anodic inhibitor is insufficient or too high, the acceleration of corrosion rate is sometimes observed, namely inducing localized attacks of the metal surface. Therefore, anodic inhibitors are also known as "dangerous or risky" inhibitors. These inhibitors are often inorganic substances and constitute "oxidizing" inhibitors and 3-D layer forming inhibitors, as will be explained below.

Cathodic inhibitors

These inhibitors act by one of two ways: by slowing down the cathodic reaction involved in the corrosion process or by reducing the cathodic surface area. In a strongly acidic medium, the hydrogen evolution reaction constitutes the main cathodic process whereas in a solution having a higher pH and aerated medium, the reduction of dissolved oxygen will be the main process. [57]

Cathodic inhibitors are "safe", since they do not lead to local corrosion, and thus do not increase corrosion when added in insufficient concentrations. Cathodic inhibitors do not represent danger when added to the electrolyte in small concentrations. Nevertheless, cathodic inhibitors are often less efficient corrosion protection reagents than the anodic inhibitors [58], but due to their "security" they are used frequently. The cathodic inhibitors are, in the majority of cases, organic compounds having hetero-atom sites. However, only a small part of

inhibitors used in industrial applications acts to the cathodic reaction only. The majority of industrial inhibitors reduces both anodic and cathodic reaction rates.

Mixed kinetic inhibitors

Mixed kinetic inhibitors hinder both the anodic and cathodic reaction rates. Approximately 80% of inhibitors used in practice are organic compounds whose effect can not be distinguished solely to cathodic or to anodic reaction. In their structure they contain nitrogen, sulphur and / or oxygen, i.e. atoms with free electron pairs, which participate in the process of adsorption on the metal surface.

The efficiency of these inhibitors is related to the extent to which they are adsorbed or cover the surface. Mixed inhibitors protect the metal in three possible ways: by physical or chemical adsorption and by forming a surface film. [53]

b. According to the thickness of the protective layer

According to protection mechanism, inhibitors may be divided into two groups: 2-D and 3-D film forming inhibitors. [55, 56]

Two-dimensional surface film inhibitors

Two-dimensional (2-D) layer inhibition presumes a strong interaction between the inhibitor and the corroding surface of the metal such as covalent bonding. [47, 53, 54] This layer can affect the basic corrosion reactions in different ways:

- By blocking reactions over the whole surface of electrodes, through adsorption of a stable inhibitor, thus the fraction of surface covered by inhibitor is relatively high, or close to unity;

- By blocking reactive sites such as crystal imperfection kinks or ledges by the adsorption of stable inhibitors on a relatively low level of surface coverage;

◙ Coverage of the reactive metal surface - in this case, adsorption process is followed by electrochemical or chemical reactions of inhibitor to form a 3-D film.

This kind of inhibitor is characterized by formation of a 2-D layer at the corroding metal surface with the inhibitor. According to the concentration and / or potential, varies the part of the surface covered by inhibitor.

Some organic molecules, having a long hydrophobic chain and adsorption centre, may form a well organised adsorbed layer (self assembling molecules; SAM). These inhibitors are particularly efficient making the metal surface hydrophobic with a good barrier layer.

Three-dimensional surface covering inhibitors

These inhibitors form a layer constituted of more than mono-molecular thickness at the corroding metal surface. The layer thus formed consists mainly of poorly soluble compounds such as corrosion products, inhibitors and coatings. 3-D layer inhibition mainly occurs in neutral media, with formation of porous or compact layers. Inhibitor efficiency strongly depends on the properties of the 3-D layer formed, especially its porosity and chemical stability towards aggressive medium. With organic inhibitors, two types of surface films may be formed: polymeric films and complexes with corrosion products and inhibitors.

Recently, the surface layer formed by sol-gel methods of nano-particles of silane or silicate base compounds attracts the interests of many corrosion scientists. The effect expected is essentially based on the high barrier properties of the surface film thus obtained.

c. According to the chemical nature

According to their chemical nature inhibitors are divided into organic and inorganic. Nowadays, another aspect of inhibitors focuses the interests of corrosion scientists: biodegradability of compounds.

Organic inhibitors

The most common corrosion inhibitors in use are organic corrosion inhibitors. They protect as mixed or adsorption inhibitors. [39, 50, 53] They form a protective layer of adsorbed molecules on the surface of the metal. The coverage of metal surface by inhibitor generally increases with its concentration, and at higher concentrations, another parallel reaction may take place such as the oxidation or the reduction of inhibitor molecules themselves. Therefore, the concentration of the inhibitor in the solution is critical; for each inhibitor in any solution there is an optimal concentration. [48]

Inorganic inhibitors

The use of inorganic inhibitors as an alternative to organic compounds is based on the possibility of degradation of organic compounds with time and temperature. [59]

Oxidizing agents such as chromate, molybdate or manganate ions may induce the passivation of steel, iron or aluminium alloys. [60, 61] Chromate is generally accepted as an efficient corrosion inhibitor. However, the main disadvantage is the toxicity of chromium (VI) oxidation state. This is the reason for the search of less toxic alternatives. [59, 62]

Biodegradable inhibitors

Another relative aspect in the chemical nature of an inhibitor is the bio degradability. Some inhibitors are noxious to the environment, thus the decrease of their concentration in soils or in river waters is an important aspect that should be taken into consideration in the choice of inhibitors. I n other terms, the protection of environment becomes a keen interest in these days. To meet this requirement, green inhibitors, essentially obtained by extraction of active substances from plants attract many people. These inhibitors are studied largely by economically under-developing countries where the valorisation of their natural resources becomes a keen factor.

d. According to oxidizing and reducing properties

The majority of organic inhibitors presents their protective effect without redox reactions, however many inorganic inhibitors act by oxydizing or reducing properties.

Oxidizing inhibitors

As stated above for inorganic inhibitors, some of them make or reinforce the passivity of corroding metals. They present a strong oxidizing property.

Reducing inhibitors

For closed cooling systems, hydrazine, N_2H_2, or sulphite, SO_3^-, are added into water. These substances reduce the concentration of oxygen dissolved in the cooling water. Since in weakly acid to alkaline medium, the reduction of dissolved oxygen constitutes the partial cathodic reaction, and then the corrosion rate decreases substantially.

e. According to the risk in protection effectiveness and hazards

There are two different ideas about the risk of inhibitor use. The failure or worsening of corrosion protection due to inappropriate use of an inhibitor and hazards induced by an inhibitor to human beings, by its toxicity or noxiousness, or to the environment.

Risky to corrosion protection

The oxidizing inhibitors reinforce the passivity, but if the concentration of which is insufficient; this type of inhibitors may fail to provide complete passivation of metals. At the surface area, a surface without a passive film appears. Then, at the large surface area, where the passive film is present, cathodic process will take place, whereas a fast active dissolution reaction will occur at the bare metal leading to the local corrosion. This type of inhibitor is therefore classified also as a "dangerous" or "risky" inhibitor, as stated above.

When using anodic inhibitors, it is necessary to determine the critical inhibitor concentration below which the inhibitor becomes "dangerous", and also the concentration above which the complete passive layer will be formed.

Generally, the cathodic and mixed inhibitors do not induce such a risk.

Hazards to health or environment

Chromate for instance is known to be carcinogenic and its use is now forbidden. Some derogation is accorded to the aircraft industry and the finding its alternative compounds is one of the main topics of corrosion scientists in this field.

Other highly efficient inhibitors, such as benzotriazole for copper and copper alloys are also suspected to be carcinogenic and harmful to the environment.

f. According to the corrosive media

The inhibitor effect depends often on the solutions pH.

Inhibition of acid solutions

In acid solutions, the inhibition action is due to adsorption on oxide-free metal surfaces. In these media, the main cathodic process is hydrogen evolution. [55, 63] Corrosion inhibition in acid solutions can be accomplished by the use of a large variety of organic compounds. Among those used for this purpose, there are triple-bonded hydrocarbons; acetylenic alcohols, sulfoxides, sulfides, aliphatic carboxylate and mercaptans; aliphatic, aromatic, or heterocyclic compounds containing nitrogen; and many other families of simple organic compounds products of reactions between two different compounds, such as amines and aldehydes. [48]

Incorrect choice or use of organic inhibitors in acid solutions may lead to corrosion stimulation and / or hydrogen penetration into the metal. The latter induces the hydrogen

embrittlement, particularly dangerous for metal under stress. In general, stimulation of corrosion is neither related to the type nor structure of the organic molecule. Stimulation of iron corrosion in acid medium was observed with mercaptans, sulfoxides, azoles, triazole derivatives, nitrites, and quinoline. This adverse action depends on the type of acid. Many investigations were devoted to the inhibiting and / or stimulating phenomena of organic compounds on ferrous as well as nonferrous metals. Organic inhibitors have a critical concentration value, below or beyond which inhibition ceases and stimulation may occur. Therefore, it is essential that when organic inhibitors are used, constant monitoring of the solution should take place, to ensure that the inhibitor concentration does not fall outside the critical values.

Generally, it is accepted that the first stage in protective action of inhibitors in aggressive acid media is adsorption of the inhibitors onto the metal surface.

Inhibition of near neutral solutions

Because of the differences in the mechanisms of the corrosion process between acid and near-neutral solutions, the inhibitors used in acid solutions usually have little or no inhibition effect in near-neutral solutions. In almost neutral solutions, the corrosion process of metals results in the formation of sparingly soluble surface products such as oxides, hydroxides, or salts. The cathodic partial reaction is oxygen reduction.

The inhibitive effect is manifested through the increase in oxide covered surface or maintenance of the protective properties of oxides or surface layers in aggressive solutions. Corrosion inhibitors for metals in neutral solutions can slow down the corrosion process by: [63]

- Stabilization of the passive oxide film and reduction of its dissolution rate;
- Repassivation of the surface by promoting the reformation of the oxide;
- Sealing of the damaged area of oxide film by forming insoluble surface compounds;

⧫ Hamper the adsorption of aggressive anions by competitive adsorption of the inhibiting anions.

Among the organic corrosion inhibitors for neutral media are salts of organic acids such as benzoates, salicylates, tartarates and azelates [64, 65]; organic compounds containing phosphorus (phosphonium) and a variety of heterocyclic compounds such as azoles.

Their major disadvantage is that they are often toxic and can lead to localized corrosion if they are added in a too small concentration.

g. According to application

Inhibitors are applied in various processes in different industries. [47] Some of the most common are used in petroleum production, for steel pipelines, for drinking water and water in cooling systems, for acids, in automobiles, for paints [66] etc.

2.6.4 INHIBITORS FOR COPPER AND COPPER ALLOYS

Copper and many of its alloys are resistant to corrosion in presence of organic compounds such as amines [67-69], amino acids [70], azoles [50, 68, 71-82], thiazoles [83, 84], alcohols [84, 85], etc. Various studies have shown that compounds involving heteroatoms such as nitrogen, sulfur and phosphorus exhibit good protective effects towards copper. [4, 59]

One of the most effective and most commonly used inhibitors for copper and its alloys is benzotriazol (BTA). A lot of research was performed on BTA for the protective effect on copper corrosion in various electrolyte media; those containing chloride ions [86], very acidic [86], nearly neutral [87], or very alkaline solutions [88], and also in the conditions of atmospheric corrosion [89].

Benzotriazol is an organic compound that in its structure contains a phenol ring and triazole, with the formula $C_6H_5N_3$. The presence of nitrogen atoms in the triazole ring allows

their adsorption on copper. Generally, BTA, is an anodic corrosion inhibitor for copper, whose mechanism of action is chemisorption (in rare cases, physical adsorption) on the copper surface following the Langmuir isotherm. In chloride containing media formation of a Cu(I)-BTA complex takes place.

The mechanism of complex formation can be described by the following reactions:

$$Cu_{(s)} + BTAH_{(aq)} \rightarrow Cu:BTAH_{(ads)} \qquad (2.29)$$

where $Cu:BTAH_{(ads)}$ indicates that BTAH (BTA in acid form) is adsorbed on the copper surface. In presence of oxidants or the anodic polarization it can be oxidized to the protecting complex:

$$Cu:BTAH_{(ads)} \rightarrow Cu(I)\text{-}BTA_{(s)} + H^+_{(aq)} + e^- \qquad (2.30)$$
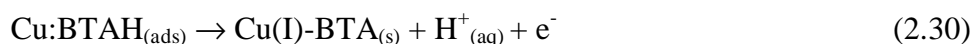
According to this reaction, it can be seen that the increase of BTA concentrations shifts the reaction towards the creation of a larger amount of the Cu(I)-BTA complex as confirmed by many experiments. [87-89] It was also reported that increasing the pH favours the creation of complexes. [88, 90]

Despite of the excellent protective properties of BTA, its application shall be restricted and in the future replaced by other corrosion inhibitors because of its toxicity. [91, 92]

Another kind of azole typed compound that has received much attention is imidazole and its compounds. [59] Imidazol is a planar, heterocyclic aromatic organic compound containing two nitrogen atoms that form a five-membered ring. One of the nitrogen atoms is pyrole type, and the other pyridine. The structure of imidazoles shows that these molecules have two sites suitable for linking to the surface: nitrogen atom with a free sp^2 pair and the aromatic ring. Imidazoles are favourable as corrosion inhibitors due to the strong protective properties, and towards BTA they have the advantage that they are non-toxic.

The mechanism of protective action is the same as for other azole compounds: adsorption of molecules on the surface of copper and creating a protective complex layer with copper. Efficiency increases as the concentration increases, while the increase in temperature has a negative effect. The introduction of substituents in the imidazole molecule influences the protection efficiency but not the inhibition as well as the benzene ring mechanism. The following groups have proven to be especially favourable: the phenyl group [73], the mercapto group [28], the presence of more heteroatoms as potential active centres for bonding with copper.

Imidazoles have proved to be effective corrosion inhibitors in various media, such as: nitric acid [93], sulphuric acid [73, 74], hydrochloric acid [86, 94], sodium chloride [76, 94, 95], sodium hydroxide [88], as well as atmospheric corrosion [82].

3. EXPERIMENTAL METHODS AND CONDITIONS

In this chapter the principles of the experimental methods used will be presented and then the conditions at which various measurements were carried out.

3.1. EXPERIMENTAL METHODS

Morphology and structure of the patina formed on the surface of the bronze electrode were characterized by Scanning Electron Microscopy (SEM) and Energy Dispersive X-ray Spectroscopy (EDS). EDS supplies the elemental composition of patina, and its crystal structure was further refined by Micro-Raman Spectroscopy. These local methods characterizing micrometric scale are particularly well adapted to identify the patina formed of fine particles. The corrosion and corrosion protection mechanisms of bronze and bronze electrodes covered with patina were then studied by electrochemical methods, particularly by the polarization measurements and electrochemical impedance spectroscopy.

3.1.1. SCANNING ELECTRON MICROSCOPY (SEM)

Scanning electron microscopy (SEM) is a method for high-resolution imaging of surfaces. Instead of visible light used for imaging in optical microscopy, SEM uses electrons. The advantages of SEM over optical microscopy consist of much higher scale resolution and greater depth of field, up to 100 times, than optical microscopy.[96]

SEM generates an incident electron beam above the sample chamber. The electrons are produced by a thermal emission source, such as heated tungsten filament, or by a field emission cathode. The energy of the incident electrons can be as low as 100 eV or as high as 30 keV depending on the evaluation objectives. The electrons are focused into a small beam by a series of electromagnetic lenses in the SEM column. The electron beam is scanned in a

raster pattern over the surface for imaging. The beam can be focused to a final probe diameter as small as 1 nm with a field-effect gun electron emitter (FEG-SEM). [97, 98]

Samples must be compatible with at least a moderate vacuum. For high-resolution secondary electron imaging, the sample environment is at a pressure of less than 10^{-5} Torr ($1.3 \cdot 10^{-3}$ Pa). [97]

The morphology and crystallographic structure of artificial patinas were examined with Scanning Electron Microscopy (SEM; Leica Stereoscan 440 controlled by LEO software).

3.1.2. ENERGY DISPERSIVE X-RAY SPECTROSCOPY (EDS)

Energy Dispersive X-Ray Spectroscopy (EDS) is a chemical microanalysis technique used in conjunction with SEM. This technique detects X-rays emitted from the sample during bombardment by an electron beam to characterize the elemental composition of the analyzed volume. [97]

The EDS X-ray detector measures the relative abundance of emitted X-rays versus their energy. The measured X-ray energy values are compared with known characteristic X-ray energy values to determine the presence of an element in the sample. Elements with atomic numbers ranging from that of boron to uranium can be detected. The minimum detection limits vary from approximately 0.1 to a few atom percent, depending on the element and the sample matrix. Semi-quantitative results are available using mathematic corrections based on the analysis parameters and the sample composition. Greater accuracy is obtained using known standards with similar structure and composition to that of the unknown sample. The quantitative determination of boron, carbon and nitrogen is difficult because they are too light and close to beryllium since the electron gun and SEM column are composed of boron

oxide. Generally, X-ray response concerns the elements found in about 1 μm depth, therefore for a very thin film, the EDS contains also the substrate material.

The morphology and crystallographic structure of artificial patinas were examined with Scanning Electron Microscopy coupled by X-ray Elemental Energy Dispersion Spectroscopy (EDS analyses; Princeton Gamma-Tech, model Spirit) at 20 keV. The standard used for quantitative micro-analyses of oxygen was MgO while C and N were not taken in account for the quantitative analysis.

3.1.3. RAMAN SPECTROSCOPY

Raman spectroscopy is a technique for analyzing material that achieves both chemical and structural information of studied species. The Raman Effect is a phenomenon of change in wavelength that accompanies the scattering of light by a material medium. It was discovered theoretically by Smekal in 1923, and confirmed experimentally in 1928 by Raman. [99] A Raman spectrum gives full information on the chemical composition and organization of the crystalline material. [100] The principle and the collected information are related to infrared spectroscopy, but contrary to this method, Raman spectroscopy allows in situ analysis in aqueous solutions.

When the oscillating electric field of an incident light beam interacts with a molecule, a small oscillating dipole moment is induced in the molecule as a consequence of its polarizability, . Polarizability itself is a measure of the change in the dipole moment of a molecule induced by an electric field, and in the simplest case, where the electric field E and induced dipole moment μ are in the same direction, $\mu = \alpha \cdot E$.

For lower molecular symmetries, μ and E must be treated as vectors and may not be in the same direction. Under these circumstances, the polarizability has the form of a tensor.

The rapidly varying electric field of the incident electromagnetic radiation can, therefore, cause a rapid fluctuation in the dipole moment of the molecule. The magnitude of this oscillation depends on the polarizability of the molecule, but is generally small.

It is known that such an oscillating dipole radiates light at the same frequency at which it oscillates. The emitted light needs to be in different direction to the incident beam, and the effect is that a small proportion of the incident light is scattered by the molecule. When the frequency of the incident light is unchanged by the scattering process, i.e. the scattering is elastic, the phenomenon is known as Rayleigh scattering. However, the molecules themselves may also undergo vibrational excitation, at frequencies dictated by their normal modes of vibration. If the molecular symmetry is such that the incident electromagnetic radiation can induce an electronic dipole change in the molecule and a vibrational transition can couple to the electronic dipole change, then a Raman transition may take place. In general, the coupling is weak and the magnitude of this inelastic scattering is small, being produced by only 1 incident photon in 10^{10}. Thus this, the normal Raman (NR) effect yields relatively weak emission bands. [101]

The Raman spectra were recorded with a Labram microspectrometer / laser line. Samples were irradiated with a helium neon laser at λ =633 nm for the chemical patina and at λ =514 nm for the electrochemical patina. The laser power was set at 0.1 mW and 1 mW. The diameter of the laser beam is about 1 μm. The volume of sample by which the Raman spectrum was collected is about 1 μm^3. It is important to recall that the metal gives no Raman spectrum.

3.1.4 STEADY STATE POLARIZATION CURVES

Two methods were used to collect current – potential relationship; a wide ($\pm$150 mV vs. E_{OC}) potential range and a narrow one ($\pm$20 mV vs. E_{OC}). The potential sweep

rate was, for both cases, at 0.166 mV·s^{-1}. From the polarization curves thus obtained corrosion parameters were determined by Tafel extrapolation method and polarization resistance measurements respectively.

a. Tafel Extrapolation Method

As described in §2.5.1, the main contribution of the overpotential η under the electrode polarization is the activation overpotential. That is, the current flowing across the electrode interface is governed by the activation process for the charge transfer reaction. This reaction near the thermodynamic equilibrium is expressed through the Butler-Volmer equation: [96, 102-104]

$$j = j_0 \left[e^{\frac{(1-\alpha)\cdot n\cdot F\cdot \eta}{R\cdot T}} - e^{-\frac{\alpha\cdot n\cdot F\cdot \eta}{R\cdot T}} \right] \quad (3.1)$$

Where:

j – Overall current density (A·cm^{-2});

j_0 – Exchange current density (A·cm^{-2});

   – Tafel transfer coefficient ($0 < \alpha \leq 1$);

F – Faraday constant (96485 C·mol^{-1});

n – Number of electrons exchanged;

   – Overpotential (V);

R – Gas constant (8.315 J·mol^{-1}·K^{-1});

T – Temperature (K).

Stern and Geary [105] applied Eq. (3.1) to the corroding electrode. For this system, the reaction is no longer around the thermodynamic equilibrium because the nature of the anodic and cathodic processes is completely different. The anodic process is the active dissolution of metal and the cathodic process will be for instance the hydrogen evolution reaction. Even in

this situation, the overall current density j will be expressed by the sum of anodic and cathodic current densities. The Tafel coefficient α should however be different for two distinct reactions. When Eq. (3.1) is rewritten it describes the overall current density which undergoes through the phase interface, on which an anodic and a cathodic reaction take place, which are not under diffusion control. This equation is known as the Wagner – Traud equation:

$$j = j_a - j_c = j_{\text{corr}}\left[e^{\frac{(1-\alpha_a)\cdot n_a \cdot \text{F}\cdot\eta}{\text{R}\cdot T}} - e^{-\frac{\alpha_c \cdot n_c \cdot \text{F}\cdot\eta}{\text{R}\cdot T}} \right] \qquad (3.2)$$

where:

j_{corr} – Corrosion current density ($A\cdot cm^{-2}$);

a (subscript) – Anodic reaction;

c (subscript) – Cathodic reaction;

η – Overpotential, $E - E_{\text{corr}}$ (V);

E_{corr} – Corrosion potential (V).

Eq. (3.2) can also be written as:

$$j = j_a - j_c = j_{\text{corr}}\left(e^{\frac{\eta}{b_a}} - e^{-\frac{\eta}{b_c}} \right) \qquad (3.3)$$

where:

$$b_a = \ln(10)\cdot\frac{\text{R}\cdot T}{(1-\alpha_a)\cdot n_a \cdot \text{F}} \qquad (3.4)$$

$$b_c = \ln(10)\cdot\frac{\text{R}\cdot T}{\alpha_c \cdot n_c \cdot \text{F}} \qquad (3.5)$$

Where:

b_a – Tafel slope for anodic process ($V\cdot dec^{-1}$);

b_c – Tafel slope for cathodic process (V·dec^{-1}).

One gets the Tafel plot (log ($|j|$) – E) by transformation of Eq. (3.3):

$$\log(|j|) = \log(j_{corr}) + \left[\frac{\eta}{b_a} - \frac{\eta}{b_c}\right]$$
(3.6)

Eq. (3.6) is drawn in Fig. 3.1 to illustrate how various corrosion parameters can be determined graphically.
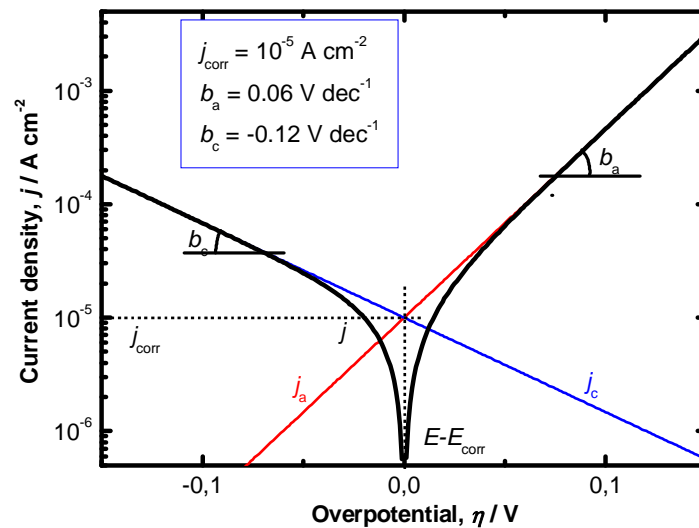
Figure 3.1: Tafel plot for determination of corrosion parameters

(parameters used are indicated in the insert).

At sufficiently high overpotential, that is far from E_{corr} (| | > 50 mV), it may be assumed that only one of the partial current densities determines the overall current density, j. For highly anodic domain, thus:

$$\log(|j|) \approx \log(j_a) = \log(j_{corr}) + \left(\frac{\eta}{b_a}\right)$$
(3.7)

Similarly, at sufficiently cathodic potential:

$$\log\left(|j|\right) \approx \log\left(|j_c|\right) = \log(j_{corr}) - \left(\frac{\eta}{b_c}\right) \tag{3.8}$$

Eqs. (3.7) and (3.8) can be rewritten into:

$$\eta = -b_a \log(j_{corr}) + b_a \log\left(|j|\right) \tag{3.9}$$

$$\eta = b_c \log(j_{corr}) - b_c \log\left(|j|\right) \tag{3.10}$$

Eqs. (3.9) and (3.10) represent the anodic and cathodic Tafel equations.

From the intersection of the extrapolated Tafel lines, $\log(j_a)$ and $\log(|j_c|)$, the corrosion current density, j_{corr}, and the corrosion potential, E_{corr}, can be determined as presented in Fig. 3.1.

The slopes of the anodic and cathodic branches allowed the evaluation of the Tafel slopes.

b. Polarization Resistance Measurements

Since Tafel extrapolation method imposes a polarization of great magnitude, about 0.15 V to obtain the linear domain for both anodic and cathodic reactions, it may modify the surface state before reaching the corrosion potential. Then, the corrosion potential, E_{corr}, and the corrosion current density, j_{corr}, may be influenced by very high polarization. This is the reason why only a narrow potential domain around the open circuit potential is also applied. [102-106] From the reciprocal of the slope of the linear part of the polarization curve, polarization resistance, R_p (dE/dj), and b_a and b_c values determined above, E_{corr} and j_{corr} are evaluated.

$$R_p = \frac{E}{j} \tag{3.11}$$

Wagner and Traud [107] have empirically found, as early as 1938, the relationship between the polarization resistance and the corrosion current density. This empirical relationship was further verified by Bonhoeffer and Jena twenty years later. [39] Independently, Stern and Geary, quoted earlier, have shown theoretical background of this important relationship. For small overpotentials ($\eta = E-E_{corr} \approx 0$) the Wagner-Traud Eq. (3.2) can be expanded into the Taylor series close to the corrosion potential. Limiting the Taylor expansion for the first order one gets:

$$\frac{j}{E} = \frac{1}{R_p} = j_{corr} \cdot \ln(10) \cdot \left(\frac{1}{b_a} + \frac{1}{b_c} \right) \qquad (3.12)$$

From Eq. (3.12), one gets the so called Stern – Geary equation: [106]

$$j_{corr} = \frac{b_a \cdot b_c}{\ln(10) \cdot (b_a + b_c) \cdot R_p} = \frac{B}{R_p} \qquad (3.13)$$

where:

$$B = \frac{b_a \cdot b_c}{\ln(10) \cdot (b_a + b_c)} \qquad (3.14)$$

B – Stern – Geary coefficient (V).

Since the potential – current relationship is linear in small potential areas around the corrosion potential E_{corr} ($E_{corr} \pm 5$ mV or 10 mV), the polarization resistance, R_p, can be determinated from the slope of the polarization curve or it can be calculated from the corrosion current, j_{corr}, and b_a and b_c, if they are calculated by the Tafel extrapolation method.

The potential – current relationship near the corrosion potential, E_{corr}, is illustrated in Fig. 3.2.
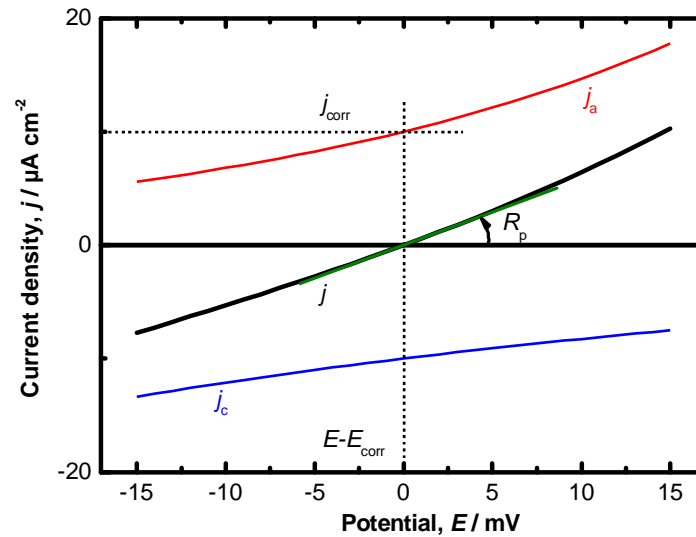
Figure 3.2: Polarization resistance determination from the polarization curve

in the vicinity of the corrosion potential

(Values of corrosion parameters are the same as for Fig 3.1).

In this figure, the partial anodic and cathodic current densities are also presented for the sake of clarity, though these characteristics are not accessible experimentally. It can also be seen that if R_p is determined from $\Delta E = \pm 15$ mV as stated by Mansfeld [106], the error induced for its estimation is 4 % in the example presented in Fig. 3.2.

c. Determination of the Inhibiting Efficiency

The inhibiting efficiency, z in %, is defined by the ratio between the corrosion rate in inhibited ($v_{corr,inh}$) and in the uninhibited system ($v_{corr,0}$):

$$z = 100 \cdot \frac{v_{corr,0} - v_{corr,inh}}{v_{corr,0}} \tag{3.15}$$

From the electrochemical measurements, the corrosion rate is obtained in the form of the corrosion current density. According to the Faraday law, the corrosion rate, v, can be expressed as:

$$v = \frac{j_{corr} \cdot M}{n \cdot F} \qquad\qquad (3.16)$$

where:

M – Atomic mass of the corroding metal (g·mol^{-1}).

The inhibiting efficiency is thus calculated in terms of the corrosion current density by:

$$z = 100 \cdot \frac{j_{corr,0} - j_{corr,inh}}{j_{corr,0}} \qquad\qquad (3.17)$$

3.1.5. ELECTROCHEMICAL IMPEDANCE SPECTROSCOPY (EIS)

The *dc* current used for the polarization methods is determined by the rate determining step, whereas the impedance method supplies other precious information on the electrode process, for instance, double layer capacitance, surface relaxation of reaction intermediates or the diffusion process. Besides, for the bronze electrode covered by a patina layer, *dc* current flow used for steady-state method may disturb deeply the patina layer itself, the formation of oxide or salt layer in anodic domain and the reduction of patina layer during the cathodic polarization, therefore electrochemical measurements remaining near the open circuit potential, as the case of the EIS method, are preferred.

Electrochemical impedance spectroscopy is a technique based on the response of a sample to an alternating current (*ac*) or voltage perturbation as a function of frequency. [108-115] *Ac* techniques are finding increasing applications in corrosion research due to the possibility of obtaining mechanistic data. Another advantage of the impedance technique is the use of very small perturbing signals which do not disturb the electrode under investigation.

One of the main particularities of electrochemical impedance spectroscopy (EIS) is that purely electrical model can be used to represent electrochemical behaviour. An electrode

interface undergoing an electrochemical reaction is typically analogous to an electrical circuit consisting of a specific combination of resistors and capacitors. This particularity is based on the fact that the response of an electrochemical system to a perturbing signal is limited to the linear domain. Once a particular electrical model is chosen, each circuit element shall be allocated to a physical or chemical property of the system and their numerical values can be extracted by regression calculation of the impedance data on the basis of the circuit model. The use of Kramers – Kronig [116] transforms of impedance data allowed, in certain cases, discarding wrong measurements.

In order to understand the particularity of EIS, the current response under *dc* regime induced by potential perturbation will be described first.

a. *DC* Regime

In the *dc* regime, the current – potential relationship is defined by Ohm's law:

$$E = I \cdot R \tag{3.18}$$

where:

E – Potential or voltage (V);

I – Current (A);

R – Resistance ( ).

Resistance is a scalar entity which has a value of a real number and is the only element that allows the flow of electrons in the *dc* regime.

Fig. 3.3 illustrates the current response followed by a step-wise potential change ΔE. It is important to recall again that the electrochemical system is essentially non-linear, thus Ohm's law applies only with a small perturbing signal.
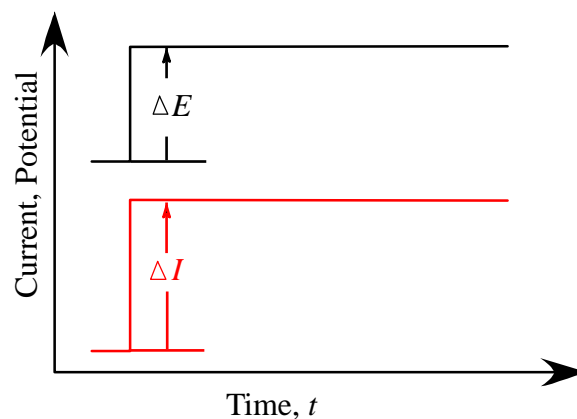
Figure 3.3: Potential, E, and current, I, in the dc regime.

It can be noticed that with a wide potential or current domain, Eq. (3.18) is no longer valid for an electrochemical system. Equations such as the Wagner-Traud Eq. (3.2) shall be used.

b. *AC* Regime

In the *ac* regime potential is no longer constant, and it becomes time-varying. *AC* signal may be in any form. Often, a sine-wave signal is superimposed around the steady-state polarization (E_0, I_0), but any form of perturbing signal can be employed, since they are linked with Laplace transformation. For the sine-wave perturbation, the potential change will be expressed as follows:

$$E(t) = E_0 + |\Delta E| \cdot \sin(\omega \cdot t) \tag{3.19}$$

where:

$E(t)$ – Instantaneous potential (V);

E_0 – *DC* bias potential around which Z will be determined (V);

$|\Delta E|$ –Amplitude of *ac* signal (V);

ω - Pulsation of perturbing signal (= 2π f; rad·s^{-1});

t – Time (s).

If $|\Delta E|$ *is* sufficiently small; the resulting current response is also sine wave of the same angular frequency, ω, with phase shift, φ:

$$I(t) = I_0 + |\Delta I| \cdot \sin(\omega \cdot t + \varphi) \tag{3.20}$$

Where:

$I(t)$ – Instantaneous current (A);

I_0 – *DC* current around which Z is determined (A);

$|\Delta I|$ – Amplitude of the *ac* signal (A);

φ – Phase-shift (rad).

Fig. 3.4 illustrates the time change of the potential and current.
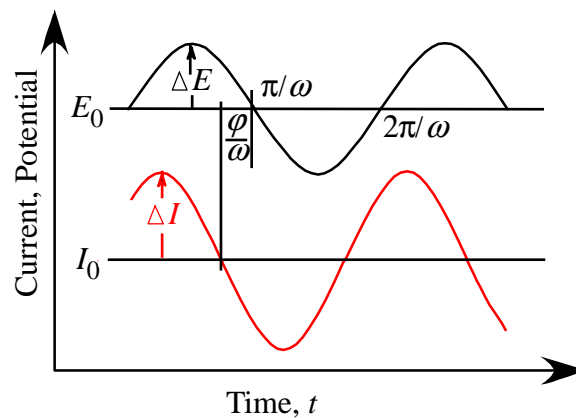
Figure 3.4: Potential E(t), and current change I(t) under ac signal.

The impedance Z is then defined as:

$$Z(\omega) = \frac{E}{I} = \frac{|\Delta E| \cdot \sin(\omega \cdot t)}{|\Delta I| \cdot \sin(\omega \cdot t + \varphi)} = |Z(\omega)| \cdot \exp(-j \cdot \varphi) \tag{3.21}$$

where:

Z – Impedance (complex number) (Ω or $\Omega \cdot cm^2$);

j – Imaginary number $\sqrt{-1}$.

The impedance Z is complex number, therefore, it is often presented in the complex or Gaussian plan with its real (Z') and imaginary (Z'') components:

$$Z(\omega) = |Z(\omega)| \cdot [\cos(\varphi) + j \cdot \sin(\varphi)] \qquad (3.22)$$

Where:

$$|Z| = \sqrt{(Z')^2 + (Z'')^2} \qquad (3.23)$$

$$\tan\varphi = \frac{Z''}{Z'} \qquad (3.24)$$

The impedance Z can be expressed also by the real and imaginary component:

$$Z(\omega) = \frac{E(\omega)}{I(\omega)} = Z'(\omega) + j \cdot Z''(\omega) \qquad (3.25)$$

The representation in complex plane is illustrated on Fig. 3.5. It is worth to recall that in electrochemistry, generally the capacitive component ($Z'' < 0$) is represented above the real axis.
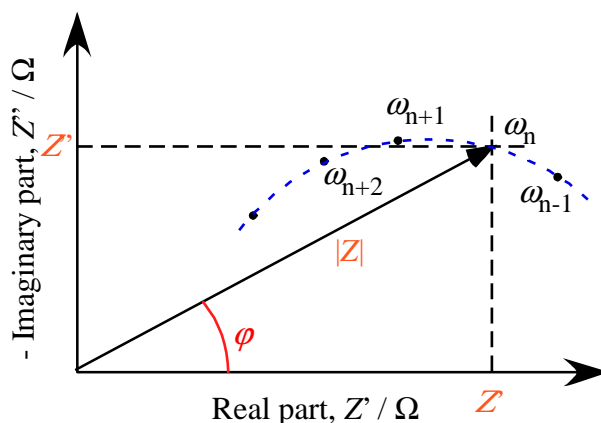
Figure 3.5: Impedance in the complex or Gaussian plan.

Since impedance depends on the frequency ω, the impedance diagram is drawn with different values of parameters ω. The impedance Z will be represented also by the modulus $|Z|$ and phase-shift φ with respect to frequency, f, in Hz, as it will be described in detail later

(§3.1.5-d). The electrochemical impedance $Z(\omega)$ collected at the electrode interface may be represented with one or many equivalent electrical circuits.
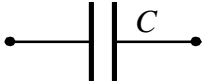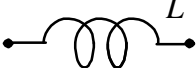
I. Equivalent Circuit Elements

Electrical elements such as resistors, capacitors or inductors depend on the perturbing frequency with a power law of integer number, 0, -1 and 1 respectively. These elements will be called no frequency distributed systems, in contrast to the elements depending on non integer numbers.

No frequency distributed elements

The basic element composing equivalent circuits are given in Table 3.1. [108]

Table 3.1: Basic equivalent circuit elements and corresponding impedance equation.

Circuit element	Resistor	Capacitor	Inductor
Impedance	$Z = R + 0 \cdot \mathrm{j}$	$Z = 0 + \dfrac{1}{\mathrm{j} \cdot \omega \cdot C}$	$Z = 0 + \mathrm{j} \cdot \omega \cdot L$

It may be noticed that the impedance of a resistor has no imaginary component. Thus, the phase-shift is zero, that is, the current is in phase with the potential in the whole frequency domain. Both current and impedance are independent of the frequency. In an electrochemical cell, resistive elements such as electrolyte resistance, charge transfer resistance, polarization resistance or resistance of an oxide or inhibitor film can be observed.

Conversely, the impedance of a capacitor has no real component. Its imaginary component is a function of both capacitance and frequency. The impedance of a capacitor varies inversely with the frequency. At high frequencies a capacitor acts as a short circuit and

its modulus |Z| tends to zero. At low frequencies (approaching *dc*) a capacitor acts as an open circuit and the impedance tends towards infinite. Capacitive elements that can be observed in electrochemical cells are double layer capacitance and coating or oxide layer capacitance. A redox process gives rise also to a capacitive behaviour and known as a blocking electrode.

The third simple electrical component is the inductor. Like a capacitor, the current through an inductor is always π/2 (rad) out of phase with the potential perturbing signal, but in the opposite direction – the current lags to the voltage. It acts as a short circuit at low frequencies and as large impedance at high frequencies. Inductive behaviour of an electrochemical system may, for example, arise from some types of adsorption processes.

For an electrochemical system, there are, in addition to that presented in Table 1, frequency distributed elements such as the diffusion impedance (or Warburg impedance) and a Constant Phase Element (CPE) which will be presented in the next paragraph.

CPE

Very often, when experimental results are fitted with a capacitance, a systematic divergence is observed. To overcome this difficulty, so called *Constant Phase Element* (CPE) was introduced. It is purely empirical and the impedance of this element can be expressed by:

$$Z(\omega) = \frac{1}{Y_0 \cdot (j \cdot \omega)} \qquad \text{where } Y_0 \text{ and } n \ (0 < n \leq 1) \text{ are constant} \qquad (3.26)$$

When the exponent of the constant phase element (*n*) is equal to 1, CPE identifies to an ideal capacitor. Some attempts were made to explain the origin of the CPE behaviour, particularly using a concept of fractal objects, but no definite theory is established. However, since this element introduces the distribution of the time constant, non-ideal capacitive behaviour is usually explained by the influence of surface roughness or non-uniform current distribution due to the heterogeneity of the surface reactivity.

Diffusion impedances

The first distributed element introduced into electrochemistry was *Warburg impedance* where the thickness of diffusion layer is infinite. [117] It is obtained from the solution of the Fick's second law, the diffusion equation, for one-dimensional diffusion of a particle in a semi-infinite space. Impedance function for infinite-length diffusion is:

$$Z_W = \frac{\sigma}{\sqrt{\omega}} - \frac{j \cdot \sigma}{\sqrt{\omega}} \qquad (3.27)$$

where:

$$\sigma = \frac{R \cdot T}{n^2 \cdot F^2 \cdot A \cdot \sqrt{2}} \cdot \left(\frac{1}{c_{ox} \sqrt{D_{ox}}} + \frac{1}{c_{red} \sqrt{D_{red}}} \right) \qquad (3.28)$$

Z_W – *Warburg impedance* (Ω);

σ – *Warburg coefficient* ($\Omega \cdot s^{-0.5}$);

c_{ox} – Concentration of oxidant in the bulk ($mol \cdot cm^{-3}$);

c_{red} – Concentration of reductant in the bulk ($mol \cdot cm^{-3}$).

On a rotating electrode or when stirring of the electrolyte is applied a diffusion layer of finite length, , is formed (Nernst diffusion layer) and diffusion impedance can be written as:

$$Z_{dif} = R_d \cdot \frac{\tanh \sqrt{j \cdot \omega \cdot T_D}}{\sqrt{j \cdot \omega \cdot T_D}} \quad \text{where} \quad T_D = \frac{\delta^2}{D} \qquad (3.29)$$

For $\omega \gg 1/T_D$, Z_{dif} identifies to the Warburg impedance, Z_W, since the concentration modulation is damped down (tanh( ) $\approx$ 1) before arriving at the Nernst diffusion layer thickness. Therefore, one can identify:

$$R_d = \sigma \cdot \sqrt{T_D} \qquad (3.30)$$

II. COMBINATION OF DIFFERENT ELEMENTS

Equivalent electrical circuit will be constructed by a combination of different elements to yield the total impedance, Z.

Table 3.2: Connecting impedance elements.
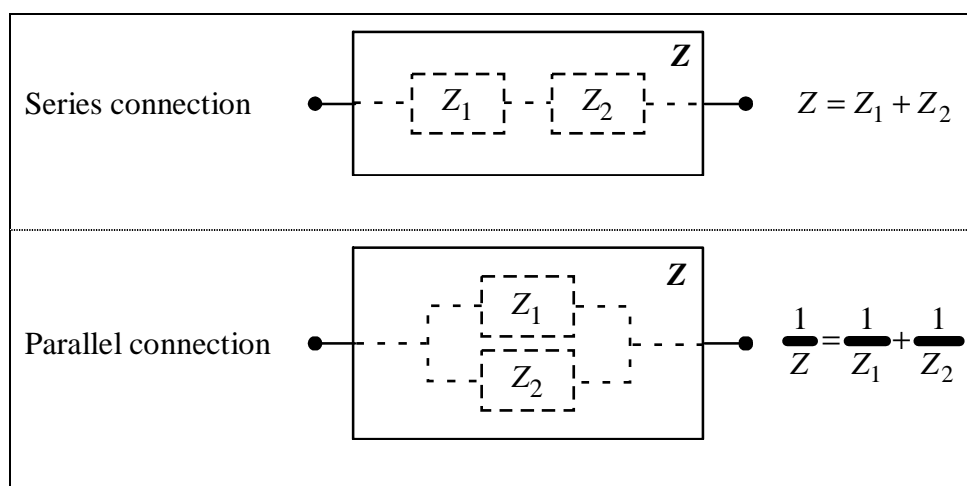
When two impedance elements are connected *in series*, the same current flows through them, but the potential of each element is different When the impedance elements are connected in parallel, the applied potential is the same, but the current flow will be shared to each element but. Table 3.2 illustrates these two combinations for two impedance elements Z_1 and Z_2.

III. SIMPLE ELECTRICAL CELL

Some basic concept of impedance behaviour at the electrode interface will be described briefly.

Double layer capacitance

A typical electrochemical cell is one in which a metallic electrode is immersed in an electrolyte solution. The electrochemical double layer will then be created on the surface of the electrode (Fig. 3.6).
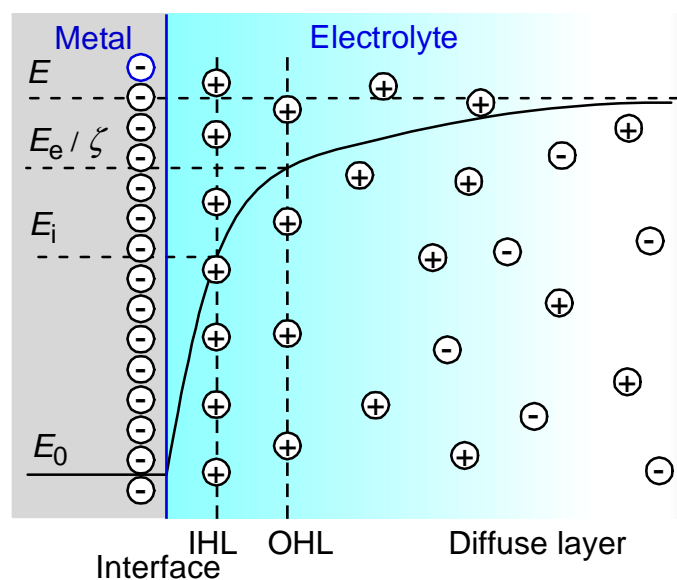
Figure 3.6: Electrochemical double layer.

The electrical neutrality is fulfilled in the solution bulk, but not at the interface. At the electrode side of interface (metal or electronic conductor), the charge is supported by electrons. In contrast at the electrolyte side, the charge is brought by ions, forming thus the space charge. The overall local charge is damped down and tends to zero when the distance from the metallic surface increases. This zone is named "*diffuse layer*" or "*Gouy-Chapman layer*". The ions cannot reach to the metal surface because of its ionic radius with solvents, and then there is a minimum distance between the electrode surface and the ions. This distance constitutes the "*Outer Helmholtz layer,* OHL". When there is specific adsorption, the distance between metal and adsorbed species is shorter than the "Outer Helmholtz layer", and this layer is named "*Inner Helmholtz layer*, IHL". Since there is a compact layer ("inner and outer Helmholtz layer" and the diffuse layer, the electrical charge of the interface is called "*Double layer capacitance*". Indeed, this interface conserves the electrical charge, and behaves as a capacitor. [118]

Capacitive behaviour of an electrode interface may be modified by the potential (charge at the electrode interface), adsorption (modifying the value of IHL),

electro-adsorption and -desorption, and by the presence of the insulating dielectric layer, which consists of an anode or organic layers.

The thickness of the diffuse layer is defined by the Debye length κ^{-1}, in the ideal case:

$$\kappa^{-1} = \sqrt{\frac{\varepsilon \cdot \varepsilon_0 \cdot R \cdot T}{2 \cdot F^2 \cdot K}} \qquad (3.31)$$

where:

κ^{-1} – Debye length in electrolyte (nm);

ε – Relative permittivity (80 in water at 25 °C);

ε_0 – Permittivity of void ($8.84 \cdot 10^{-14}$ F·cm);

K – Ion strength (mol·cm^{-1}).

Equation 3.31 will be rewritten approximately at room temperature to:

$$\kappa^{-1} = \frac{10}{\sqrt{K(\mathrm{mM})}} \qquad (3.32)$$

For the corrosion test solution used in this study, the ionic strength is roughly equal to 6.4 mM. Thus, the Debye distance is approximately 4 nm ($4 \cdot 10^{-7}$ cm). By adding the thickness of OHL, ca. $3 \cdot 10^{-8}$ cm, one can evaluate the double layer capacitance of an ideally flat electrode as:

$$C_{dl} = \frac{\varepsilon \cdot \varepsilon_0 \cdot A}{d} \qquad (3.33)$$

where:

d – Thickness of double layer (OHL+ $^{-1}$, nm).

One gets then, $C_{dl} = 16$ µF·cm^{-2}. This value is somewhat smaller than that often encountered in the literature, but one should be aware that the solution used is dilute and also the surface was considered ideally flat.

Simplest electrochemical cell

The simplest electrical model of an electrochemical cell is presented on Fig. 3.7. It consists of the solution (electrolyte) resistance, R_e, which arises due to the finite conductivity of the electrolyte and characterizes a potential drop between the reference electrode and the working electrode; polarization resistance, defined as the slope of the polarization curves, R_p, (cf. Eq. 3.8) and the capacitance of the double layer, C_{dl}.
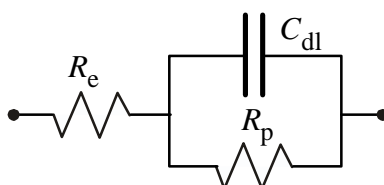
Figure 3.7: Simples equivalent circuit at the electrode interface.

Randles circuit

Randles circuit is an equivalent electrical circuit which represents this faradaic reaction, where the faradaic impedance Z_F is represented by the charge transfer resistance, R_t, in series with Warburg impedance, Z_W, in parallel with the double layer capacitance, C_{dl}, and this circuit is then connected to the electrolyte resistance R_e. Fig. 3.8 depicts the Randles circuit. This is the first representation of electrochemical impedance by an electrical equivalent circuit, and thus sometimes, the circuit in Fig. 3.7 is also called Randles circuit.
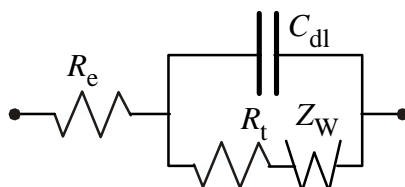
Figure 3.8: Randles circuit.

IV. IMPEDANCE PLOTS

As shown in Eq. (3.22), the impedance is a complex number, and can be represented by two different diagrams, Nyquist plot in complex plane and Bode plot with the modulus and argument as shown in Eqs. (3.24) and (3.25).

Nyquist plot

Fig. 3.9 shows the impedance spectrum for the equivalent circuit presented in Fig. 3.7 in Nyquist plot. It gives the imaginary impedance component (Z'') against the real impedance component (Z') at each excitation frequency f.
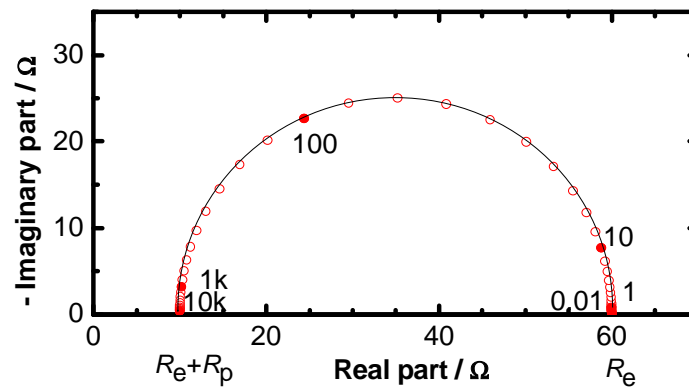
Figure 3.9: Nyquist plot for a simple electrochemical system presented in Fig. 3.7.

$R_e = 10\ \Omega$, $R_p = 50\ \Omega$, $C = 50\ \mu F$; parameters are frequency in Hz.

It can be seen that the high frequency limit of impedance is equal to the solution resistance, R_e. The low frequency limit impedance is the sum of solution and polarization resistance ($R_e + R_p$). As shown in Fig. 3.9, the frequency corresponding to the apex of the semicircle, f_m, can be used to calculate the capacitance, C:

$$C = \frac{1}{2 \cdot \pi \cdot f_m \cdot R_p} \qquad (3.34)$$

Fig 3.10-a shows the impedance spectrum of the Randles circuit (Fig. 3.8) whereas Fig. 3.10-b is relative to the case where the thickness of the diffusion layer is finite, Eq. (3.29).
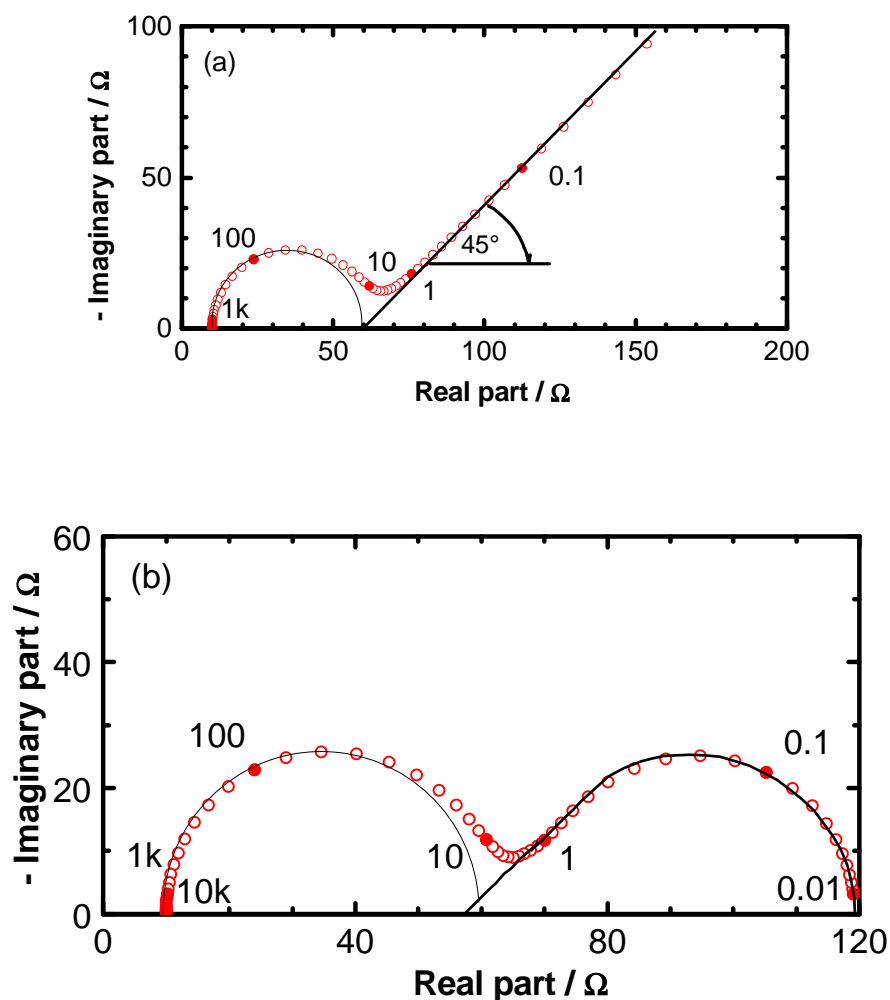
Figure 3.10: Randles circuit with Warburg impedance (a) and

Nernst diffusion layer impedance (b):

$R_e = 10\ \Omega$, $R_t = 50\ \Omega$, $D = 10^{-5}\ cm^2 \cdot s^{-1}$, $T = 297$ K (25 °C), $d = 5 \cdot 10^{-3}\ cm$ (50 μm).

In Fig. 3.10-a, the Warburg impedance with the unit slope can be clearly seen (it is important to note that the scale length of the real and imaginary components are identical, orthonormalized scale). In a simple situation, the Warburg element manifests itself in EIS spectra by a line with an angle of 45 degrees in the low frequency region. Values of the

charge transfer resistance and Warburg coefficient depend on physico-chemical parameters of a system under investigation. The low frequency limit of the impedance is infinite. When the thickness of the diffusion layer is finite, the real part of the low frequency limit is also finite, and the impedance plot bends towards the real axis. It can also be seen that this diffusion impedance behaves as Warburg for the high frequency side.

The Nyquist plot has several advantages. Primary, this plot format makes it easy to see the effect of the solution resistance. The shape of the curve does not change when the solution resistance, R_e, changes, but it shifts along with the real axis. Diffusion impedance can be seen through the unit slope. The depressed feature of the capacitive loop is often observed, and this shape is associated with the CPE element. The main drawbacks of the Nyquist plot are two folds. First, this diagram does not make explicitly *ac* frequency appear. Second; if huge and small impedance networks are in series, the small impedance circuit is difficult to see since the larger impedance controls plot scaling.

Bode plot

The second one to represent EIS data is the Bode plot. Generally, in this mode, two graphs, $\log(|Z|) - \log(f)$ and $\varphi - \log(f)$ are drawn, Fig. 3.11 shows the same impedance data as Fig. 3.9, but in Bode plot.

The modulus $|Z|$ shows a sigmoid curve whereas the phase-shift depicts a bell-shaped curve. At medium frequencies, $\log(|Z|) - \log(f)$ curve is a straight line with slope of -1. Extrapolation of this line to the axis $\log|Z|$ at $= 1$, i.e. $\log(\omega) = 1$ or ($f = 0.16$ Hz), allows the determination of C due to the following expression:

$$\log|Z(\omega = 1)| = \log\left(\frac{1}{C_{dl}}\right) \qquad\qquad (3.32)$$
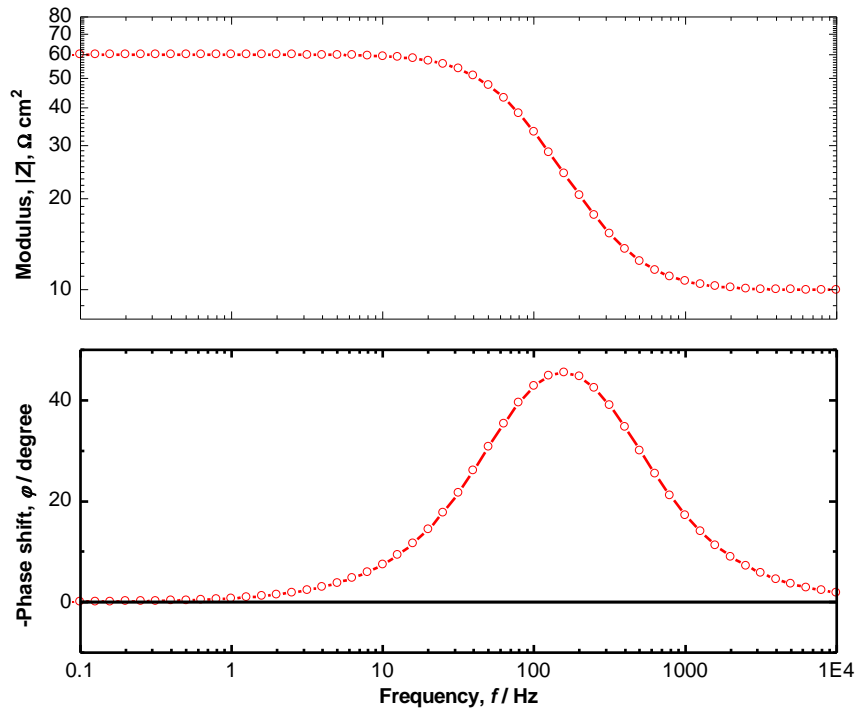
Figure 3.11: Bode plot of the impedance spectrum presented in Fig. 3.9.

The phase angle gives the maximum at:

$$\omega_{(\varphi=\max)} = \sqrt{\frac{1}{C_{dl} \cdot R_{ct}}\left(1+\frac{R_{ct}}{R_e}\right)} \qquad (3.33)$$

It is important to note that this maximum frequency is different from the maximum frequency f_m in the Nyquist plot.

Fig. 3.12 presents the impedance spectra presented in Fig. 3.10.

In the Bode plot, observation of the diffusion behaviour is more difficult, since the phase angle reaches to 45 ° very slowly. In this plot, the diffusion impedance is revealed by the slope of $\log(|Z|) - \log(f)$ equal to -0.5. Nevertheless, one may notice that the diffusion behaviour observed on Fig. 3.10-b can be hardly identified.

While for the simple systems, as the one presented in Figs. 3.9 and 3.11, parameters of the equivalent circuit can be extracted directly from the impedance plots, for more

complicated systems, it is necessary to perform a regression calculation of the measured impedance data with the selected model. In this work this procedure was performed by a Simplex program based on the Nedler - Mead algorithm. [119]
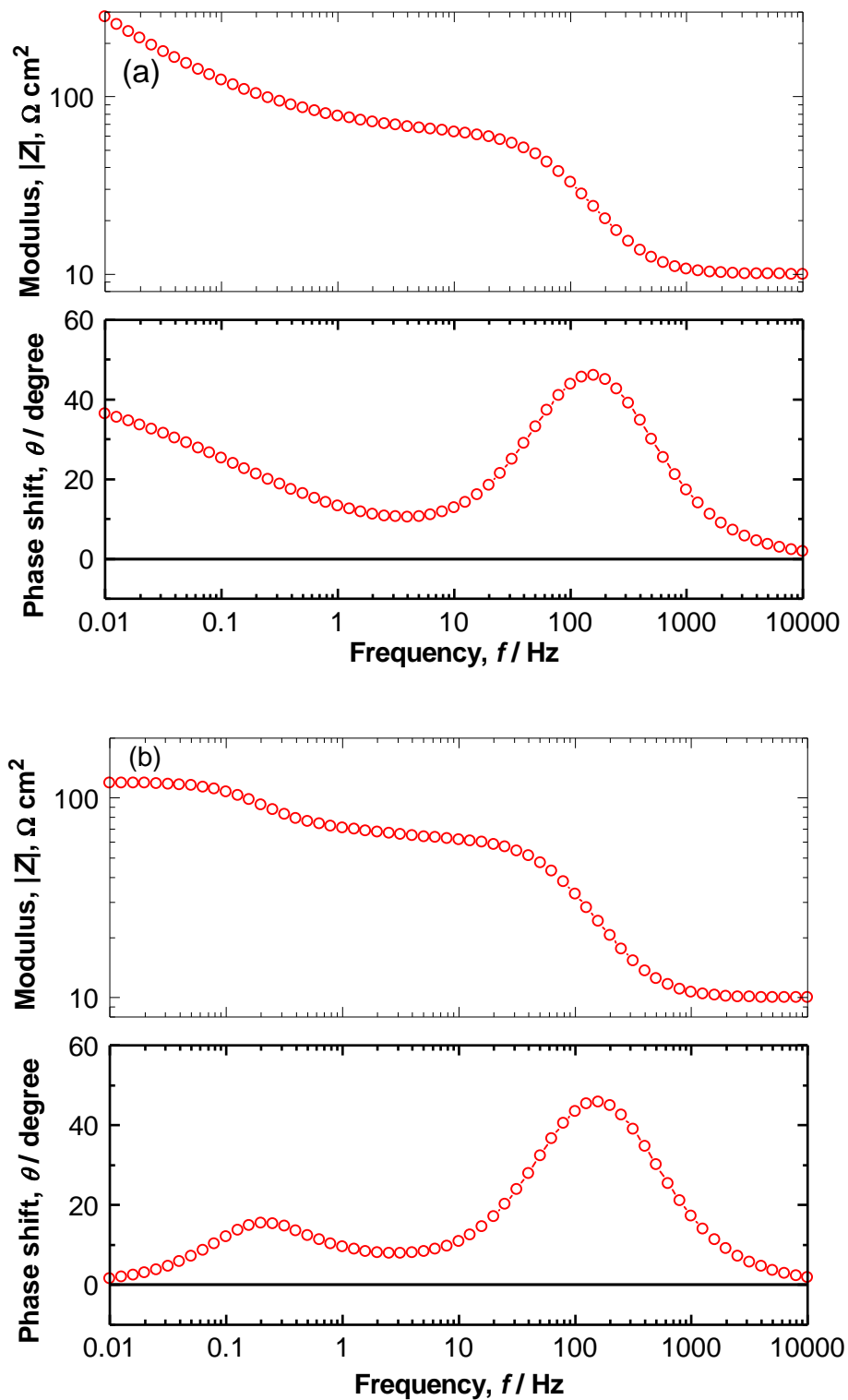
Figure 3.12: Bode plot of the impedance spectra presented in Fig. 3.10.

3.2. MODELLING OF COPPER DISSOLUTION

Let us consider the case where copper dissolves into cupric ions involving intermediate cuprous species. As can be seen in Chapter 5, the dissolution of bronze will, indeed, take place through the cuprite.

$$Cu \Leftrightarrow Cu^I_{(s)} + e^- \qquad (3.37a)$$

$$Cu^I_{(s)} \rightarrow Cu^{2+}_{(sol)} + e^- \qquad (3.37b)$$

The reaction rates of the first step will be represented by K_1 (forward) and K_{-1} (backward) and that of the second step by K_2. It is assumed that these reactions follow the Tafel law with Tafel constant respectively b_1, b_{-1}, and b_2.

Material balance:

$$\Gamma \frac{d\theta}{dt} = K_1 \cdot (1 - \theta) + (K_{-1} - K_2) \cdot \theta \qquad (3.38)$$

where:

- maximum surface concentration ($mol \cdot cm^{-2}$) ;

θ - molar fraction of surface species with respect to Γ.

Charge balance:

$$\frac{1}{F} \cdot I = K_1 \cdot (1 - \theta) + (K_{-1} + K_2) \cdot \theta \qquad (3.39)$$

From these two equations, the polarization curve and the faradaic impedance Z_F will be derived.

Steady-state; dθ/dt = 0

The steady state is defined as invariance of the surface coverage, thus dθ/dt=0, then one gets:

$$K_1 \cdot (1-\theta) + (K_{-1} - K_2) \cdot \theta = 0 \tag{3.40}$$

This equation leads to:

$$K_1 \cdot (1-\theta) = -(K_{-1} - K_2) \cdot \theta \tag{3.41}$$

$$\theta = \frac{K_1}{K_1 - K_{-1} + K_2} \tag{3.42}$$

Introducing Eq. (3.38) into Eq. (3.39), one obtains the steady state current:

$$I = 2 \cdot F \cdot K_2 \cdot \theta = \frac{2 \cdot F \cdot K_1 \cdot K_2}{K_1 - K_{-1} + K_2} \tag{3.43}$$

IMPEDANCE

From the Taylor expansion of Eq. (3.38) limited to the first order, one gets the following equation under sine-wave potential perturbation:

$$\begin{aligned} j \cdot \omega \cdot \Gamma \cdot d\theta = &[b_1 \cdot K_1 \cdot (1-\theta) + (b_{-1} \cdot K_{-1} - b_2 \cdot K_2) \cdot \theta] \cdot dE \\ &- (K_1 - K_{-1} + K_2) \cdot d\theta \end{aligned} \tag{3.44}$$

By substituting $K_1(1-\theta)$ by Eq. (3.41), one yields:

$$\frac{d\theta}{dE} = -\frac{[(b_1 - b_{-1}) \cdot K_{-1} - (b_1 - b_2) \cdot K_2] \cdot \theta}{j \cdot \omega \cdot \Gamma + K_1 - K_{-1} + K_2} \tag{3.45}$$

Similarly, the current response to a small potential perturbation can be expressed as:

$$\frac{1}{F} \cdot dI = [b_1 \cdot K_1 \cdot (1-\theta) + (b_{-1} \cdot K_{-1} + b_2 \cdot K_2) \cdot \theta] \cdot dE - (K_1 - K_{-1} - K_2) \cdot d\theta \tag{3.46}$$

$$\frac{1}{F}\cdot\frac{dI}{dE} = -\left[(b_1 - b_{-1})\cdot K_{-1} - (b_1 + b_2)\cdot K_2\right]\cdot\theta - (K_1 - K_{-1} - K_2)\cdot\frac{d\theta}{dE} \quad (3.47)$$

dI/dE is a reciprocal of the faradaic impedance Z_F, then this impedance can be written as:

$$\frac{dI}{dE} = \frac{1}{Z_F} = \frac{1}{R_t} - \frac{F\cdot(K_1 - K_{-1} - K_2)\cdot\left[(b_1 - b_{-1})\cdot K_{-1} - (b_1 - b_2)\cdot K_2\right]\cdot\theta}{j\cdot\omega\cdot\Gamma + K_1 - K_{-1} + K_2} \quad (3.48)$$

where:

$$R_t = -\frac{1}{F\cdot\left[(b_1 - b_{-1})\cdot K_{-1} - (b_1 + b_2)\cdot K_2\right]\cdot\theta} \quad (3.49)$$

It is worth to note that R_t depends not only on K_2, directly related to *dc* anodic current (cf. Eq. (3.43)) but also on the rate of the redox process through K_{-1}. Eq. (3.49) can be expressed formerly by the following equation:

$$\frac{1}{Z_F} = \frac{1}{R_t} + \frac{1}{j\cdot\omega\cdot L + \rho} \quad (3.50)$$

In this equation, one can identify the equivalent circuit elements inductance, *L*, and resistance, ρ, respectively as:

$$L = -\frac{\Gamma}{F\cdot(K_1 - K_{-1} - K_2)\cdot\left[(b_1 - b_{-1})\cdot K_{-1} - (b_1 - b_2)\cdot K_2\right]\cdot\theta} \quad (3.51)$$

$$\rho = -\frac{K_1 - K_{-1} + K_2}{F\cdot(K_1 - K_{-1} - K_2)\cdot\left[(b_1 - b_{-1})\cdot K_{-1} - (b_1 - b_2)\cdot K_2\right]\cdot\theta} \quad (3.52)$$

The time constant of this circuit   will be evaluated readily from Eq. (3.50) by:

$$\tau = \Gamma\cdot(K_1 - K_{-1} + K_2) \quad (3.53)$$

ANALYSES OF FARADAIC IMPEDANCE

It will be seen how the faradaic impedance will be represented by an equivalent electrical circuit, and also some digital simulation of this equation will be presented.

Equivalent circuit

Eq. (3.50) will be represented in Fig. 3.13-a:
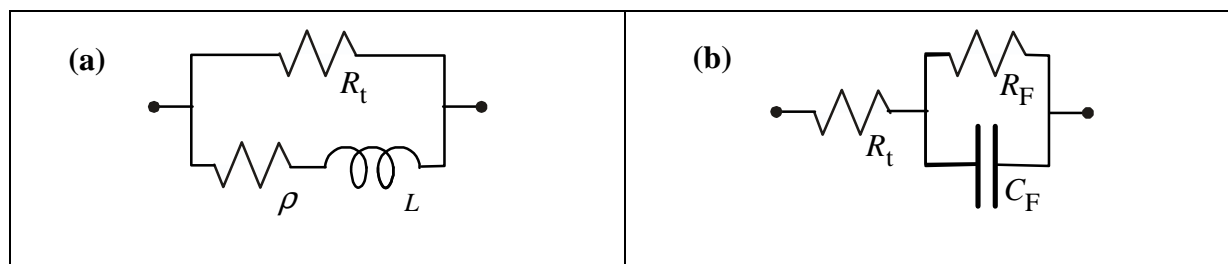
Fig 3.13: Equivalent electrical circuit of the electrochemical reaction involving one relaxation time constant (cf. Eq. (3.50)). (a) Faradaic impedance exhibiting an inductive behaviour (b) that a capacitive behaviour.

It can be seen that both L and ρ are negative since K_{-1} is negative when the redox process is faster than the dissolution one, that is $(K_1 - K_{-1} - K_2) > 0$, and then this dynamic electrical behaviour will be represented by a parallel connection of C_F and R_F as illustrated in Fig. 3.13-b. [120-122]

The electrical circuits (a) and (b) represent the identical dynamic behaviour. Let the low frequency limit of the impedance, the polarization resistance, be expressed as $R_{p,a}$ and $R_{p,b}$, then they will be calculated according to Eqs (3.54) and (3.55) respectively.

$$\frac{1}{R_{p,a}} = \frac{1}{R_t} + \frac{1}{\rho} \tag{3.54}$$

$$R_{p,b} = R_t + R_F \tag{3.55}$$

Since these two equations are identical:

$$R_{p,a} = R_{p,b} = R_p \tag{3.56}$$

Then, one yields:

$$R_F = R_p - R_t = -\frac{R_t^2}{R_t + \rho} \tag{3.57}$$

It can be seen that if K_2 is equal to zero, that is, the reaction presented earlier have no dissolution step:

$$\rho = -R_t \tag{3.58}$$

Thus, R_F is infinite besides in the virtue of Eq. (3.55), $R_{p,a}$ is also infinite. Therefore, the faradaic impedance exhibits *the blocking electrode behaviour*.

To make further calculation easier, A and B should be defined:

$$A = -\left[(b_1 - b_{-1})\cdot K_{-1} - (b_1 + b_2)\cdot K_2\right] \tag{3.59}$$

$$B = (b_1 - b_{-1})\cdot K_{-1} - (b_1 - b_2)\cdot K_2 \tag{3.60}$$

With Eqs. (3.49), (3.52) and (3.54), one can yield:

$$\frac{1}{R_p} = \frac{1}{R_t} + \frac{1}{\rho} = F\cdot\theta\cdot\left[A + \frac{(K_1 - K_{-1} - K_2)\cdot B}{K_1 - K_{-1} + K_2}\right] \tag{3.61}$$

$$\frac{1}{R_p} = F\cdot\theta\cdot\left[\frac{(K_1 - K_{-1})\cdot(A+B) + K_2\cdot(A-B)}{K_1 - K_{-1} + K_2}\right] \tag{3.62}$$

Now, it can be derived that:

$$A + B = 2\cdot b_2\cdot K_2 \text{ and } A - B = -2\cdot\left[(b_1 - b_{-1})\cdot K_{-1} - b_1\cdot K_2\right] \tag{3.63}$$

Therefore:

$$R_p = \frac{1}{2\cdot F\cdot\theta}\cdot\frac{K_1 - K_{-1} + K_2}{K_2\cdot\left[b_2(K_1 - K_{-1}) - (b_1 - b_{-1})\cdot K_{-1} - b_1\cdot K_2\right]} \tag{3.64}$$

When taking into account Eq. (3.43) one gets:

$$I\cdot R_p = \frac{K_1 - K_{-1} + K_2}{b_2\cdot(K_1 - K_{-1}) - (b_1 - b_{-1})\cdot K_{-1} + b_1\cdot K_2} \tag{3.65}$$

If the surface coverage is high, that means $K_2 << (K_1-K_{-1})$, then one yields:

$$I \cdot R_p = \frac{1}{b_2 - (b_1 - b_{-1}) \cdot [K_{-1}/(K_1 - K_{-1})]} \approx \frac{1}{b_2} \tag{3.66}$$

Therefore, when the dissolution of Cu through a large amount of Cu(I) is taking place, Stern – Geary relationship remains valid. It is worth to emphasize that Epelboin et al. showed that in presence of a redox process R_p will be more closely correlated with the corrosion current. In contrast, with combination of irreversible consecutive dissolution steps, R_t shall be used. [123]

The expression of C_F will be derived. For Fig. 3.13-a, at sufficiently high frequencies, Eq. (3.50) will be reduced to:

$$\left. \frac{1}{Z_a} \right|_{\to \infty} = \frac{1}{R_t} + \frac{1}{j \cdot \omega \cdot L} = \frac{R_t + j \cdot \omega \cdot L}{j \cdot \omega \cdot L \cdot R_t} \tag{3.67}$$

Therefore:

$$\left. \frac{1}{Z_a} \right|_{\to \infty} = \frac{j \cdot \omega \cdot L \cdot R_t}{R_t + j \cdot \omega \cdot L} = \frac{j \cdot \omega \cdot L \cdot R_t \cdot (R_t - j \cdot \omega \cdot L)}{R_t^2 + (\omega \cdot L)^2} = \frac{\omega^2 \cdot L^2 \cdot R_t + j \cdot \omega \cdot L \cdot R_t^2}{R_t^2 + (\omega \cdot L)^2} \tag{3.68}$$

Then the imaginary part of Z_a at sufficiently high frequencies becomes:

$$\text{Im}(Z_a(\omega \to \infty)) = \frac{\omega \cdot L \cdot R_t^2}{(\omega \cdot L)^2} = \frac{R_t^2}{\omega \cdot L} \tag{3.69}$$

Similarly, for the circuit 1b, one calculates its impedance Z_b by:

$$Z_b = R_t + \frac{1}{\dfrac{1}{R_F} + j \cdot \omega \cdot C} \tag{3.70}$$

Consequently at high frequencies where $R_F \gg \omega C$, one gets:

$$\left. Z_b \right|_{\to \infty} \approx R_t + \frac{1}{j \cdot \omega \cdot C} = R_t - \frac{j}{\omega \cdot C} \tag{3.71}$$

Then:

$$\text{Im}\left(Z_b\left(\omega \to \infty\right)\right) = -\frac{1}{\omega \cdot C} \tag{3.72}$$

Since Z_a and Z_b represent the same impedance; with Eqs (3.69) and (3.70), one gets:

$$C_F = -\frac{L}{R_t^2} = \left[\frac{\Gamma}{\left(K_1 - K_{-1} - K_2\right) \cdot F \cdot \theta \cdot B}\right] \cdot \left(F \cdot \theta \cdot A\right)^2 = \frac{\Gamma \cdot F \cdot \theta \cdot A^2}{\left(K_1 - K_{-1} - K_2\right) \cdot B} \tag{3.73}$$

Then with Eq. (3.42) the faradaic capacitance C_F will be calculated by:

$$C_F = \cdot -\frac{\Gamma \cdot F \cdot A^2 \cdot K_1}{\left(K_1 - K_{-1} + K_2\right) \cdot \left(K_1 - K_{-1} - K_2\right) \cdot B} \tag{3.74}$$

In case where no dissolution of Cu(I) is taking place as examined above for R_F, $K_2 = 0$, then one can verify readily $A = B$. Introducing $(b_1 - b_{-1}) = F/R \cdot T$, Eq. (3.74) reduces into:

$$C_F = \frac{\Gamma \cdot F^2 \cdot K_1 \cdot K_{-1}}{R \cdot T \cdot \left(K_1 - K_{-1}\right)^2} \tag{3.75}$$

When there is no dissolution of Cu or K_2 is very small compared with $(K_1 - K_{-1})$, C_F is maximal at $K_1 = K_{-1}$ and values:

$$C_F = \frac{\Gamma \cdot F^2}{4 \cdot R \cdot T} \tag{3.76}$$

It is demonstrated therefore that the mathematical expression of the faradaic impedance and the theoretical values of each equivalent circuit element. At room temperature, the maximum faradaic capacitance values therefore 2.52 mF·cm^{-2} for mono-molecular coverage of Cu(I). When there is a reaction intermediate that involves a redox process, the faradaic impedance will be revealed by a capacitive behaviour. This is an important feature for analyzing the experimental data, besides when the surface coverage by the intermediate species is high, the polarization resistance, the low frequency limit of the faradaic impedance

is closely related to the corrosion rate, and not the charge transfer resistance. In contrast, this resistance indicates the rate of exchange current density of the redox process with the substrate copper.

Digital applications

Because of the contribution of non-faradaic components in the experimental impedance spectrum, two elements R_e and C_{dl} were added to the circuit 3.13-b.
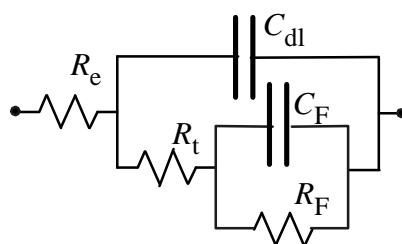
Figure 3.14: Equivalent electrical circuit involving non-faradaic component;

Electrolyte resistance R_e and double layer capacitance C_{dl}.

First, let us consider the particular case where K_2 is equal to zero, that is there is no dissolution of cuprous surface species. This situation corresponds to the Nernst equation with Cu and Cu^I species, and is known, as mentioned earlier, as *the blocking electrode behaviour.* The faradaic resistance is in a series connection with the parallel connection of charge transfer resistance, R_t, and faradaic capacitance, C_F. Fig. 3.15 displays the results of the digital simulations.
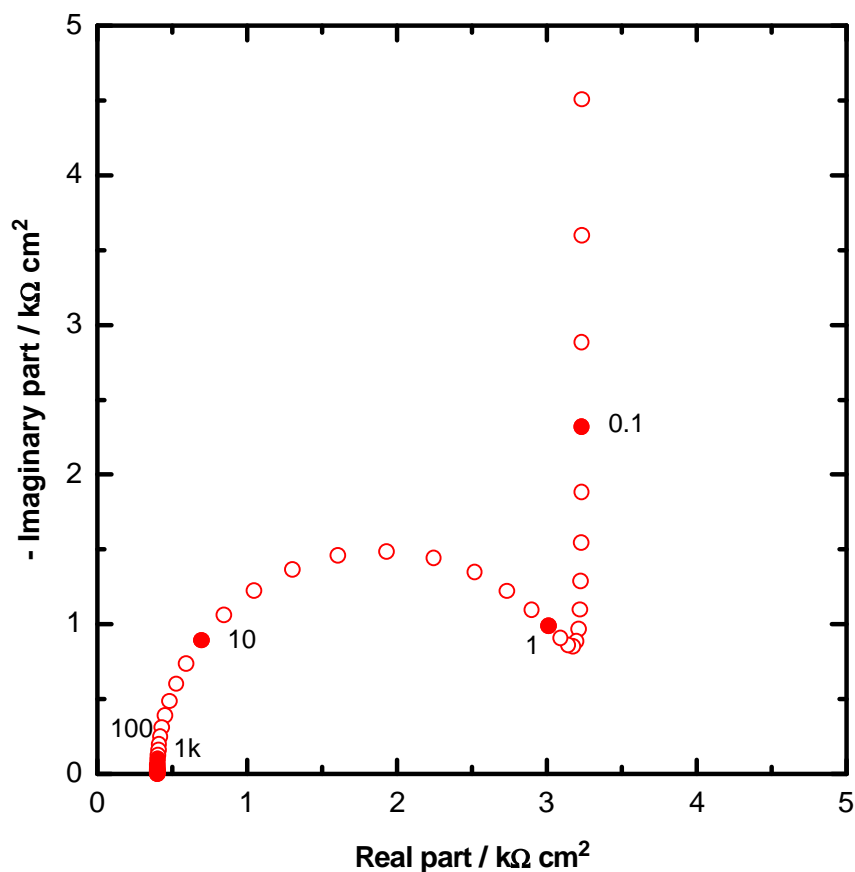
Figure 3.15: Impedance calculated for a redox process.

$R_e = 400 \; \Omega \cdot cm^2$, $C_{dl} = 16 \; \mu F \cdot cm^{-2}$, $K_1 = 1 \cdot 10^{-9} \; mol \; s^{-1}$, $K_{-1} = -0.1 \cdot K_1$, $K_2 = 0$

$\Gamma = 2.27 \cdot 10^{-9} \; mol \cdot cm^{-2}$, $T = 300 \; K$, $b_1 - b_{-1} = 2 \cdot F/R \cdot T$.

The capacitance, C_F, calculated according to the kinetic variables given in the figure caption, is ca. 0.66 mF·cm^{-2} for the monomolecular Cu^I_s without the dissolution step ($K_2 = 0$). The examined potential corresponds to the potential about 60 mV more positive to the equilibrium potential of Cu(0)/Cu(I). When there is the chemical dissolution of $Cu^I_{(s)}$ so that the corrosion process of Cu electrode takes place, the impedance diagram presented in Fig. 3.16 will be obtained.
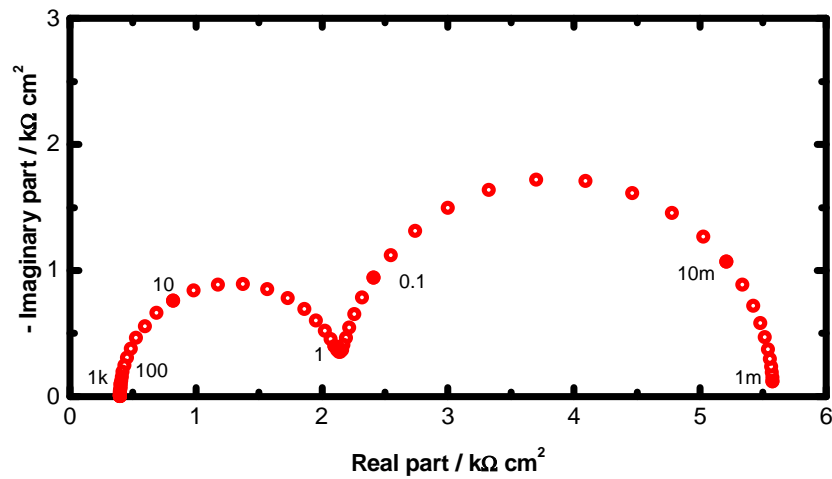
Figure 3.16: Impedance calculated for dissolution of Cu involving adsorbed cupric species.

$R_e = 400\ \Omega \cdot cm^2$, $C_{dl} = 16\ \mu F \cdot cm^{-2}$, $K_1 = 1 \cdot 10^{-9}\ mol \cdot s^{-1}$, $\alpha_1 = 0.5$, $K_{-1} = -0.1 \cdot K_1$, $K_2 = 0.1 \cdot K_1$,

$b_2 = 12 V^{-1}$, $\Gamma = 2.27 \cdot 10^{-9}\ mol \cdot cm^{-2}$, $T = 300\ K$, $b_1 - b_{-1} = 2F/R \cdot T$.

This figure corresponds well to the equivalent electrical circuit presented in Fig. 3.13-b. The faradaic capacitance in this case is higher, because of the current flow through the electrode (virtual charge at Cu(0) is increased) and values 1.61 mF·cm^{-2}. Fig. 3.17 shows some calculated polarization data with the dissolution step.

It can be noticed the change of *j-E* curve in the Tafel plot when θ is close to 0.5, because *q* increases much slower (in semi-logarithmic scale, and some saturation effect of θ is taking place. In Fig. 3.17-b, it can be seen that the faradaic capacitance, C_F, is maximum at this inflexion point, and decreases slowly beyond this potential. C_F is maximal at -0.05 V and values 2.27 mF·cm^{-2}. Fig. 3.17-c shows that above 0 V, θ increases slowly with the parameters' value used here.

Figure 3.17: Current density j (a), Faradaic capacitance C_F (b), and Conversion rate θ (c): Parameter values are the same to Fig. 3.16.
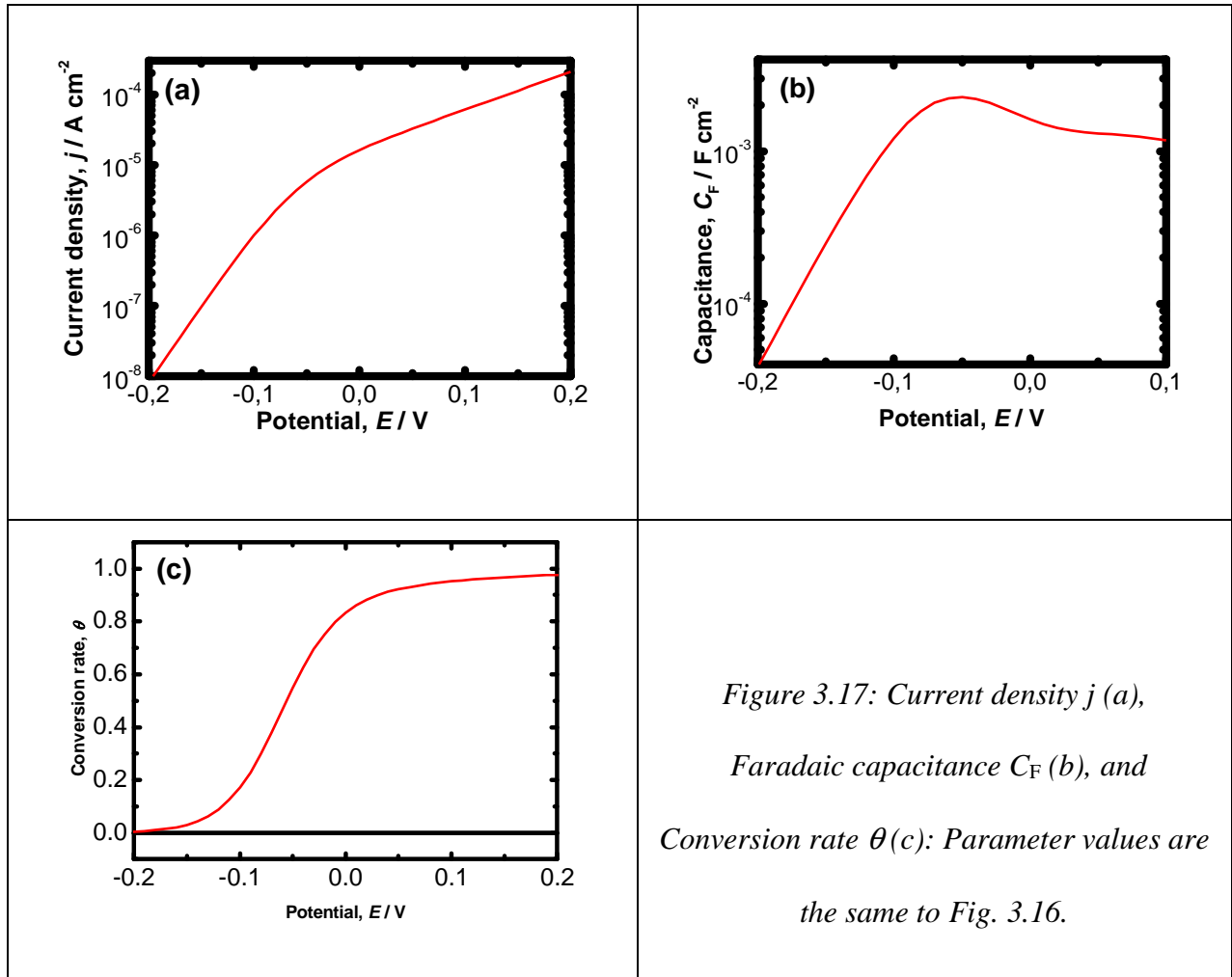
The corrosion process is taking place together with the cathodic process, in parallel with the anodic dissolution reaction. For instance, resistance R_c, representing the polarization resistance of the cathodic process, will be added in parallel to the equivalent circuit representing the anodic process. However, in this case, the number of time constants of the system remains the same, and it is impossible to extract separately all elements constituting the electrode behaviour. This is the reason that we will use also the circuit shown in Fig. 3.14 for the corroding system. The polarization resistance in this case is more closely related to the corrosion current density, j_{corr}, as stated above.

3.3. ADSORPTION ISOTHERMS

The protective effectiveness of 2-D film forming inhibitors is closely related to its adsorption. The adsorption isotherm links the relationship between the bulk concentration and the surface concentration of the adsorbent (adsorbed species).

The adsorption isotherm is determined by the equality of the electrochemical potential for the bulk and adsorbed species. With the standard electrochemical potential $\mu^{0,B}$ and $\mu^{0,A}$, one gets the following relationship: [124, 125]

$$\mu^{0,A} + R \cdot T \cdot \ln(a^A) = \mu^{0,B} + R \cdot T \cdot \ln(a^B) \qquad (3.77)$$

where:

μ - Electrochemical potential (J·mol^{-1});

a – Activity;

Superscript A and B – Adsorbed and Bulk species.

The standard free energy of the adsorption, ΔG_i^0, is therefore expressed as:

$$G_i^0 = \mu^{0,A} - \mu^{0,B} \qquad (3.78)$$

Thus:

$$a^A = a^B \cdot \exp\left(\frac{-G_i^0}{R \cdot T}\right) = \gamma \cdot a^B \qquad (3.79)$$

where:

$$\gamma = \exp\left(\frac{-G_i^0}{R \cdot T}\right) \qquad (3.80)$$

There are basically two well established types of adsorption isotherms: the Langmuir adsorption isotherm and the Freundlich adsorption isotherm.

3.3.1. LANGMUIR ISOTHERM

The Langmuir adsorption isotherm describes quantitatively the structure of a layer of molecules on an adsorbent surface as a function of the concentration of the adsorbed material in the liquid in which it is in contact. In a modified form it can also describe a bi-layer deposition. The Langmuir isotherm involves assumptions of:

- No interactions between the absorbed species on the electrode surface,

- No heterogeneity of the surface,

- High bulk activities.

The fractional surface coverage, θ, occupied by adsorbent is expressed as: [126]

$$\frac{\theta}{1-\theta} = K \cdot a \tag{3.81}$$

where for a dilute solution, the activity, a, can be replaced by the concentration, c. θ increases gradually with respect to the adsorbent concentration, c, and K stands for the adsorption equilibrium constant related to its free energy G_{ads}: [127, 128]

$$K = \frac{1}{c_{solvent}} \cdot \exp\left[-\frac{G_{ads}}{R \cdot T}\right] \tag{3.82}$$

where:

$c_{solvent}$ – molar concentration of the solvent, which in the case of water is 55.5 mol·dm^{-3};

R – the gas constant (8.315 J·mol^{-1}·K^{-1});

T – the thermodynamic temperature (298 K).

The Langmuir isotherm assumes that all adsorption sites are equivalent and that the binding of adsorbate upon adsorbent occurs independently of the nearby sites being occupied or not i.e. no lateral interaction exercise between them. [129]

3.3.2. FREUNDLICH ISOTHERM

The Freundlich isotherm is expressed as: [76]

$$\theta = \mathrm{K} \cdot a^{n} \qquad\qquad (3.83)$$

Therefore, this isotherm follows exponential law in form. It often represents an initial surface adsorption followed by a condensation effect resulting from extremely strong solute-solute interaction.

As In case of the Langmuir isotherm, the activity, a, for a dilute solution can be replaced by the concentration, c.

Langmuir-type adsorption is more common than the Freundlich one. When there is an interaction between adsorbed species, often Temkin or Frumkin adsorption isotherms are used.

3.4. EXPERIMENTAL CONDITIONS

In this section, we will describe experimental conditions used in this work.

3.4.1. ELECTRODES

Investigations were performed on the Cu-6Sn (wt %) bronze plate of 0.5mm in thickness. The composition of this alloy, determined according to DIN 17660 is given in Table 3.3.

Table 3.3: Elemental composition of the Cu-6Sn bronze.

	Sn	Pb	Zn	Fe	P	Cu
wt-%	6.10	0.01	0.10	0.02	0.11	93.66
at-%	3.36	0.003	0.10	0.02	0.23	96.28

Percentage normalized with analyzed elements

Two types of electrodes were prepared; one for electrochemical measurements embedded into epoxy resin, and another for bronze covered by chemically processed patina.

a. Specimens for Electrochemical measurements

The electrodes were prepared from a bronze sheet of Cu-6Sn (wt%) diphase alloy, 0.5 mm in thickness, by cutting it into a rectangular plate of 10mm×10 mm. On the back side of this plate, a copper wire was soldered, and then they were covered with cataphoretic paint (PGG W975 + G323) to avoid the electrolyte infiltration. The bronze plate thus prepared was then embedded into epoxy resin (Buehler; Epoxycure). After that, the electrodes were worked in a cylinder of 14 mm diameter and of about 15 mm height, the bronze surface is set approximately at the centre of the cylinder. On these samples, electrochemical patina was synthesized.

b. Specimens for Chemical patination

For these series of experiments, the same bronze sheet was cut-out in ribbons of 10 mm in width and 50 mm in length.

3.4.2 PATINA FORMATION

The present studies were performed, in addition to bare electrodes without patina (Chapter 4), on three types of artificial patinas (Chapter 5): a chemical patina (named "*sulphate patina*" for the sake of simplicity); patina prepared by a combination of a chemical procedure and acceleration of the formation by heating of the specimen (named *"chloride patina"*), and lastly electrochemical patina (called just *"electrochemical patina"*).

a. Synthesis of Sulphate patina in CuSO₄ aqueous solution

The bronze sheets were first cleaned according to ASTM G1-03 (2003). [130] Then, on clean surface, sulphate patina was formed as follows:

The bronze sheet was partially (approximately one half) immersed in 15 mM $CuSO_4$ solution during 336 hours (two weeks) at room temperature. The solution was neither stirred nor aerated by bubbling but at the thermodynamic equilibrium with the surrounding atmosphere. After the patina formation, the patinated bronze specimens were washed with distilled water and dried at room temperature. Fig. 3.18 shows a bronze specimen partially covered with the sulphate patina thus obtained.
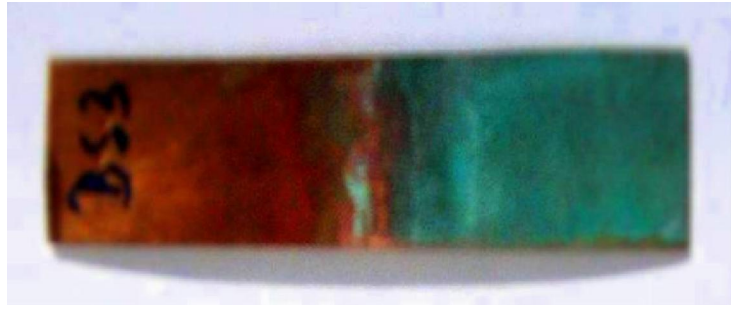
Figure 3.18: Bronze sample with sulphate patina synthesized

in 15 mM CuSO$_4$ for two weeks.

The sulphate patina thus obtained is, as can be seen in Fig. 3.18, dark green and adheres well to the bronze surface. In this solution, the formation of sulphate containing copper salts such as bronchantite, antlerite or posnjakite are expected.

b. Synthesis of Chloride patina in NH$_4$Cl

The bronze plate was prepared following a 5 step procedure:

- The bronze ribbon was degreased in petroleum,

- Washed in the detergent solution,

- Pickled in 5% H$_2$SO$_4$ for several seconds,

- Neutralized by dipping the specimen in 7% NaOH,

- Washed with running water abundantly and rinsed with distilled water.

After that, artificial patina on the bronze plate was synthesized as follows:

The bronze plate was heated in hot air to 200-300 °C. The 33 wt-% NH$_4$Cl aqueous solution was applied 4 times with a brush on the hot plate of bronze. Between applications the sample was left to dry in air for approximately 20 minutes. Once the chloride patina was formed, the patinated specimen was rinsed with distilled water. Fig. 3.19 illustrates a bronze sample withthe chloride patina.

Figure 3.19: Bronze sample with the chloride patina formed

by chemical – thermal procedure.

The obtained patina covers the bronze almost uniformly and its colour is green in agreement with the formation of atacamite or paratacamite expected in presence of chloride.

c. Synthesis of Electrochemical patina in Na_2SO_4 / $NaHCO_3$ Solution

For the preparation of the electrochemical patina, bronze electrodes were first polished with SiC paper up to 2000 grade, and then degreased with ethanol. Six electrodes were set simultaneously in an electrode holder made of poly-methylmethacrylate, and electrical leads were linked in parallel. Electrodes were transferred into an electrochemical cell under potential regulation. Fig. 3.20 presents shematically the experimental setup used.

The electrodes were dipped in synthetic urban rain composed of an aerated solution of 0.2 g·L^{-1} Na_2SO_4 + 0.2 g·L^{-1} $NaHCO_3$ at 30 °C. The pH value of the solution was not adjusted, but $NaHCO_3$ set it at about 8.5. As a counter electrode, a nickel wire surrounding cylindrical cell wall was used, and as reference electrode a saturated calomel electrode (SCE). After a stable open circuit potential (OCP) was reached – which was usually about -0.05 V versus SCE after about 30 minutes of immersion, patina was synthesized under potential control:

- At –0.20 V vs. OCP during 60 seconds,
- At +0.14 V vs. OCP during the next 48 h,
- At +0.12 V vs. OCP during another 48 h.
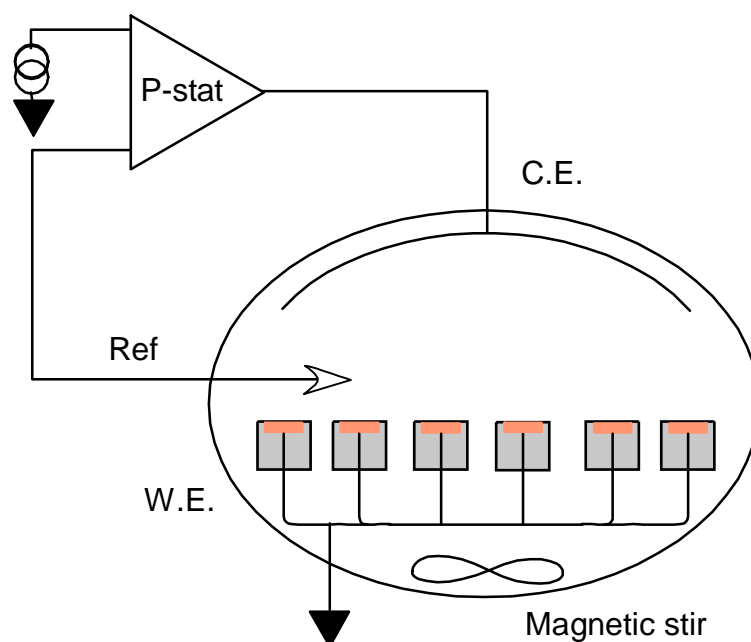
Figure 3.20: Experimental setup for simultaneous patination of six bronze electrodes.

P-stat, Ref, C.E. and W.E.are respectively:

potentiostat, calomel reference electrode, counter and working electrode.

Fig. 3.21 presents a picture of the parallel connection with the patina formed on the electrodes.
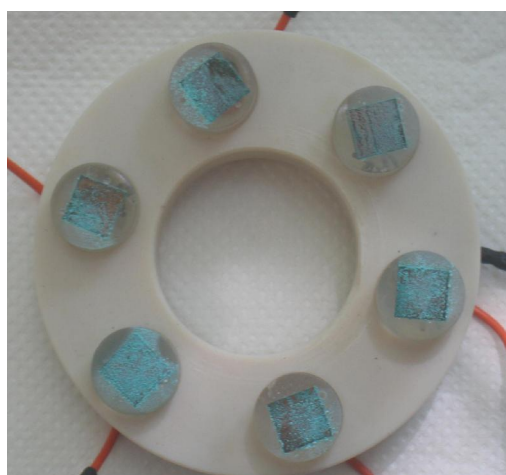
Figure 3.21: Parallel connection of six electrodes

for the electrochemical patination.

The electrode is covered with a mixture of blue and green patina upon reddish or dark red substrate. The formation of carbonate and sulphate patina together with cuprite or tenorite is very possible.

3.4.3. INHIBITORS

In this work the inhibiting efficiency of three imidazole derivatives as corrosion inhibitors of bare bronze or patinated bronze was studied. Their molecular structures are presented in Figure 3.22.

On bare bronze, optimal concentrations of these inhibitors were investigated and on bronze covered with patina, the optimal inhibitor concentrations determined in previous results on copper were used. [76, 95]

4-methyl-1-phenylimidazole	*4-methy1-1-p-tolylimidazole*	*1H-Benzimidazole*
(PMI)	*(TMI)*	*(BZI)*
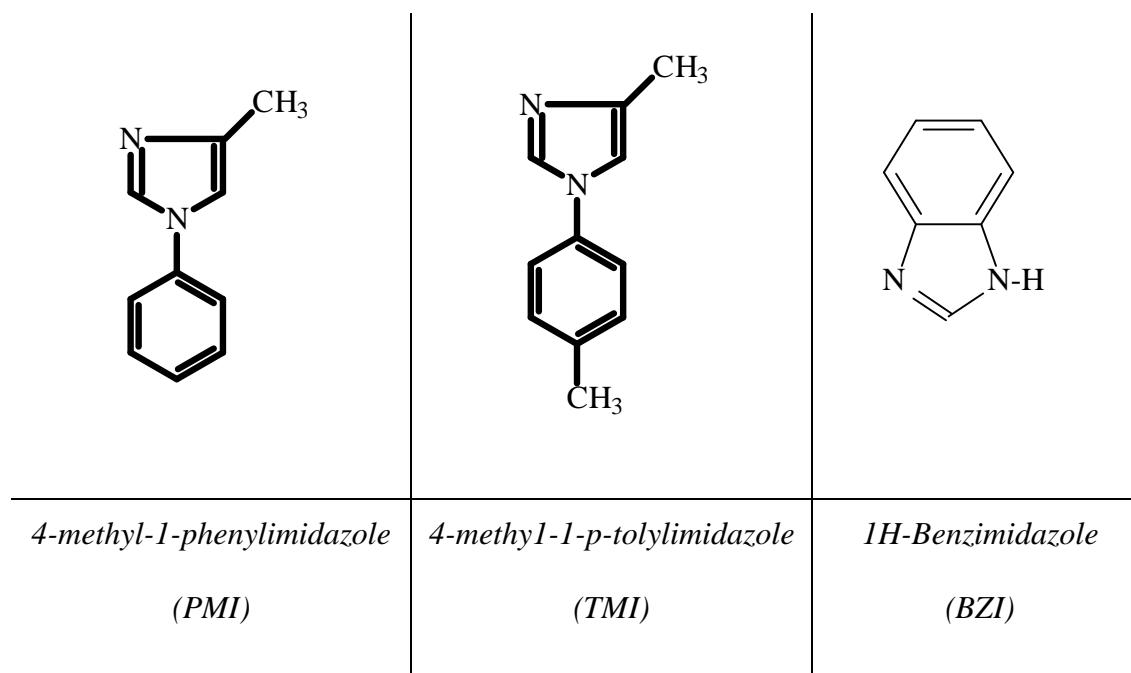
Figure 3.22: Molecular structure of investigated imidazoles: PMI, TMI and BZI.

3.4.4 CORROSION TEST SOLUTION

Electrochemical measurements were conducted in a test solution containing 0.2 $g \cdot dm^{-3}$ Na_2SO_4 + 0.2 $g \cdot dm^{-3}$ $NaHCO_3$ acidified to pH 3 or 5 by addition of dilute sulphuric acid at room temperature. These solutions constitute markedly simplified artificial very acid and acid rain in urban atmosphere. The presence of sulphate represents the pollution by sulphur dioxide frequently induced by petroleum in nowadays, and coal in ancient time. The presence of carbonate ions is due to the natural composition of air, i.e. 0.033 %. For the inhibitor investigations each inhibitor was dissolved in the Na_2SO_4 / $NaHCO_3$ solution.

3.4.5. ELECTROCHEMICAL MEASUREMENTS

Polarization measurements were conducted in a conventional three-electrode cell (~ 100 cm^3 volume). A saturated calomel electrode (SCE) was used as the reference and a Pt plate as the counter electrode. All potentials are reported vs. SCE.

Electrochemical measurements were conducted after 1 hour immersion (if not differently specified) in the test solution with or without the inhibitor to avoid too important change of the open circuit potential during the collection of polarization or impedance data.

The data used for the Tafel extrapolation or the polarization resistance measurements were collected using the EG&G potentiostat / galvanostat Model 263A. For impedance measurements, frequency response detector 1025 was coupled to the above device. Experiments were monitored with PowerSine software.

4. RESULTS AND DISCUSSION ON BARE BRONZE

In this chapter, the efficiency of corrosion protection of some imidazole molecules on bare Cu-6Sn (masse percentage) bronze will be examined. Different electrochemical methods were applied to evaluate the inhibitive efficiency in a solution simulating strongly (pH 3) or mildly (pH 5) acid rain in urban environment; 0.2 g·dm^{-3} Na$_2$SO$_4$ + 0.2 g·dm^{-3} NaHCO$_3$ acidified by addition of dilute H$_2$SO$_4$.

Tafel extrapolation method: the plotting of polarization (current – potential) curves on a wide potential range that allows determination of the corrosion potential at zero overall current, E_{corr}, the anodic and cathodic Tafel slope, b_a and b_c, the corrosion current density, j_{corr}, and the inhibiting efficiency, z (cf. §3.1.4-a).

Polarization resistance method: since the Tafel extrapolation method imposes polarization of a great magnitude, it may modify the surface state before reaching the corrosion potential. Then, the corrosion potential (potential of zero overall current), and the corrosion current density may be based on this very high polarization. This is the reason why only a narrow potential domain around the open circuit potential was applied. E_{corr} and j_{corr} were evaluated from polarisation resistance, R_p (dE/dj), b_a and b_c values determined earlier (cf. §3.1.4-b).

Adsorption isotherm: from the inhibitive efficiency, z, the adsorption isotherm was tentatively determined to know how these imidazoles are adsorbed on the bronze electrode surface on the basis of the free adsorption energy ΔG_{ads} (cf. §3.1.6).

Electrochemical impedance spectroscopy: finally, the inhibitive efficiency evaluated by the potential scan methods (Tafel extrapolation and polarization resistance) was validated by electrochemical impedance spectroscopy. In this method, the perturbing signal is

- -

considered to be sufficiently small so that the bronze electrode remains at its open circuit conditions (cf. §3.1.5).

Three imidazole derivatives used as corrosion inhibitors for Cu-6Sn bronze were: 4-methyl-1-phenylimidazole (PMI), 4-methyl-1-*p*-tolylimidazole (TMI) and 1-H benzimidazole (BZI).

- -

4.1 PROTECTIVE EFFECT OF PMI IN pH 3 SOLUTION

The effect of PMI addition in the solution simulating strongly acid rain, evaluated by various experimental methods, will be presented in this section.

4.1.1 TAFEL EXTRAPOLATION METHOD
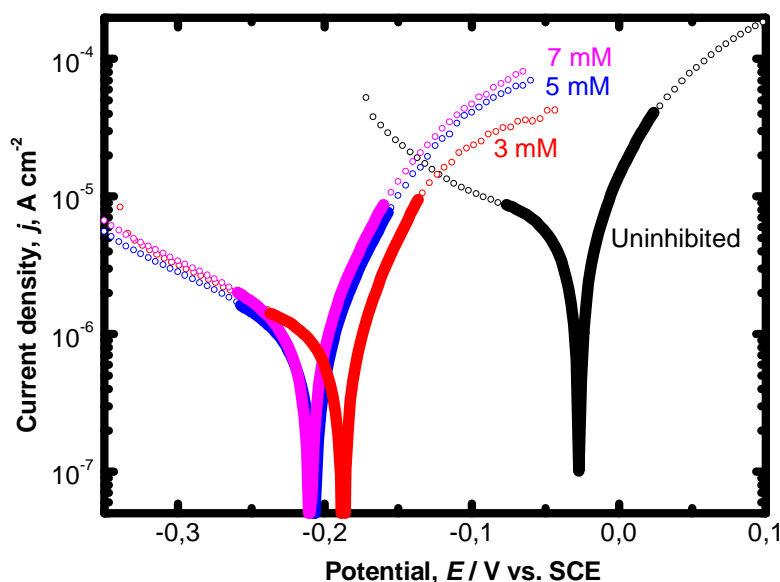
Figure 4.1: Wide range polarization curves of bare bronze

in Na₂SO₄ / NaHCO₃ at pH 3 with different PMI concentrations.

Results obtained by anodic and cathodic polarizations of bronze in wide potential range (Fig. 4.1) show that with addition of inhibitor the cathodic branches shift markedly towards smaller current densities, whereas the anodic branches exhibit higher current densities for a given potential. As a whole, the corrosion potential shifts towards more negative values. PMI is therefore a cathodic inhibitor. These curves do not exhibit sufficiently wide linear domain, namely for the anodic side, to determine unambiguously the Tafel lines. Therefore, the results obtained were fitted with non-linear square method to determine the corrosion parameters. For this sake we used the Origin software that allows defining a user

- -

function and carrying out a simplex regression method with this function for the first step to find the approached parameters' value and then the non-linear least square method. For these calculations, we used the potential domain of ±50 mV with respect to the corrosion potential, E_{corr}. The user defined function corresponds to the Wagner-Traud Eq. (3.2), but written in a slightly different form to match Origin's syntax:

$$Y = \text{abs}\left(j_c * \left(\exp\left(B_a * \left(E_{corr} - X\right)\right) - \exp\left(B_c * \left(E_{corr} - X\right)\right)\right)\right) \tag{4.1}$$

where:

Y – Dependent variable (Current density, $A \cdot cm^{-2}$);

X - Independent variable (Potential, V vs. SCE);

j_c – Corrosion current density ($A \cdot cm^{-2}$);

E_{corr} – Corrosion potential (V vs. SCE);

B_a, B_c – Anodic and cathodic Tafel constant (V^{-1}).

The results of the fitting calculations are summarized in Table 4.1. In this table, the Tafel slope, b, was calculated from the Tafel constant, B, with Eqs. (3.6) and (3.7). To illustrate the fitted curve, only one point over ten in experimental data is displayed. In other terms, 100 experimental points were used, 0.5 mV per step, to fit the polarization curve. A good agreement between experimental and fitted polarization curves can be noticed. Too large potential domain to perform fitting calculations induces often systematic devergency with the experimental curve since the system is no longer entirely determined by the Tafel law for each branch.

- -

Table 4.1: Corrosion parameters of bare bronze in Na_2SO_4 / $NaHCO_3$ at pH 3 with different

PMI concentrations, determined by the Tafel extrapolation method.

c, mmol·dm^{-3}	/	1	2	3	5	7	10
E_{corr}, mV	-27.8	-44.1	-140	-188	-207	-210	-224
b_a, mV·dec^{-1}	65.6	36.4	68.2	55.6	58.2	57.9	64.8
$-b_c$, mV·dec^{-1}	365	216	150	514	260	219	294
j_{corr}, µA·cm^{-2}	7.79	1.71	1.52	1.26	1.14	1.31	4.10
z, %	/	78.0	80.5	83.8	85.4	83.2	47.4

The value b_a remains ca. 60 mV·dec^{-1}. This value is often observed for anodic dissolution of solid metals. As for b_c, it is relatively high in absence of PMI, suggesting that the cathodic reaction is partially governed by the reduction of dissolved oxygen under convective diffusion control. It was worth to recall that the limiting current density of reduction of dissolved oxygen for stationary electrode, as it was the case here, can be estimated according to the Fick's first law between 10 to 20 µA·cm^{-2}. The corrosion current density decreases in presence of the corrosion inhibitor. The smallest value is observed at the concentration 5 mmol·dm^{-3}. At this concentration, the inhibiting efficiency is 85 %.

4.1.2 LINEAR POLARIZATION

Fig. 4.2 depicts results obtained by the polarization of the bronze electrode in a narrow potential range. The figure shows that in presence of inhibitor, the polarization resistance, R_p, increases. The potential domain of ±20 mV with respect to the corrosion potential, E_{corr}, is too wide to ensure the linear response of the system: therefore, data concerning ±5 mV with respect to E_{corr} were used for the linear fitting calculation by means of a built-in function in Origin software. The results of the non-linear least square regression

- -

calculation are superimposed to the experimental data, and fairly good agreement can be seen between experimental and calculated data.
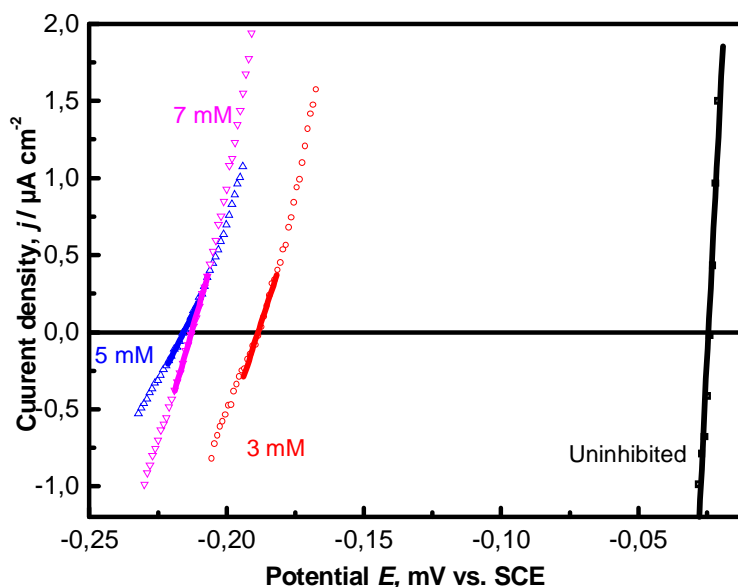
Figure 4.2: Linear polarization curves of bronze in Na₂SO₄ / NaHCO₃

at pH 3 with different PMI concentrations.

Fig. 4.2 shows that in presence of inhibitor, the corrosion potential shifts towards more negative values and also the slope of the polarization curve decreases. Therefore, in agreement with the Tafel extrapolation method, PMI is a cathodic corrosion inhibitor.

The potential domain used was narrow, ±20 mV with respect to the corrosion potential, however, the polarization curves are not completely linear. Thus, the polarization resistance was determined from the experimental data collected in ±5 mV around the corrosion potential. The calculated data are superimposed also on this figure. Similarly to the case of the Tafel plot, only one tenth of experimental points were displayed. Since the experiments collected I and E data at the potential step of 0.1 mV, there were 100 experimental data values to evaluate R_p and E_{corr}.

Table 4.2: Corrosion parameters of bare bronze in Na_2SO_4 / $NaHCO_3$ at pH 3 with different

PMI concentrations, determined by the polarization resistance method.

C, mmol·dm^{-3}	/	1	2	3	5	7	10
E_{corr}, mV	-25.0	-42.3	-152	-188	-215	-212	-228
B, mV	24.1	13.7	20.2	21.8	20.6	19.9	22.6
R_p, k ·cm^2	2.58	5.72	18.4	18.1	26.2	14.8	7.81
j_{corr}, µA·cm^{-2}	9.34	2.41	1.24	1.21	0.79	1.34	2.89
z, %	/	74.2	86.7	87.0	91.5	85.6	69.1

The corrosion potential, E_{corr}, is very close to that determined as zero overall current with a large potential scan, that is, large polarization did not disturb significantly the corroding system. The constant linking the polarization resistance and the corrosion current density, Stern – Geary coefficient, B, (Eq. (3.14)) is slightly higher in absence of inhibitor, 24 mV, because the cathodic process is controlled partially by the diffusion process. This coefficient becomes about 20 mV in presence of inhibitor, values often reported in the literature for the metallic corrosion at active state. R_p increases with increasing PMI concentration up to 5 mmol·dm^{-3} and then, it decreases. At this concentration the inhibitor efficiency is 92 %.

The Tafel extrapolation method and the linear polarization method both indicate that the optimal inhibiting efficiency of PMI is at the concentration 5 mmol·dm^{-3} and the inhibiting efficiency is slightly greater than 90 %.

- -

4.1.3 ADSORPTION ISOTHERM

From the data obtained by the Tafel extrapolation method, the fractional surface coverage, θ, was calculated for each inhibitor concentration, c, as follows:

$$\theta = \frac{j_{corr,0} - j_{corr}}{j_{corr,0}} \qquad [4.2]$$

Where $j_{corr,0}$ and j_{corr} stand respectively for the corrosion current density in absence and in presence of inhibitor. This equation considers implicitly that the corrosion rate at the surface area covered by the inhibitor is zero, thus it cannot be applied if there is an acceleration of the corrosion rate in presence of the organic inhibitor. Consequently, one may emit certain criticism to Eq. (4.2), but when the surface coverage is low, or the concentration of organic species in the solution is low, this equation allows at least qualitatively the nature of bonding between the alloy surface and the organic compound. Then, c/θ or c change was fitted with various isotherms. The best fit was obtained with the Langmuir-type isotherm as is shown in Fig. 4.3.
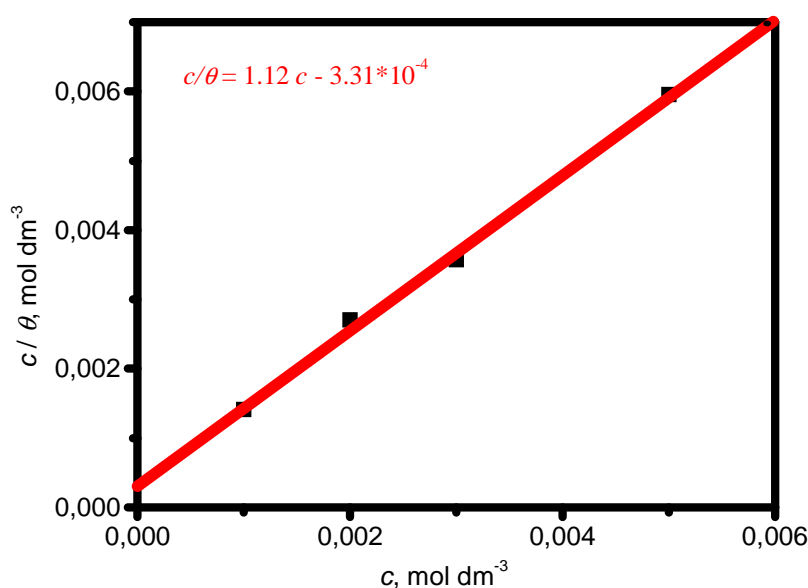
Figure 4.3: Langmuir adsorption isotherm for PMI upon bare bronze in Na$_2$SO$_4$ / NaHCO$_3$ at pH 3.

Adsorption energy was determined from the Langmuir isotherm according to Eqs. (3.81) and (3.82):

$$G_{ads} = -29.8 \text{ kJ·mol}^{-1}$$

The adsorption free energy, G_{ads}, is negative which reveals the spontaneity of the adsorption process and the stability of the adsorbed layer on the bronze surface. The G_{ads} value of -40 kJ·mol^{-1} is usually accepted as a threshold value between chemisorption and physisorption. Smaller energies in absolute value are consistent with the electrostatic interaction between the charged molecules and the charged metal (Van der Waals force), physisorption, and the greater energies in absolute value involve charge sharing or transfer from organic molecules to the metal surface to form a coordinate type of bond, chemisorption. [131] Consequently, the interaction between the inhibitor and the bronze surface is spontaneous physisoption by attractive force.

4.1.4 ELECTROCHEMICAL IMPEDANCE SPECTROSCOPY (EIS)

EIS measurements were carried out after a one hour stabilization period at the open circuit potential. Fig. 4.4 shows the results obtained by electrochemical impedance spectroscopy.

- -
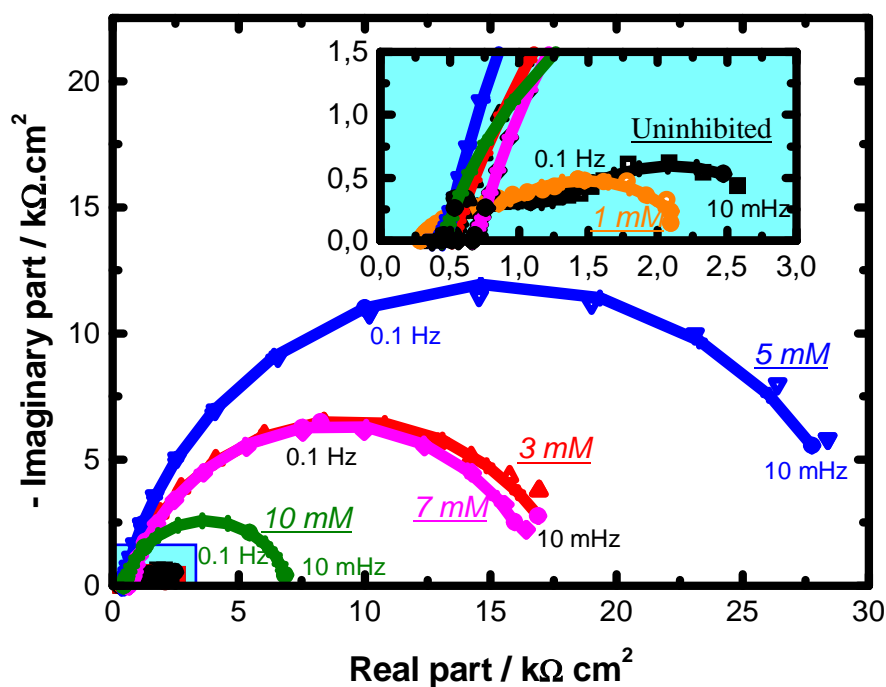
Figure 4.4: Impedance diagrams of bare bronze in Na₂SO₄ / NaHCO₃

at pH 3 in presence of PMI in different concentrations:

Symbols present experimental, while (— + —) presents the calculated data.

The insert is an enlarged scale for high frequency domain.

Experimental EIS exhibits, though often badly separated, two time constants under the capacitive loop, as well in absence as in presence of the inhibitor, at different concentrations (from 1 to 10 mmol·dm⁻³). The electrochemical process involves therefore only one reaction intermediate in addition to the contribution of the double layer capacitance. This impedance behaviour is that predicted by the model presented earlier (§3.2). For the regression calculation of this data, instead of the pure capacitances C_{dl} and C_F presented in Fig. 3.14, the Cole-Cole type distribution was used as illustrated in Fig. 4.5. For the sake of simplicity, this circuit will be named 2RC.
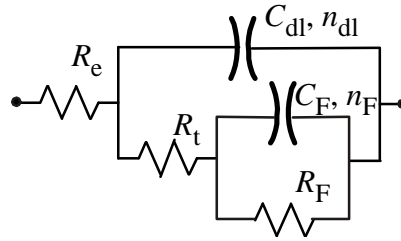
Figure 4.5: Equivalent electrical circuit (2RC) to represent experimental data.

—)(— indicates frequency distributed system coupled with its

parallel resistance (cf. Eq.(4.3)).

The impedance with Cole – Cole distribution of the time constant can be expressed by:

$$Z = \frac{R}{1 + (j \cdot \omega \cdot R \cdot C)^n} \qquad (4.3)$$

where:

n – Cole – Cole coefficient ($0 < n \leq 1$).

In this equation, C possesses well the dimension of $F \cdot cm^{-2}$, instead of CPE elements, largely used nowadays, with the remaining fractional time dimension since here $\omega R \cdot C$ is dimensionless, thus if R is expressed in Ω or $\Omega \cdot cm^2$, then C is expressed in F or $F \cdot cm^{-2}$. In this manner, the origin of the distribution of time constant is not allocated merely to the capacitance, which is the case for the CPE model. In contrast, in the Cole – Cole expression, as well as capacitance, resistance may depend on the perturbing frequency.

Lines with cross in Fig. 4.4 are the calculated data. It can be seen that the used model reproduces suitably the experimental data attesting the validity of the adopted equivalent circuit.

The results of regression calculations are summarized in Fig. 4.6. By using Stern-Geary relationship with polarization resistance $R_p = (R_t + R_F)$, as explained in §3.2,

- -

the corrosion current density was calculated, then the inhibitive efficiency of PMI in the sulphate – carbonate solution at pH 3 was evaluated. The Stern – Geary coefficient B was that presented in Table 4.2 for each PMI concentration.
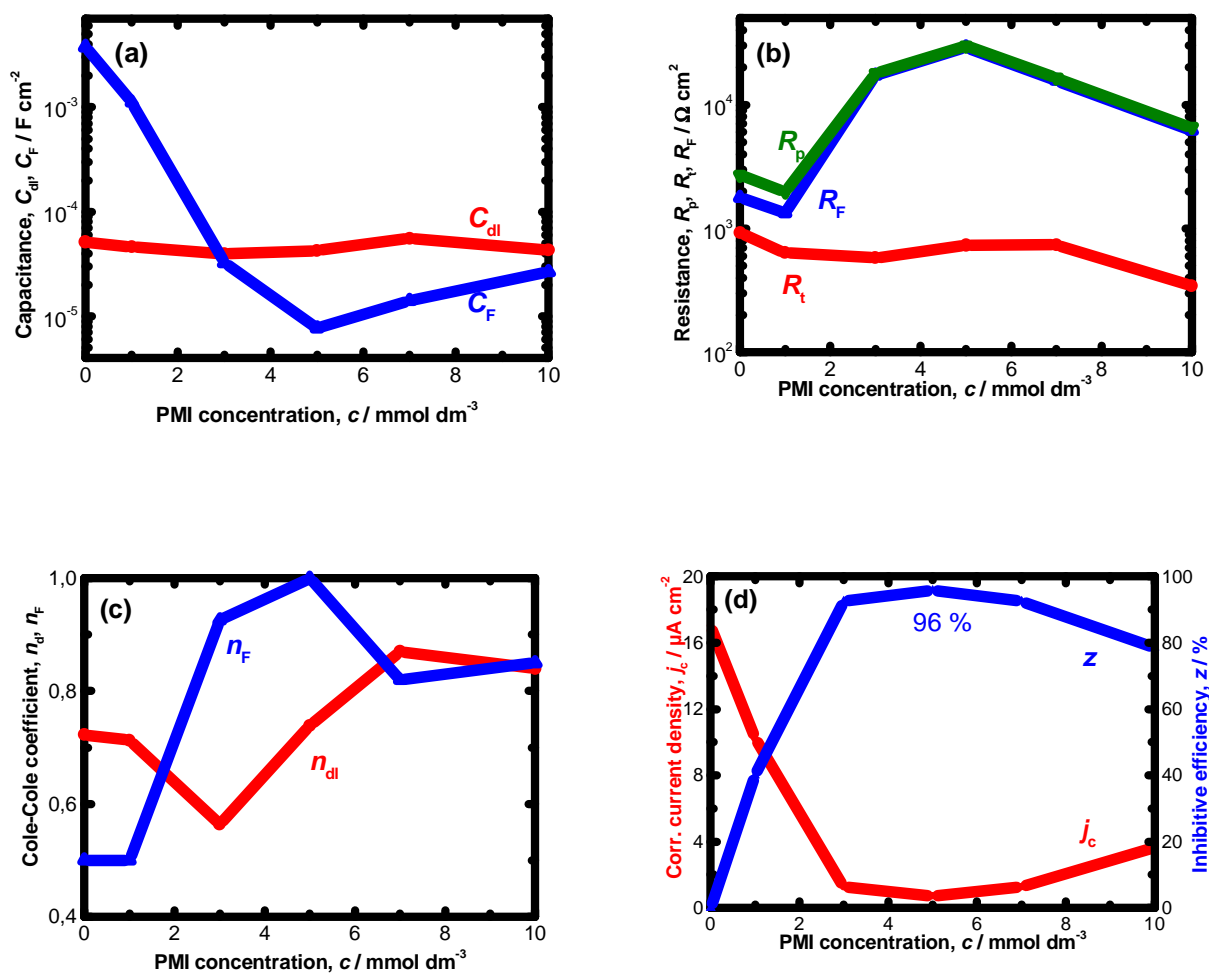
Figure 4.6: Dependence of the equivalent electrical circuit elements with respect to the PMI concentration in Na_2SO_4 / $NaHCO_3$ at pH 3.

It can be seen in this figure that C_{dl} (Fig. 4.6-a) varies little with addition of PMI. Its value is between 40 and 60 $\mu F \cdot cm^{-2}$, three to four times greater than that calculated earlier (cf. §3.2). The surface roughness and probably slightly higher ionic forces at the very vicinity of the electrode surface due to the leaching of cations by corrosion process may explain this discrepancy.

- -

The charge transfer resistance, R_t, is ca. 1 k$\Omega\cdot$cm^2 in absence of inhibitor at the solution of pH 3 and 0.5 k$\Omega\cdot$cm^2 in pH5 solution. If this resistance is mainly determined by the redox process of Cu(0) $\Leftrightarrow$ Cu(I), the exchange current density of this redox process can be estimated, according to Butler – Volmer equation, as 25 and 50 μA$\cdot$cm^{-2} respectively for pH 3 and pH 5 solution. R_t decreases slightly by addition of PMI, ca. three times when 10 mM PMI is added into the corrosion test solution, compared with its absence (cf. Fig. 4.6-b). This substance increases slightly the electrochemical reactivity of bronze. As it was observed with the Tafel extrapolation method (§4.1.1), PMI indeed increases the anodic reaction rate.

In contrast, C_F and R_F change markedly by addition of PMI. R_F is maximum at $c = 5$ mmol$\cdot$dm^{-3}, simultaneously at this concentration C_F is minimum. In other terms, the whole surface species are not involved in the redox process. This phenomenon can be explained by the inhibiting effect of PMI towards the redox process. A small value of C_F compared with that presented in Fig. 3.17-b can be explained by the potential dependence of C_F as shown earlier and also only a part of the surface species take part in the redox process. As a matter of fact, the potential range of E_{corr} observed is much more negative than that at the thermodynamic equilibrium potential (Nernst potential) involving the surface species; Cu/Cu^I or Cu/Cu^{II}. As it will be shown in the next chapter, the surface species involved in the redox process are very likely cuprous compounds. The highest value of C_F was observed at the most anodic E_{corr} potential, i.e. in absence of inhibitor.

It can be remarked also that the values of n_{dl} and n_F (Fig. 4.6-c) are small when the PMI concentration is low whereas they increase significantly at higher PMI concentrations. The presence of PMI makes the reactivity of the bronze electrode surface more homogeneous.

- -

The corrosion current density, j_c, and the inhibitive efficiency, z, are presented in Fig. 4.6-d. The inhibitive efficiency, z, is maximum at PMI concentration 5 mmol·dm^{-3}. Consequently, a good agreement between three methods (linear polarization, Tafel extrapolation method, and EIS spectroscopy) was observed.

- -

4.2 PROTECTIVE EFFECT OF PMI IN pH 5 SOLUTION

In the sulphate / carbonate solution at pH 5, PMI showed a low inhibitive effect. To illustrate it, only the EIS data will be presented. As stated earlier, three electrochemical methods supply similar z values.

4.2.1 ELECTROCHEMICAL IMPEDANCE SPECTROSCOPY

Fig. 4.7 illustrates the impedance diagram obtained in this medium for different PMI concentrations.
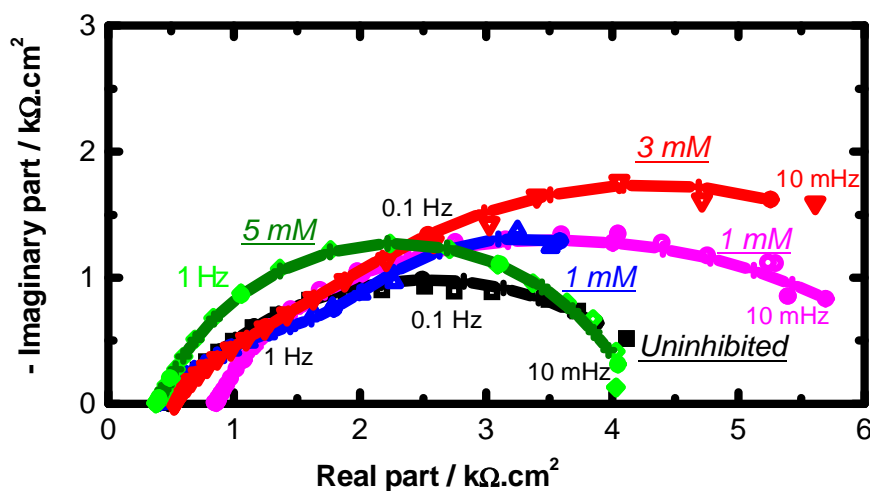
Figure 4.7: Effect of PMI on to the impedance spectra of bare

bronze in Na_2SO_4 / $NaHCO_3$ at pH 5.

It can be noticed that the chord of impedance spectra in Nyquist plot changes little by addition of PMI. Fig. 4.8 illustrates the results of the regression calculation with the 2RC circuit.
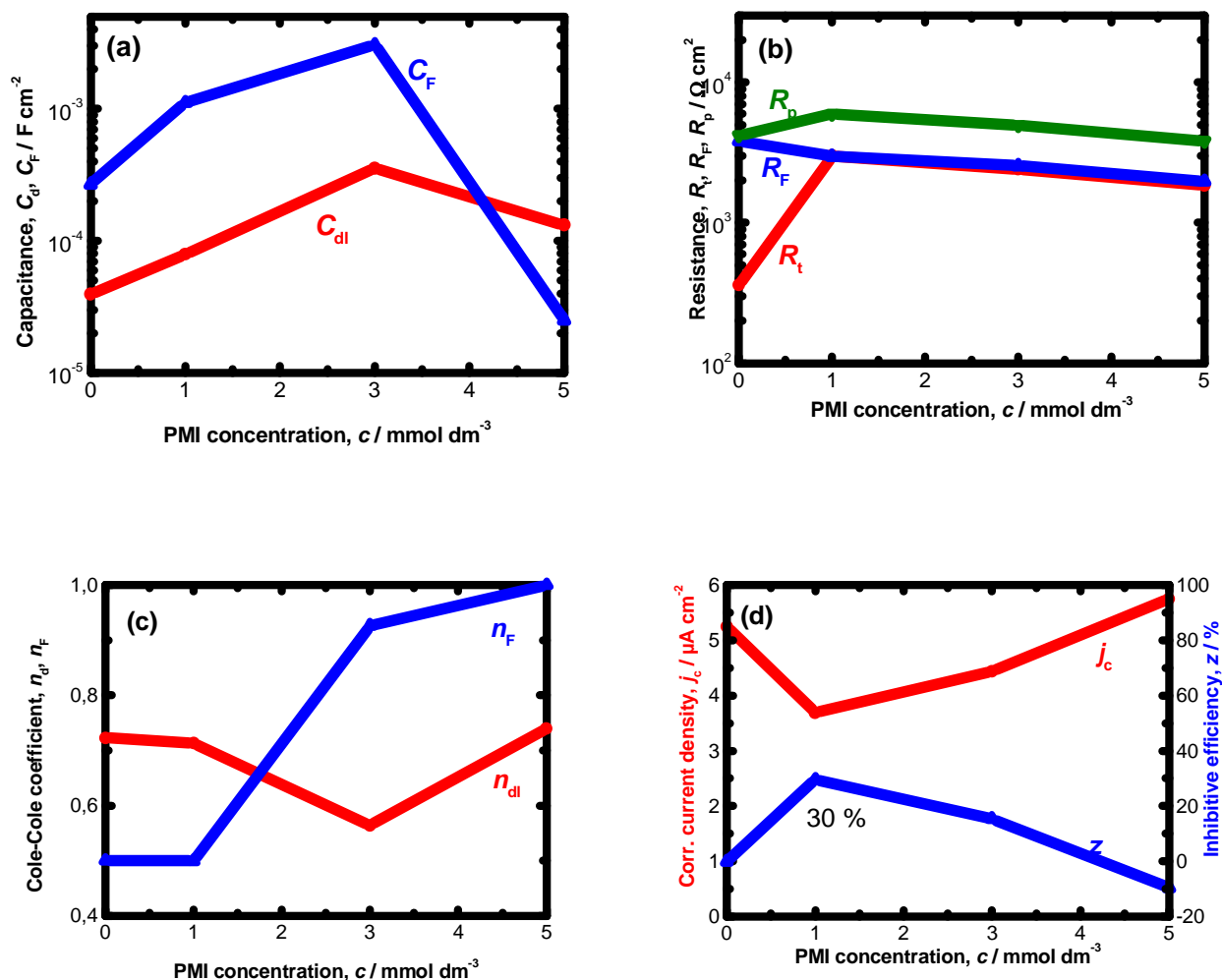
Figure 4.8: Effect of PMI on the corrosion of bare bronze

in Na$_2$SO$_4$ / NaHCO$_3$ at pH 5.

As can be seen in Fig. 4.8-a, C_{dl} is higher than in the case of the pH 3 solution indicating a more roughened electrode surface. The value of C_F which increases up to 3 mmol·dm^{-3} indicates that there is no marked protective effect towards the redox process taking place at the electrode surface, as can be seen also by the variation of R_F which remains almost constant. R_t increases slightly in presence of PMI as it was the case at pH 3. Fig. 4.8-d shows the corrosion current density, j_c, and the protective effectiveness calculated as earlier. The efficiency is maximal at the PMI concentration equal to 1 mmol·dm^{-3} and reaches only 30 %. It can be said that the protective effectiveness of PMI is strongly dependent on the

solutions pH value, and exhibits almost no protective effect in the pH 5 solution. At least, the protective effect is insufficient. Besides, the protective effect shows the maximum, therefore the monitoring of PMI concentration to ensure a protection of bronze against the urban acid rain is critical.

- -

4.3 PROTECTIVE EFFECT OF TMI IN PH 3 SOLUTION

The results related to the protective effect of TMI in the solution simulating strongly acid rain at pH 3 will be presented in this section.

4.3.1. TAFEL EXTRAPOLATION METHOD
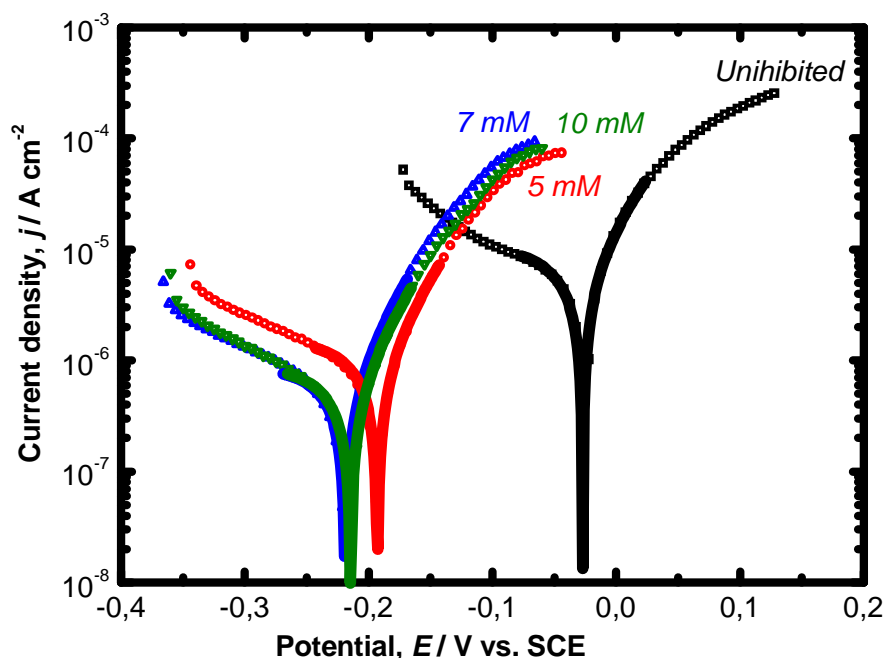
Figure 4.9: Wide range polarization curves of bare bronze in Na$_2$SO$_4$ / NaHCO$_3$

at pH 3 in presence of TMI in different concentrations.

Results obtained by the anodic and cathodic polarization of the bronze electrode in wide potential range (Fig. 4.9), show that with addition of inhibitor, the cathodic polarization curves shift towards lower currents. As a whole, the zero overall current shifts towards more negative values, and the intersection of anodic and cathodic characteristics indicates a lower corrosion current density. TMI is thus a cathodic inhibitor. The effect of TMI to the corrosion kinetics of Cu-6Sn is similar to PMI at pH 3. Corrosion parameters evaluated by the simplex

regression calculation are shown in Table 4.3. Similar to the case of PMI, only one tenth of experimental points are displayed in Fig. 4.9 to make regressed data legible.

Table 4.3: Corrosion parameters of Cu-6Sn bronze in Na_2SO_4 / $NaHCO_3$ at pH 3 with different TMI concentrations determined from the Tafel extrapolation method.

c, mmol·dm^{-3}	/	1	3	5	7	10
E_{corr}, mV	-27.8	-39.1	-186	-192	-218	-215
b_a, mV·dec^{-1}	65.6	42.1	9.80	54.6	50.7	52.1
$-b_c$, mV·dec^{-1}	365	304	262	389	338	251
j_{corr}, µA·cm^{-2}	7.79	2.00	1.30	1.02	0.643	0.552
z, %	/	74.3	83.3	86.9	91.7	92.9

It can be seen in Table 4.3 that the smallest corrosion current density is observed at the highest concentration used and the inhibitive effect reaches 93 %. b_a decreases slightly in presence of PMI and approaches to around 60 mV·dec^{-1}. For b_c, it remains relatively high in absolute value, that is the cathodic process is almost always controlled by the oxygen reduction reaction partially limited by the diffusion process. The limiting current density at higher TMI concentrations is significantly smaller than that expected for the convective diffusion on uniformly accessible surface. The presence of TMI at the bronze surface hinders markedly the surface area available for the oxygen reduction reaction.

4.3.2 LINEAR POLARIZATION

Fig. 4.2 shows the polarization curves of bronze in a narrow potential range. The figure shows that in presence of inhibitor, the polarization resistance, R_p, increases.

- -
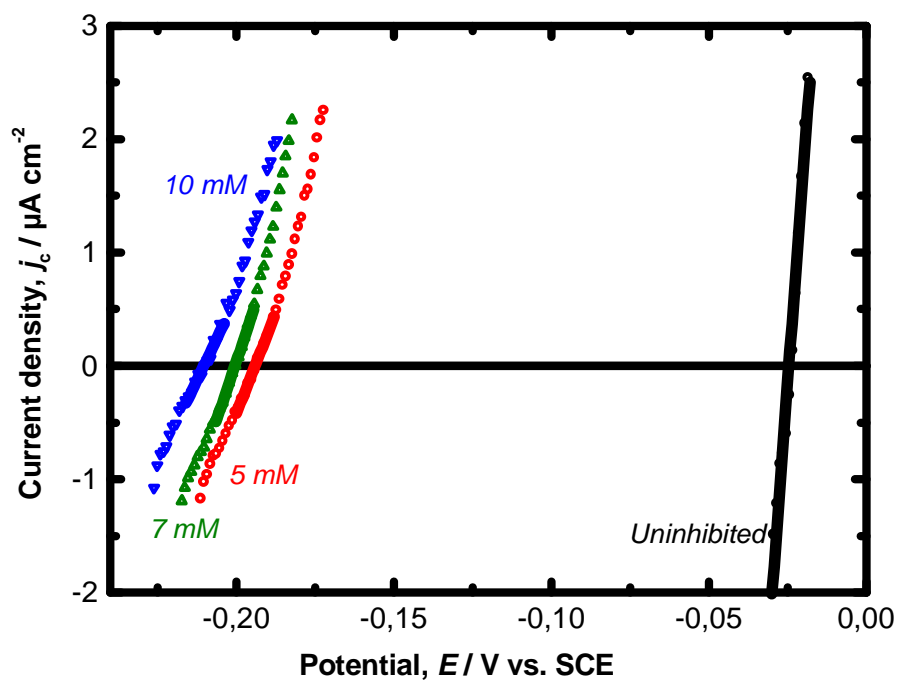
Figure 4.10: Narrow range polarization curves of bare bronze

in Na₂SO₄ / NaHCO₃ at pH 3 with different TMI concentrations.

Corrosion parameters estimated from these data are presented in Table 4.4.

Table 4.4: Corrosion parameters of bare bronze in Na₂SO₄ / NaHCO₃ at pH 3 with different

TMI concentrations, determined by the polarization resistance method.

C, mmol·dm^{-3}	/	1	3	5	7	10
E_{corr}, mV	-25.0	-37.0	-187	-194	-216	-210
B, mV	24.1	15.9	23.2	20.8	19.1	18.7
R_p, k ·cm^2	2.58	5.32	17.8	17.8	24.0	22.0
j_{corr}, µA·cm^{-2}	9.34	2.97	1.58	1.17	0.796	0.850
Z, %	/	68.2	83.1	87.5	91.5	90.1

- -

The value of the polarization resistance, R_p, increases in presence of the inhibitor and is highest at the concentration of 7 mmol·dm^{-3}. Accordingly, the corrosion current density decreases in presence of the inhibitor (TMI) and is the smallest at the concentration of 7 mmol·dm^{-3}. It can be noticed that similar inhibiting efficiencies were obtained by the Tafel extrapolation method.

4.3.3 ADSORPTION ISOTHERM

The data c/θ calculated from j_c according to the Tafel extrapolation method were fitted with various isotherms. The best fit was obtained with the Langmuir-type isotherm, and c/θ with respect to c is presented in Fig. 4.11.
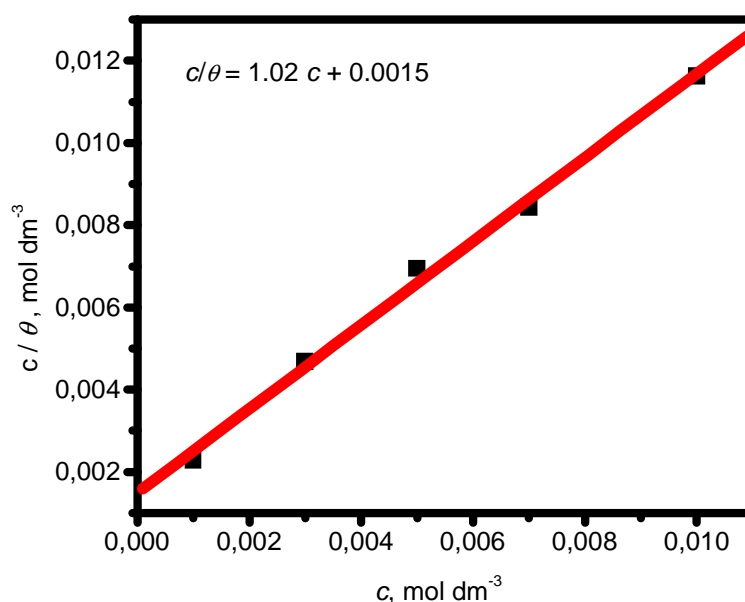
Figure 4.11: Langmuir adsorption isotherm of TMI upon bare bronze

in Na_2SO_4 / $NaHCO_3$ at pH 3.

The adsorption energy was determined from the Langmuir isotherm according to Eqs. (3.81) and (3.82):

G_{ads} = - 26.1 kJ·mol^{-1}

- -

Value of the adsorption free energy G_{ads}, indicates that the interaction between inhibitor and bronze surface is spontaneous and determined by physisorption.

4.3.4 ELECTROCHEMICAL IMPEDANCE SPECTROSCOPY

The results obtained by electrochemical impedance spectroscopy are presented in Fig. 4.12.
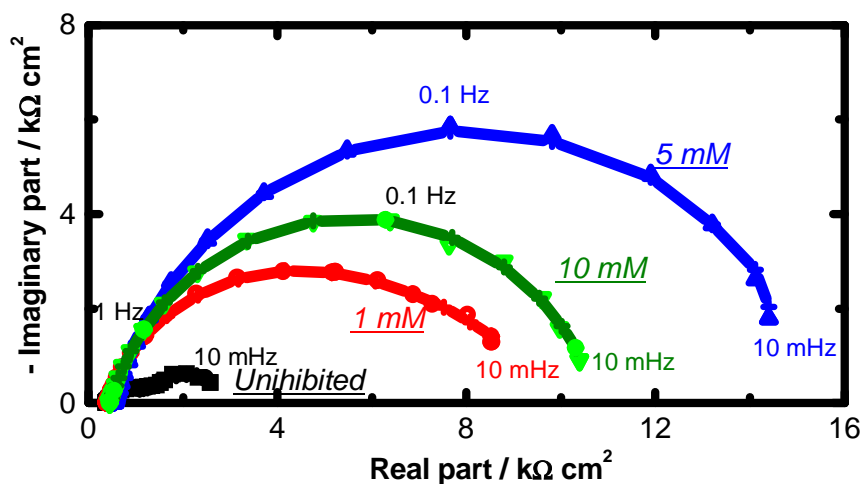
Figure 4.12: Impedance spectra for bare bronze in Na₂SO₄ / NaHCO₃ at pH 3

with different TMI concentrations.

Similar to the earlier case, these impedance spectra are constituted, though not always readily visible, of two capacitive loops. 2RC circuits were thus used to determine the circuit elements. A good agreement with experimental and calculated spectra validate the selection of the adopted equivalent circuit. The results of a simplex regression calculation are presented in Fig. 4.13.

It can be seen that C_{dl} remains essentially independent of the TMI concentration and values 30 μF·cm^{-2}, slightly higher than the theoretical value, but remains reasonable for a roughened electrode surface by corrosion process. C_F decreases continuously

with the TMI concentration indicating the inhibiting effect of this compound to the redox process taking place at the electrode surface. R_t decreases at lower TMI concentrations in agreement with the increase of the anodic reaction rate, but when TMI concentration increases, R_t increases. As can be seen in Fig. 4.13-b, further addition of TMI has small effect on the anodic reaction rate and hinders mainly the cathodic reaction rate.
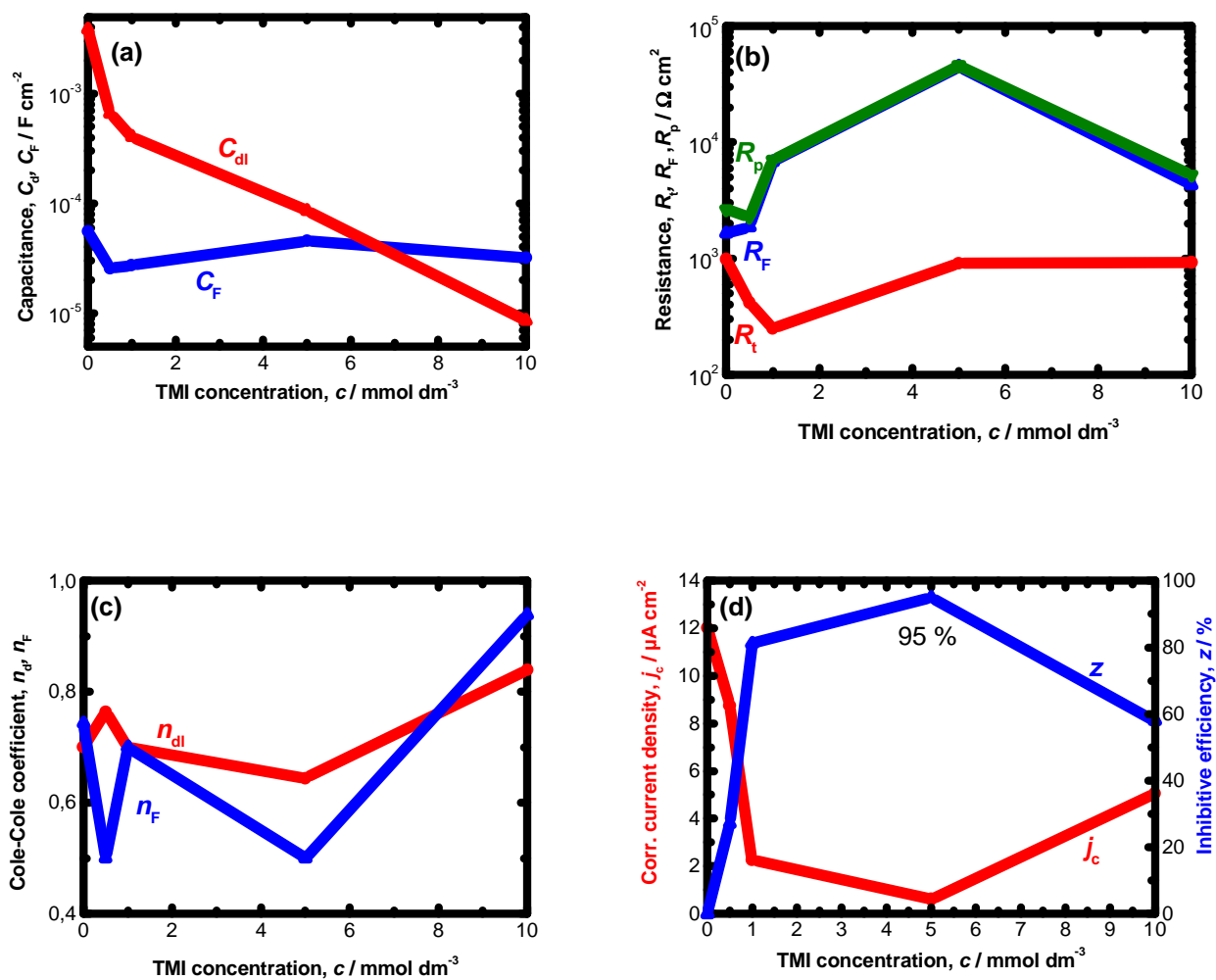
Figure 4.13: EIS data for bare bronze in Na_2SO_4 / $NaHCO_3$ at pH 3

with addition of TMI in different concentrations.

The values of n_d and n_F approache both to 1. TMI adsorbs likely at active sites making the surface distribution of the reaction rate homogeneous. Fig. 4.13-d shows the corrosion current density, j_c, and the inhibitive effect, z. The maximal protective effectiveness observed by the linear polarization method is confirmed by EIS measurements. The protective effect is as high as 95 % at the concentration of 5 mmol·dm^{-3}. TMI is an efficient corrosion inhibitor for Cu-6Sn bronze in strongly acidic urban rain.

- -

4.4 PROTECTIVE EFFECT OF TMI IN pH 5 SOLUTION

The results concerning the effect of TMI in the solution simulating weakly acidic rain will be presented in this chapter.

4.4.1 TAFEL EXTRAPOLATION METHOD
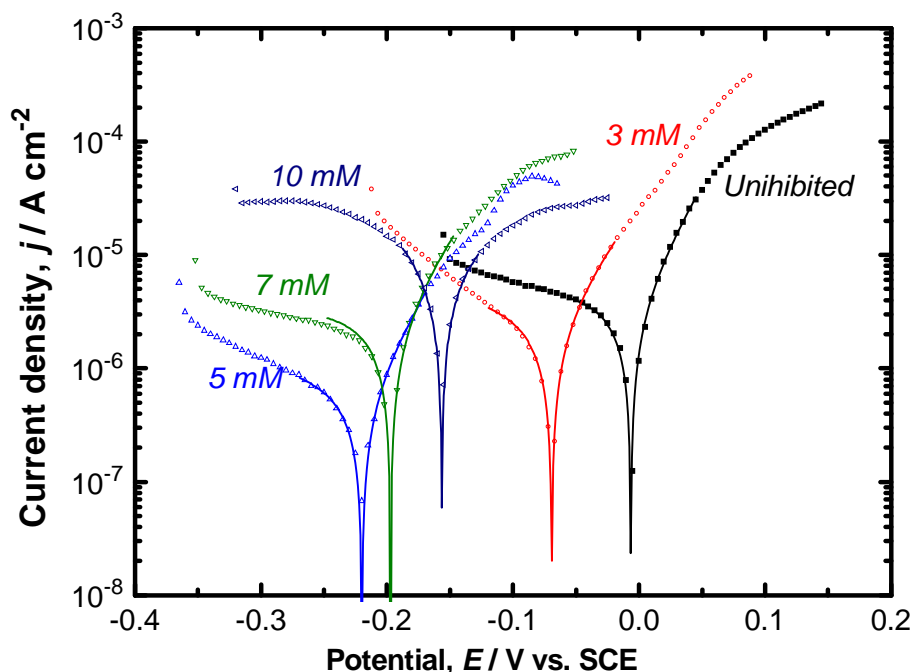
Figure 4.14: Wide potential range polarization curves of bare bronze

in Na$_2$SO$_4$ / NaHCO$_3$ at pH 5 with different TMI concentrations.

Results obtained by the anodic and cathodic polarization of bronze in wide potential range (Fig. 4.14) show that with addition of inhibitor, cathodic branches shift towards smaller currents up to the concentration of 5 mmol·dm^{-3}. Beyond this threshold concentration, the cathodic current increases. In contrast, the anodic branches shift towards the higher current direction up to 5 mmol·dm^{-3}, after which it no longer increases. As a whole, the open circuit potential displaces towards the more cathodic direction and also the corrosion current densities decrease up to 5 mmol·dm^{-3}. Consequently, TMI is a cathodic corrosion inhibitor in the solution at pH 5.

The corrosion parameters were calculated quantitatively according to Eq. (4.1) and the results are displayed in Table 4.5. The inhibitive efficiency is maximal at the concentration 5 mmol·dm^{-3} and is 84 %. At the concentration 10 mmol·dm^{-3}, the inhibitive efficiency is negative corresponding to the acceleration of the corrosion rate compared with the absence of TMI.

Table 4.5: Corrosion parameters of bare bronze in Na$_2$SO$_4$ / NaHCO$_3$ at pH 5 with different TMI concentrations, determined by the Tafel extrapolation method.

c, mmol·dm^{-3}	/	1	3	5	7	10
E_{corr}, mV	-6.40	-78.1	-69.1	-220	-197	-157
b_a, mV·dec^{-1}	54.1	141	70.2	56.7	55.0	134
- b_c, mV·dec^{-1}	736	155	405	344	401	122
j_{corr}, μA·cm^{-2}	4.01	3.04	2.99	0.656	2.00	6.61
z, %	/	24.1	25.4	83.6	50.1	-64.5

4.4.2 LINEAR POLARIZATION

Fig. 4.15 shows results obtained by the polarization of the bronze electrode in a narrow potential range. This figure illustrates that in presence of the inhibitor the slope of the polarization curve decreases corresponding to an increase of the polarization resistance.

- -
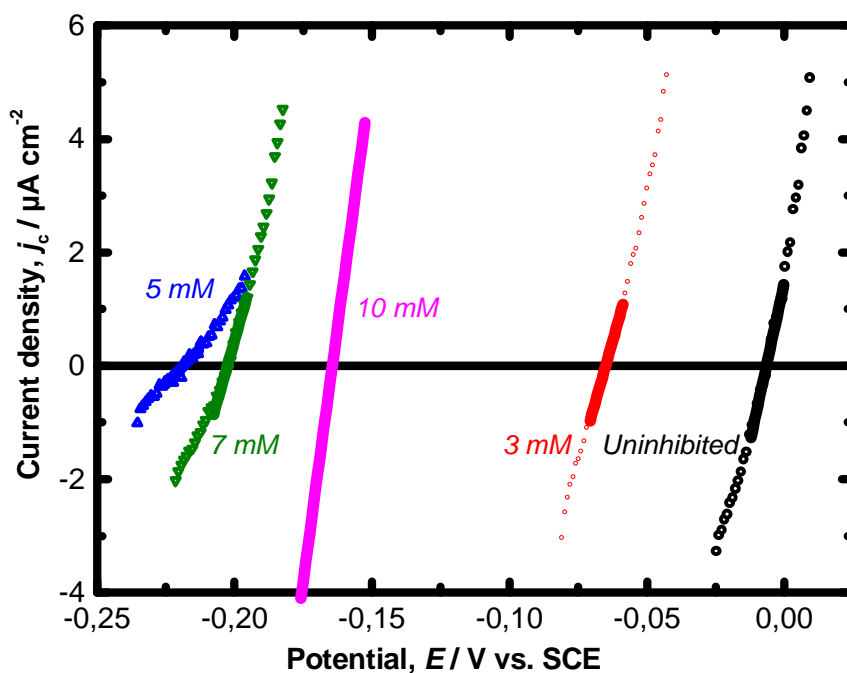
Figure 4.15: Narrow range polarization curves of bare bronze

in Na₂SO₄ / NaHCO₃ at pH 5 with different TMI concentrations.

Corrosion parameters of the bronze electrode extracted from the polarization curves in a narrow potential range (Fig. 4.15) are shown in Table 4.6.

The corrosion current density calculated from Stern – Geary relationship is in agreement with the Tafel extrapolation method. It decreases in presence of the inhibitor, and exhibits the smallest value at the inhibitor concentration 5 mmol·dm^{-3}. It can also be seen that the polarization resistance increases in presence of the inhibitor and is the highest at the concentration 5 mmol·dm^{-3}. At this concentration the inhibitive efficiency is 83 %. An excess of TMI however accelerates the corrosion rate, and at the concentration **10** mmol·dm^{-3} z is negative. This increase is essentially due to the increase of the cathodic current. One of the possibilities of this side-effect will be the reduction of TMI molecules rather than desorption of TMI from the bronze surface since the anodic current densities remain stable.

Table 4.6: Corrosion parameters of bare bronze in Na_2SO_4 / $NaHCO_3$ at pH 5

with different TMI concentrations, determined by polarization resistance method.

c, mmol·dm^{-3}	/	1	3	5	7	10
E_{corr}, mV	-7.02	-81.1	-64.9	-219	-203	-165
B, mV	21.9	31.6	26.0	21.1	21.0	28.2
R_p, k ·cm^2	4.50	8.09	7.38	25.1	7.60	3.02
j_{corr}, µA·cm^{-2}	4.87	3.91	3.51	0.84	2.76	9.44
z, %	/	19.7	27.9	82.8	43.3	-93.8

4.4.3 ADSORPTION ISOTHERM

The data obtained by Tafel extrapolation method were fitted with various isotherms with respect to the TMI concentration domain where the inhibitive effect improved with increasing inhibitor concentration, i.e. up to the optimal concentration, $c \leq 5$ mmol dm^{-3}. Unlike other cases, in this one, the data could not be fit with the Langmuir isotherm. The best fit was obtained with the Freundlich isotherm.

Adsorption energy is calculated according to the Freundlich isotherm according to Eqs. (3.82) and (3.83):

$G_{ads} = -21.3$ kJ·mol^{-1}

According to this value, the adsorption process can be allocated to physical adsorption of the inhibitor. Since only three points were used for fitting the adsorption isotherm, and also at higher TMI concentrations, the augmentation of the cathodic reaction rate was observed, the results are not very reliable, but this result indicates the tendency of TMI's adsorption to the bronze surface. The ΔG_{ads} calculated here is much higher than that at pH 3 (cf §4.3.3), but this quantitative comparison is rather uncertain as explained above.

- -
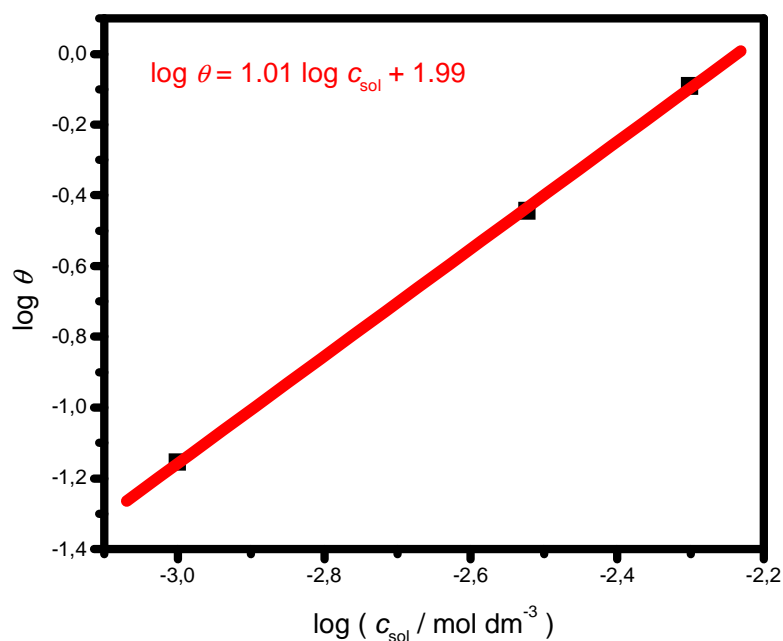
Figure 4.16: Freundlich adsorption isotherm for bare bronze in

Na₂SO₄/ NaHCO₃ at pH 5 with addition of TMI in different concentrations.

4.4.4 ELECTROCHEMICAL IMPEDANCE SPECTROSCOPY

Fig. 4.17 shows the results obtained by electrochemical impedance spectroscopy.
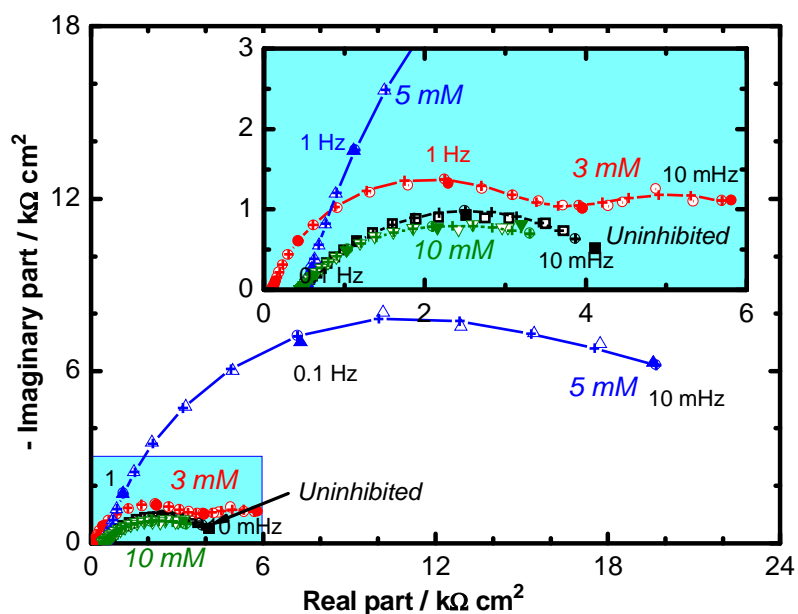
Figure 4.17: Impedance spectra for bare bronze in Na₂SO₄ /NaHCO₃ at pH 5

with addition of TMI in different concentrations.

As in the case above, two capacitive loops are sufficient to reproduce suitably the observed impedance spectra. Therefore, regression calculation to determine the value of 2RC equivalent circuit elements by a Simplex method was performed for each TMI concentration. It can be noticed that the comparison of experimental and calculated impedance spectra in Nyquist plot superimposes almost perfectly indicating the validity of the equivalent circuit adopted here. The results obtained for different parameters are presented graphically in Fig. 4.18.
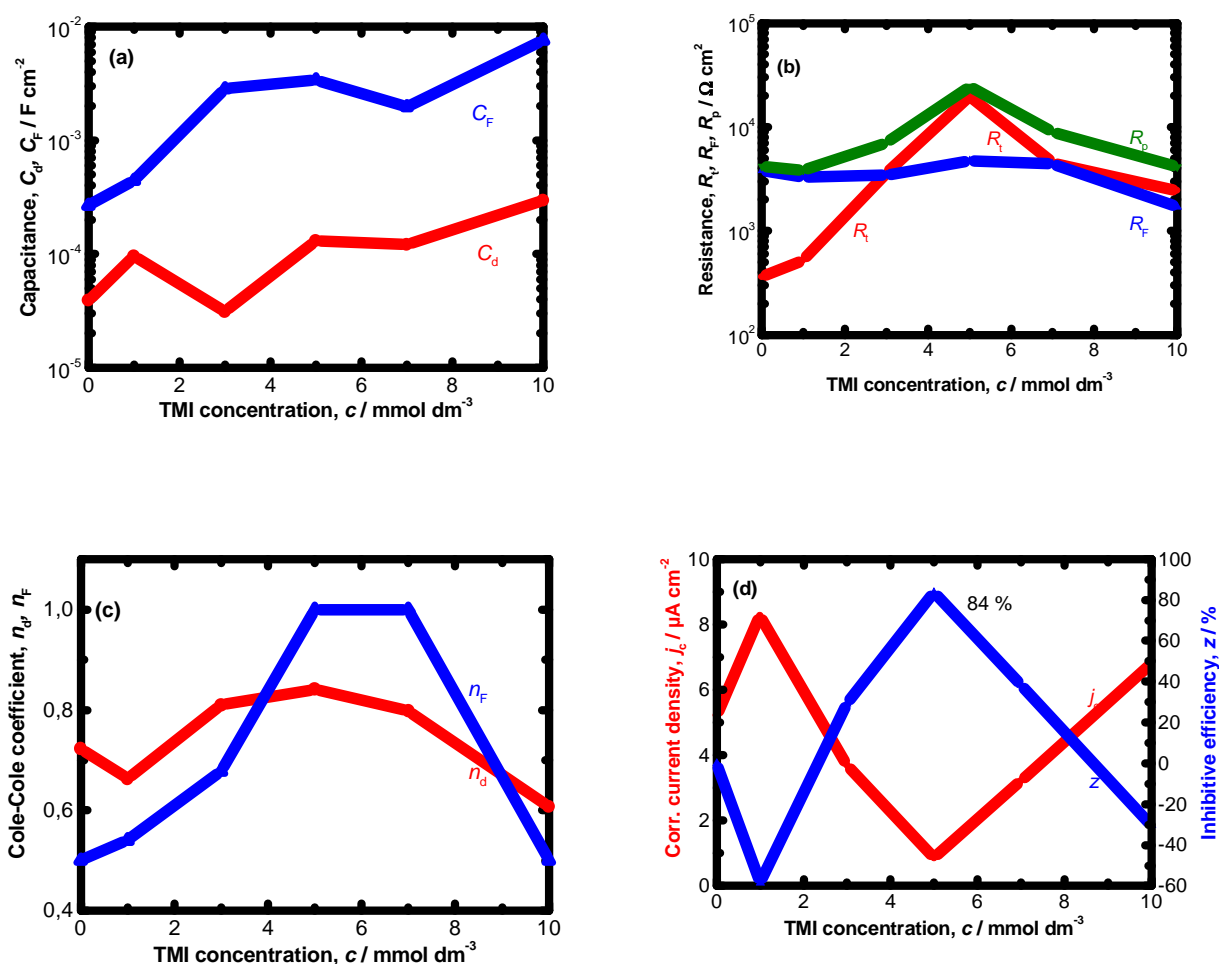
Figure 4.18: EIS data for bare bronze in Na_2SO_4 / $NaHCO_3$ at pH 5 with addition of different TMI concentrations.

It can be noticed that C_{dl} and C_F grow with the increasing TMI concentration, as it was observed for the addition of PMI in the same corrosion test solution. TMI has, therefore, no marked protective effect towards the redox process preceding the dissolution step of the reaction intermediate. The electrode surface becomes rough and certainly the corrosion products make the ionic strength at the vicinity of the electrode surface higher. As for R_t and R_F, these two resistances have a similar value, also as in the case of PMI addition at pH 5. n_d and n_F rise with the increase of the TMI concentration until 7 mmol·dm^{-3}, beyond which these parameters decrease substantially. The acceleration of the corrosion rate as shown by Tafel extrapolation and linear polarization methods corroborated here by impedance measurements (cf. Fig 4.18-d). The decrease of n_d and n_F above this threshold concentrations may indicate an enhancement of the heterogeneity of electrochemical reactivity of the bronze surface. The reduction reaction of TMI invoked above may thus take place at particular reaction sites. The maximum inhibitive effect of TMI is found again at the TMI concentration of 5 mmol·dm^{-3}, and its efficiency at this concentration is 84 %.

Three corrosion evaluation methods (Tafel extrapolation, linear polarization, and electrochemical impedance spectroscopy) exhibited coherent results and the concentration of TMI 5 mmol·dm^{-3} has the optimum protective effect against the corrosion of Cu-6Sn in weakly acidic urban rail fall. The protection of bronze statues exposed in urban area by this inhibitor is particularly dangerous or needs meticulous monitoring of the inhibitor concentration, as at lower and higher inhibitor concentrations, the corrosion rate may be higher than in the uninhibited solution.

- -

4.5 PROTECTIVE EFFECT OF BZI IN PH 3 SOLUTION

The results relative to the simplest molecular structure among three imidazoles tested (benzimidazole) in synthetic strongly acidic rain water in urban environment are presented in this section.

4.5.1 TAFEL EXTRAPOLATION METHOD
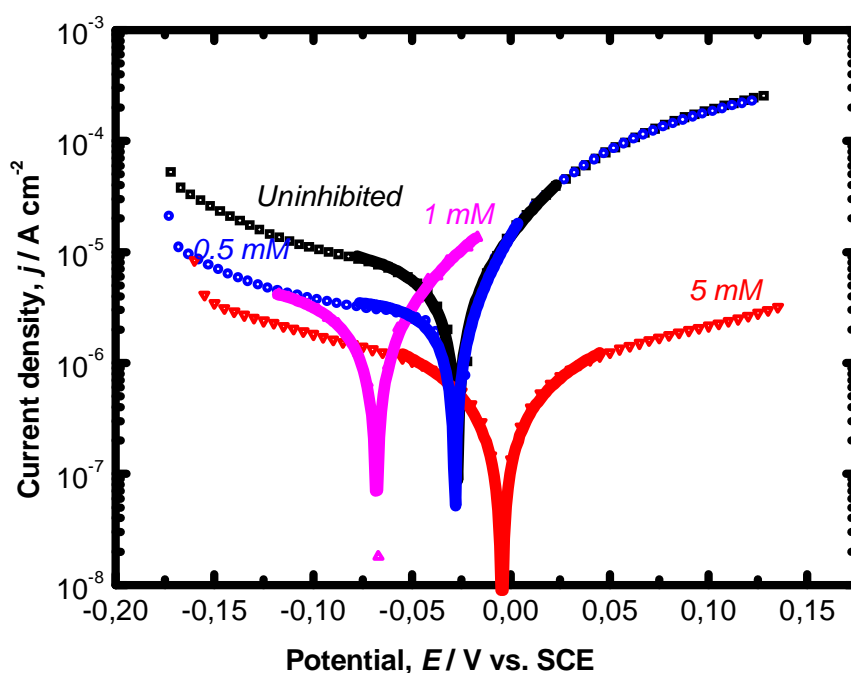
Figure 4.19: Wide range polarization curves of bare bronze
in Na_2SO_4 / $NaHCO_3$ at pH 3 with different BZI concentrations.

Results obtained by the Tafel plot (Fig. 4.19) show that the cathodic branches move towards smaller currents when BZI is added even in low concentrations. As for the anodic current density, it decreases also by addition of higher inhibitor concentrations (c > 1 mmol·dm^{-3}). This indicates that BZI is a mixed inhibitor. As a whole, it can also be seen that with addition of inhibitor the corrosion potentials shift towards the more negative direction up to 1 mmol·dm^{-3} than to the anodic direction. As a matter of fact, at the optimal

concentration (5 mmol·dm^{-3}) the decrease of the anodic current density is more marked than that of the cathodic current density, this explains the inversion of the potential shift with BZI concentration. As above, the corrosion parameters are determined from these curves with the Stern – Geary equation for the potential domain limited to ±50 mV with respect to E_{corr}. The results are displayed in Table 4.7

Table 4.7: Corrosion parameters of bare bronze in Na$_2$SO$_4$ / NaHCO$_3$ at pH 3 with different BZI concentrations , determined by the Tafel extrapolation method.

c, mmol·dm^{-3}	/	0.5	1	3	5	10
E_{corr}, mV	-27.8	-26.6	-68.0	-165	-4.3	-219
b_a, mV·dec^{-1}	65.6	57.5	79.2	53.0	140	42.0
$-b_c$, mV·dec^{-1}	365	888	352	220	154	185
j_{corr}, μA·cm^{-2}	7.79	4.05	3.76	1.60	0.722	1.40
z, %	/	48.0	51.7	79.5	90.7	82.0

According to Table 4.7, the corrosion current density decreases in presence of the corrosion inhibitor and is smallest at the concentration 5 **m**mol·dm^{-3}. At this concentration, the inhibiting efficiency reaches 91 %. At excess of BZI, the E_{corr} becomes more negative and j_{corr} increases. With the polarization curves obtained at this concentration, it was remarked that cathodic current density increases.

4.5.2 LINEAR POLARIZATION

Fig. 4.20 shows results obtained by the polarization curves in a narrow potential range. These curves indicate the decrease of its slope in presence of the inhibitor.
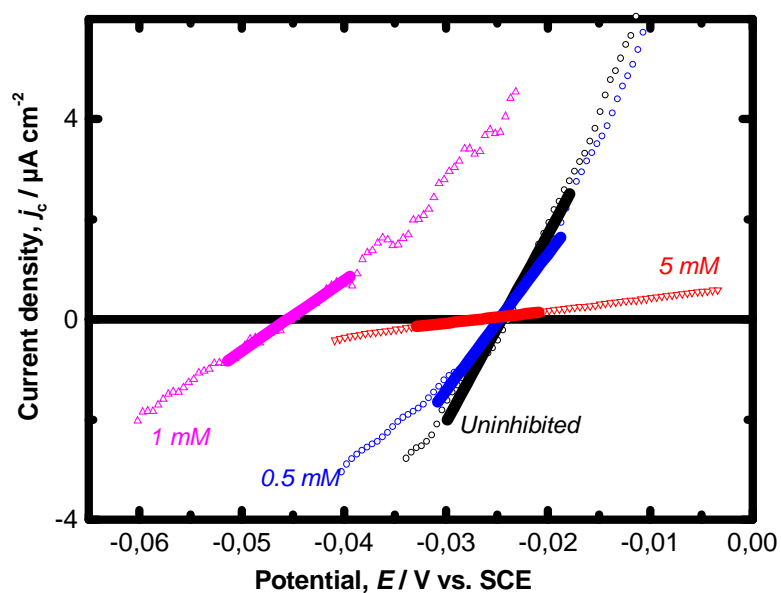
Figure 4.20: Narrow range polarization curves of bare bronze

in Na₂SO₄ / NaHCO₃ at pH 3 with different BZI concentrations.

The polarization resistance, R_p, and the corrosion potential, E_{corr}, are determined by a linear regression calculation at $j – E$ curve close to the corrosion potential $\pm$ 5 mV. Corrosion parameters of the bronze electrode obtained from these polarization curves are summarized in Table 4.8.

Table 4.8: Corrosion parameters of Cu-6Sn electrode in Na₂SO / NaHCO₃ at pH 3 with

different BZI concentrations determined by the polarization resistance method.

c, mmol·dm^{-3}	/	0.5	1	3	5	10
E_{corr}, mV	-24.8	-24.8	-45.4	-157	-26.9	-216
B, mV	24.1	23.4	25.1	19.8	31.0	15.6
R_p, k ·cm^2	2.58	3.65	7.16	11.0	41.8	13.0
j_{corr}, µA·cm^{-2}	9.34	6.41	3.50	1.80	0.74	92.6
z, %	/	31.4	62.5	80.7	92.1	87.2

- -

It can be observed that these results are in good agreement with those obtained by the Tafel extrapolation method. It can be seen also that the polarization resistance increases in presence of the inhibitor and is the highest also at 5 mmol·dm^{-3}; thus the corrosion current density is the smallest at this concentration. The inhibitor efficiency at this optimum value is 92 %.

4.5.3 ADSORPTION ISOTHERM

The data obtained by the Tafel extrapolation method allowed the evaluation of the surface coverage θ. With various isotherms, the best fit was obtained with the Langmuir-type isotherm as shown in Fig. 4.21.
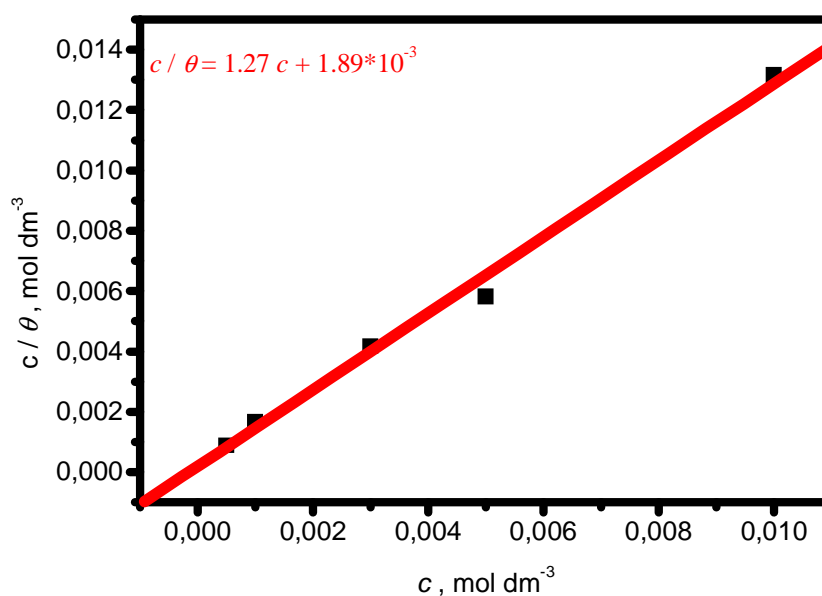
Figure 4.21: Langmuir adsorption isotherm for bare bronze

in Na$_2$SO$_4$ / NaHCO$_3$ at pH 3 with addition of different BZI concentrations.

The adsorption energy was determined from the Langmuir-type isotherm according to Eqs. (4.3) and (4.4):

$G_{ads} = - 25.5$ kJ·mol^{-1}

- -

The value of free energy of adsorption, G_{ads}, indicates that the inhibitor is linked likely to the surface by spontaneous physisorption.

4.5.4 ELECTROCHEMICAL IMPEDANCE SPECTROSCOPY

Fig. 4.22 shows the results obtained by electrochemical impedance spectroscopy.
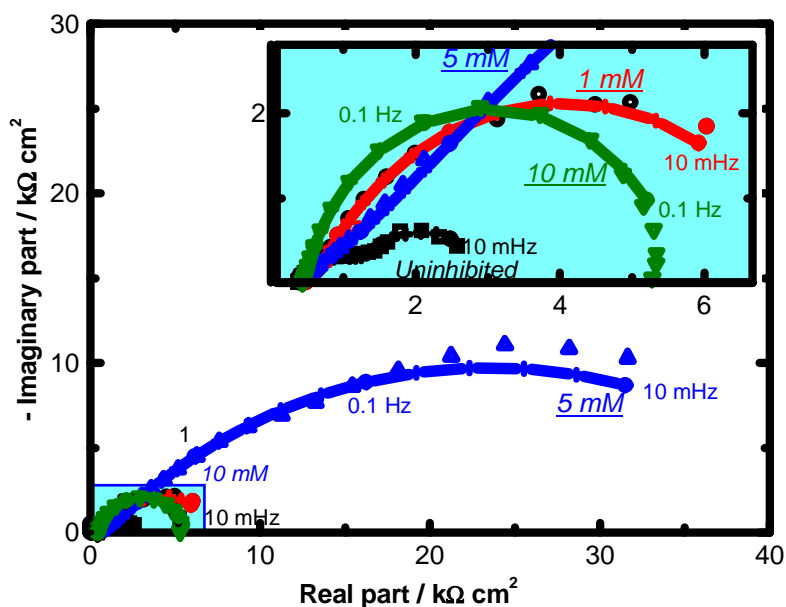
Figure 4.22: EIS for bare bronze in Na₂SO₄ / NaHCO₃ at pH 3

with different BZI concentrations.

These diagrams are also suitably represented by two capacitive loops, thus regression calculation with 2RC circuit by Simplex method was carried out. The calculated data are summarized in Fig. 4.23.

Very similar inhibitive effects were obtained by Tafel extrapolation and linear polarization methods. The inhibitive effect was maximum at 5 mmol·dm⁻³ beyond which it decreases slightly. None-the-less, the inhibitive effect remains high even at the concentration

equal to 10 mmol dm^{-3}, thus an overprotection by BZI may not damage the bronze object

exposed in the urban area.
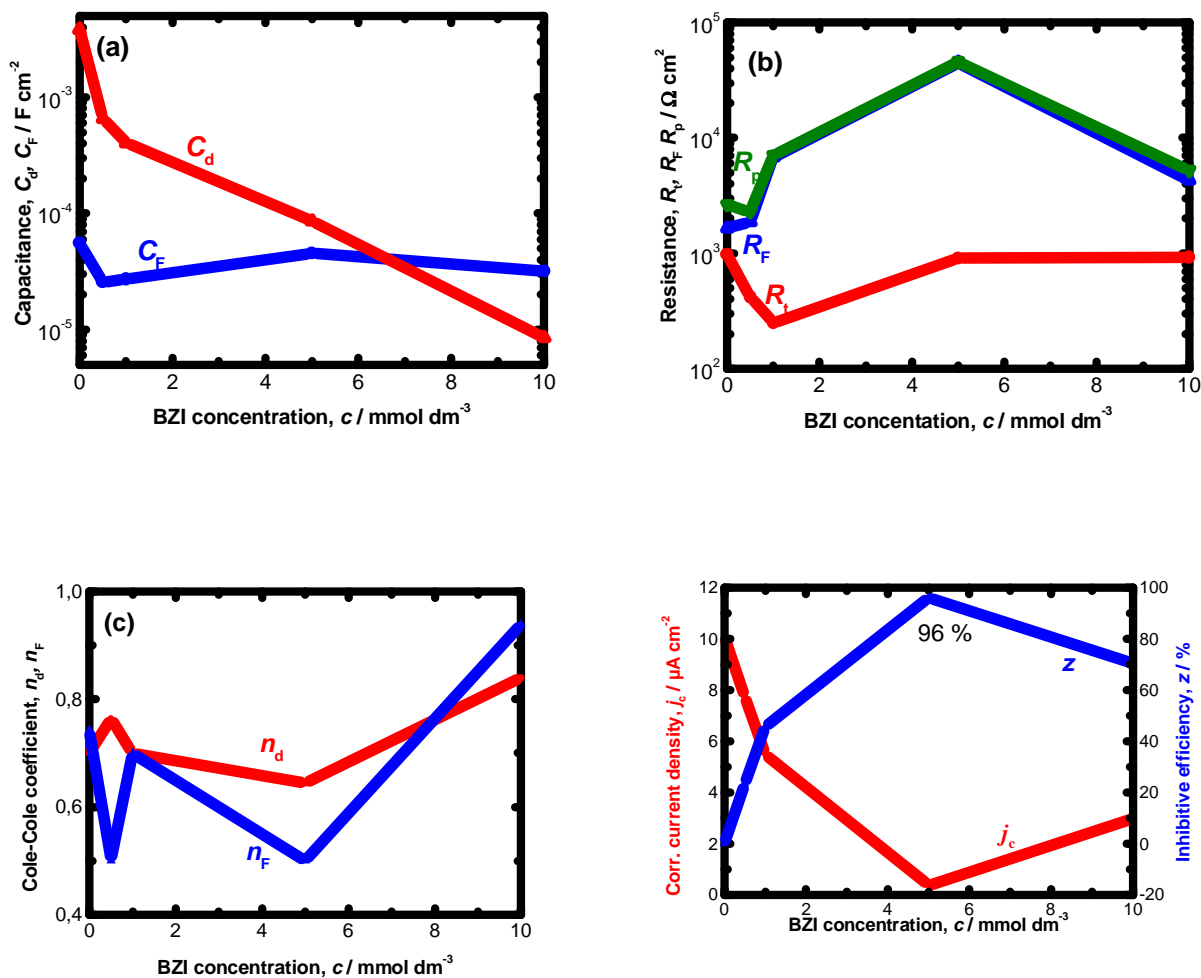
Figure 4.23: EIS data for bare bronze in Na$_2$SO$_4$ / NaHCO$_3$

at pH 3 with different BZI concentrations.

4.6 PROTECTIVE EFFECT BZI IN pH 5 SOLUTION

The effect of BZI in a solution representing mildly acid rain in urban environment will be presented in this section.

4.6.1 TAFEL EXTRAPOLATION METHOD
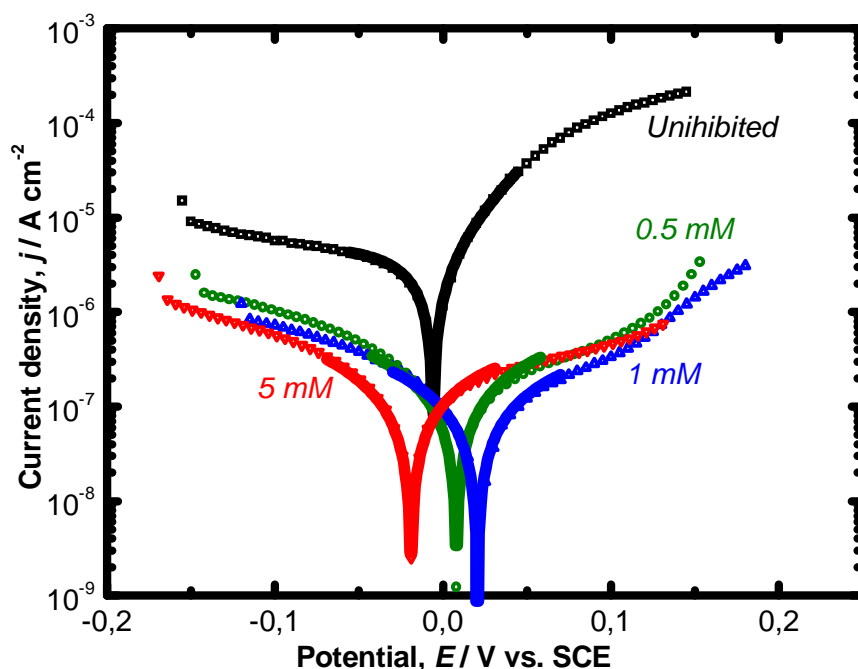
Figure 4.24: Wide range polarization curves of the Cu-6Sn bronze electrode

in Na₂SO₄ / NaHCO₃ at pH 5 with different BZI concentrations.

Results obtained by the anodic and cathodic polarization of the bronze electrode in wide potential range (Fig. 4.24) show that with addition of inhibitor both anodic and cathodic curves move towards smaller current densities indicating a mixed inhibitor property of BZI. It can be remarked also that the inhibitive effect on the cathodic process seems to no longer improve above 0.5 mmol·dm^{-3}. As for the anodic process, the current density continues, though moderately, to decrease. As a whole, the addition of inhibitor does not modify

significantly the corrosion potential. Corrosion parameters evaluated from these curves are presented in Table 4.9.

Table 4.9: Corrosion parameters of in Na_2SO_4 / $NaHCO_3$ at pH 5

with different BZI concentrations, determined by the Tafel extrapolation method.

c, mmol·dm^{-3}	/	0.001	0.005	0.01	0.05	0.1	0.5	1	5
E_{corr}, mV	-6.40	-31.0	-28.9	-6.03	26.7	-13.0	8.14	20.8	-18.3
b_a, mV·dec^{-1}	54.1	40.4	36.2	38.2	53.7	66.6	121	111	339
- b_c, mV·dec^{-1}	736	362	350	163	177	172	98.4	263	282
j_{corr}, µA·cm^{-2}	4.01	2.39	1.60	0.590	0.301	0.330	0.511	0.402	0.451
z, %	/	40.4	60.1	85.3	92.5	91.8	87.3	90.0	88.8

The corrosion current density presented in Table 4.9 decreases markedly in presence of the corrosion inhibitor even at very low concentrations, and is the smallest at the concentrations between 0.05 to 1 mmol·dm^{-3}. Further addition of inhibitor does not deteriorate the inhibitive efficiency contrary to other cases examined in this work. The inhibitive efficiency reaches 93 %.

4.6.2 LINEAR POLARIZATION

Fig. 4.25 shows results obtained by the polarization of the bronze electrode in a narrow potential range which indicates that in presence of the inhibitor the polarization resistance increases.

- -
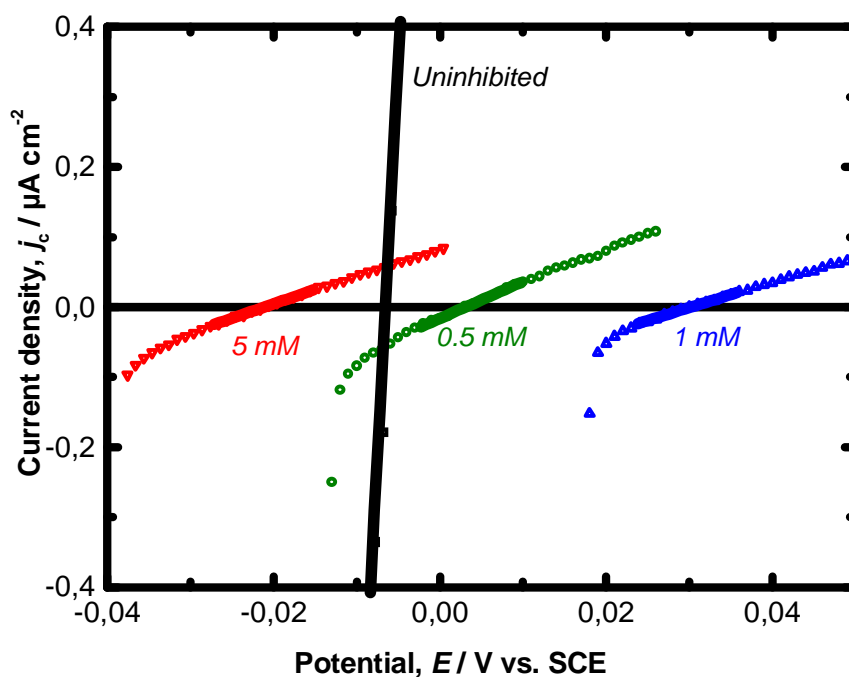
Figure 4.25: Narrow range polarization curves of bare bronze

in Na₂SO₄ / NaHCO₃ at pH 5 with different BZI concentrations.

Corrosion parameters of the bronze electrode obtained from these polarization curves are displayed in Table 4.10.

Table 4.10: Corrosion parameters of bare bronze in Na₂SO₄ / NaHCO₃ at pH 5

with different BZI concentrations, determined by polarization resistance method.

c, mmol·dm^{-3}	/	0.001	0.005	0.01	0.05	0.1	0.5	1	5
E_{corr}, mV	-7.00	-28.1	-27.3	-18.1	12.9	-10.1	2.99	1.10	-21.3
B, mV	21.9	15.6	14.3	12.6	17.2	20.3	25.7	16.5	48.5
R_p, k ·cm^2	4.50	5.21	6.20	21.0	28.6	67.5	197.2	165.0	243
j_{corr}, A·cm^{-2}	4.87	3.00	2.28	0.600	0.600	0.321	0.135	0.331	0.321
z, %	/	38.4	52.8	87.7	87.7	93.4	97.2	93.2	93.4

It can be seen that the value of polarization resistance increases in presence of inhibitor above 0.01 mmol·dm^{-3}, at which the inhibitive efficiency reaches ca. 87 %. It is important to emphasize that BZI decreases the corrosion current density at the concentration as low as 1 μmol·dm^{-3}. The concentration 0.1 mmol·dm^{-3} is sufficient to obtain marked inhibitive effect.

4.6.3 ADSORPTION ISOTHERM

The surface coverage θ evaluated from the corrosion current density according to the Tafel extrapolation method were fitted with various isotherms. The best fit was obtained with the Langmuir-type isotherm, and this relationship is illustrated in Fig. 4.26.
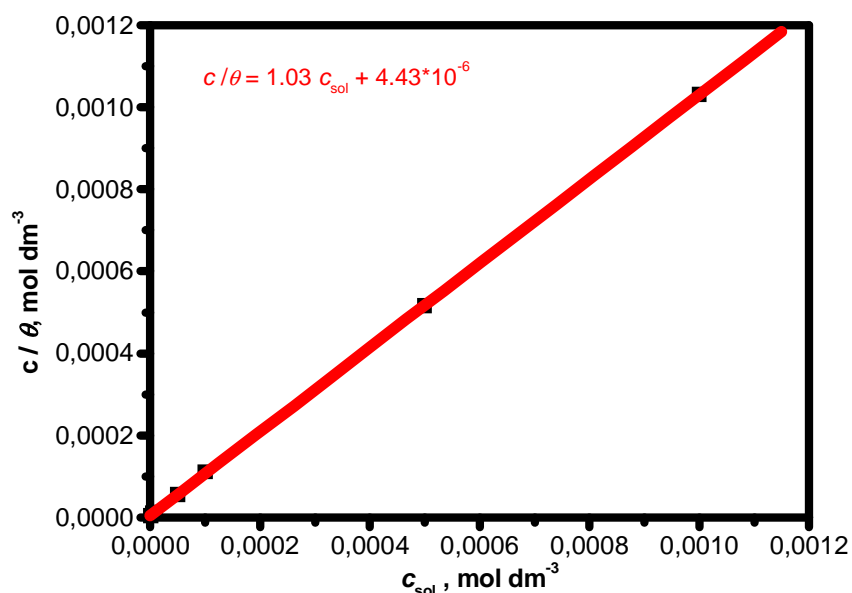
Figure 4.26: Langmuir adsorption isotherm for bare bronze

in Na$_2$SO$_4$ / NaHCO$_3$ at pH 5 in presence of BZI.

The adsorption energy determined from the Langmuir isotherm values:

G_{ads} = -40.5 kJ·mol^{-1}

- -

The value of adsorption free energy, G_{ads}, is at the threshold of physisorption and chemisorption. Since at pH 3 BZI links to the surface by physisorption, it is most likely that at pH 5 it also links by physisorption, but there is also a certain amount of chemical bounds forming on the surface.

4.6.4 ELECTROCHEMICAL IMPEDANCE SPECTROSCOPY

Fig. 4.27 shows the results obtained by the electrochemical impedance spectroscopy.
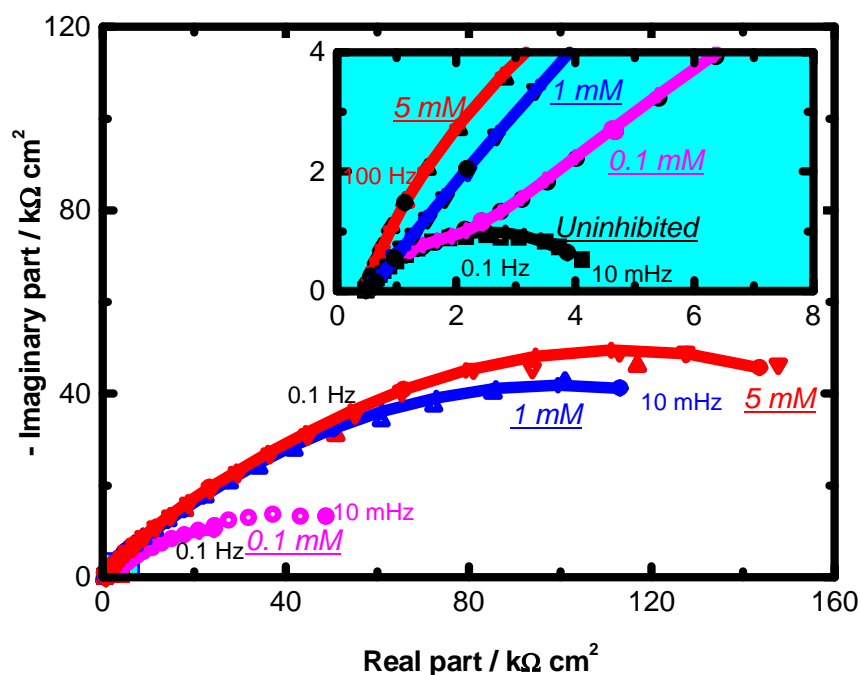
Figure 4.27: Impedance spectra for bare bronze in Na_2SO_4 / $NaHCO_3$

at pH 5 with different BZI concentrations.

The impedance spectra are very depressed even in presence of the inhibitor. However, two capacitive loops with small Cole-Cole coefficients are sufficient to reproduce suitably the experimental spectrum according to the regression calculation with a Simplex method. The calculated data are represented in Fig. 4.28. The value of the double layer capacitance, C_{dl}, is around a few $\mu F \cdot cm^{-2}$, markedly smaller than that expected for this dilute

solution medium. The surface coverage by BZI may modify deeply the double layer structure. This high adsorption effect is really reflected by good inhibiting efficiency, z, observed for the coupling pH 5 solution – BZI even at very low inhibitor concentrations. C_F is also small, a few tens $\mu F \cdot cm^{-2}$, that indicates an efficient inhibitive effect towards the redox process taking place at the electrode surface. Very small values observed at the concentration of 0.1 $mmol \cdot dm^{-3}$ will be considered to be due to a poor separation of two capacitive loops.
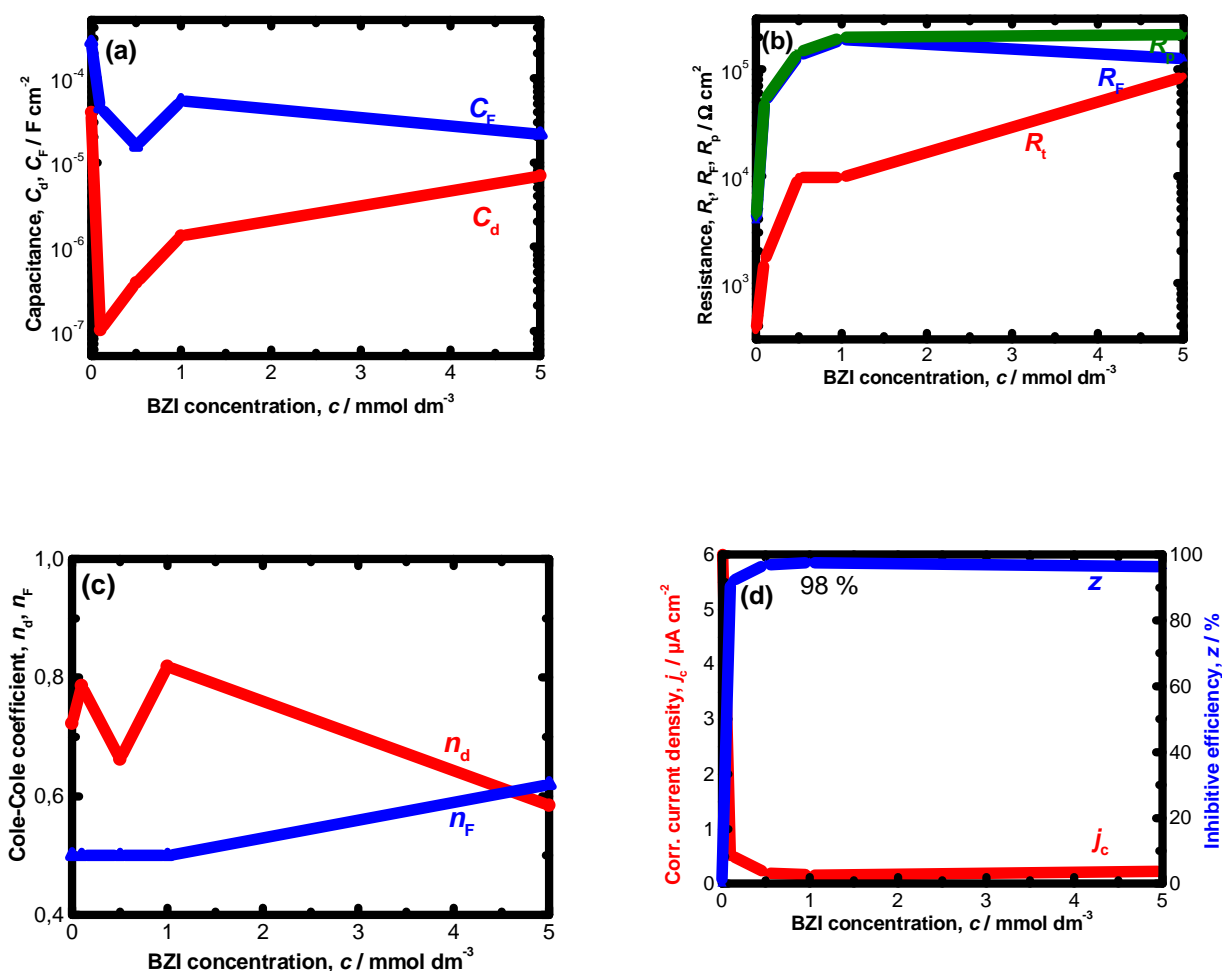
Figure 4.28: EIS data for bare bronze in Na₂SO₄ / NaHCO₃

at pH 5 with different BZI concentrations.

The resistances, especially the polarization resistance, are high, greater than 100 $k\Omega \cdot cm^2$ above the concentration as low as 0.3 $mmol \cdot dm^{-3}$. This very high R_p value is in

agreement with that determined by the linear polarization method presented above. n_d and n_F are both small, especially when inhibitor concentration is high, that is, in spite of a good inhibiting effect, the surface reactivity is highly distributed. The protective effect is high, and above 90 % for concentrations higher than 1 mmol·dm^{-3} and j_c remains small in the whole concentration domain examined.

Benzimidazole exhibits the best protection properties, as well for the inhibitive efficiency as it maintained for an excess addition to the corrosive medium. According to Material Safety Data Sheet, BZI is just harmful. However, it should be mentioned that after long immersion (over 1 month), its surface colour changes into a brown-reddish colour. Therefore, this inhibitor cannot be applied at present time to protect statues covered by green patina and exposed in urban area.

4.7. PARTIAL CONCLUSION OF THE CHAPTER

The inhibitor effect of three imidazole compounds, 4-methyl-1-phenylimidazole (PMI), 4-methyl-1-*p*-tolylimidazole (TMI) and 1-H benzimidazole (BZI) to copper-tin binary alloy (Cu-6Sn) immersed in artificial urban acid rain was examined by electrochemical methods. The polarization curves plotted with a large potential domain ($\pm$ 0.15 V) by the Tafel extrapolation method were first applied for different corrosion test systems. It was found that the cathodic branches exhibited generally rather well developed linear domain to determine the Tafel constant (or the Tafel slope).

In absence of inhibitor, the cathodic Tafel slope is huge, more than 360 mV·dec^{-1} in pH3 solution and 700 mV dec^{-1} in pH5, solution in agreement with the cathodic process controlled in major part-by the diffusion of dissolved oxygen.

Among three inhibitors examined, PMI is found not efficient at all in mildly acid rain (pH 5), even at the concentration of 5 mmol·dm^{-3}. The acceleration of the corrosion rate with respect to the uninhibited medium was recorded. Except this particular case, from E_{corr} and j_{corr} values, and also by the polarization curves, it was concluded that the imidazoles used here are cathodic inhibitors, except for BZI which decreases also the anodic reaction rate, i.e. it is a mixed inhibitor.

From the corrosion current density, the surface coverage by inhibitor was estimated, considering that the surface area is covered by inhibitor, the corrosion rate $j_{corr} = 0$. With this very rough hypothesis, the adsorption mechanism of each inhibitor is estimated. They are generally Langmuir-type and the adsorption free energy indicated that these species are linked spontaneously by physisorption.

Since large polarization may induce surface change during the collection of potential – current data, the polarization curves in narrow potential domain were also plotted. It was

- -

found that the large polarization applied for the Tafel extrapolation method does not modify significantly the corrosion potential defined as zero overall current. Thus, it is considered that the perturbation induced by large polarization is negligible in the present case.

The corrosion current density determined by the linear polarization method is in good agreement with the Tafel extrapolation method. Namely in the whole cases, the inhibiting efficiency and the optimal inhibitor concentration were found very close to each other.

The EIS measurements were carried out in the whole inhibitor – corrosion test solution systems. In all cases, impedance spectra can be represented by two capacitive loops, thus so called 2RC circuit, that is the ladder connection of two resistance and capacitance in parallel, together with the electrolyte resistance R_e in series. These impedances are in good agreement with that predicted by theory involving one reaction with cuprous intermediate with reversible process involving the substrate copper and the anodic dissolution process.

The double layer capacitance is two to four times greater than that predicted by theory, and this divergence was explained by the increase of ionic forces at the vicinity of the electrode surface and also by a roughening of electrode surface due to the corrosion process. As a whole, the double layer capacitance obtained is reasonable for the electrode system examined.

R_t decreases slightly in presence of inhibitor except for pH5 solution in presence of TMI and BZI. This variation is explained by the increase of anodic reaction rate in presence of inhibitors according to the Tafel extrapolation method. For the pH5 solution in presence of BZI, this compound induces a mixed corrosion inhibition, thus the anodic reaction rate is also reduced.

- -

The faradaic capacitance C_F, several mF cm^{-2} in absence of inhibitor, generally decreases in presence of inhibitor and becomes even a few ten's of µF cm^{-2}. In presence of inhibitor, the amount of Cu(I) available in the redox process decreases.

As foreseen by theoretical approach, the corrosion current density was estimated from the polarization resistance, sum of the charge transfer resistance and the faradaic resistance. The corrosion current densities estimated from the impedance data are fairly in good agreement with those evaluated from the Tafel extrapolation and the polarization resistance methods. This result corroborates the validity of the model proposed, and also indicates that the use of EIS alone allows the estimation of inhibitory efficiency of imidazole compounds used in this study.

The last statement is of importance for the investigation of the next chapter where the inhibitor effect can be determined only by EIS technique. A *dc* polarization should induce a deep modification of patina covering the bronze surface.

For the protection of patinated bronze, the inhibitor effect should be effective as well in strongly and mildly acidic media, thus PMI cannot be applied. BZI is found to be a good inhibitor for this purpose; however it was found that for long exposure, this substance induces a change in the patina colour. Consequently, TMI is found to be the best candidate to protect bronze objects exposed in urban environment.

- -

5. RESULTS AND DISCUSSION ON BRONZE

COVERED WITH PATINA

In the former chapter, the corrosion and protection of bare Cu-6Sn bronze in artificial acid rainwater (pH 3 and 5) in urban environment were examined. Since the majority of archaeological and cultural bronze artefacts are covered with a patina layer, often dark green to pale green, it appears relevant to study, as well the corrosion and protection of bronze covered with patina, as well as the bare one. Because a quantitative comparison study on natural patina formed during a long period is difficult to carry out and also they are generally unique, we used artificial patinas formed on Cu-6Sn bronze in short period. Three different patina formation procedures, for this sake, were applied: chemical, thermo-chemical, and electrochemical methods. The procedures for the formation of these artificial patinas were described in Chapter 3 devoted to the experimental techniques. The inhibitor examined is 4-methyl-1-*p*-tolylimidazole (TMI). The choice of this inhibitor is based on our former results in which TMI has exhibited good protective effect on electrochemical patina when the patinated specimens were dipped in a mildly acidic sulphate – carbonate medium simulating acid rain in urban environment. [26, 28]

We will examine the morphological observation of the bronze covered by these three patinas by SEM. This study will be completed by the characterization of the patinated bronze surface by EDS and micro-Raman spectroscopy. The time change of the electrochemical impedance spectra in absence and in presence of TMI will be presented. For the bronze covered with electrochemical patina, in addition to TMI, the inhibiting effect of 4-methyl-1-phenylimidazole (PMI) and 1H-benzimidazole (BZI) will be also investigated.

5.1. SULPHATE PATINA FORMED BY CHEMICAL PROCESS

The chemical patina formation was carried out by dipping Cu-6Sn bronze coupons in copper sulphate solution, thus this patina will be called "sulphate patina" for the sake of simplicity. The results concerning Cu-6Sn bronze covered by this chemical patina will be described in this section.

5.1.1 SPECTROSCOPIC MEASUREMENTS ON THE SULPHATE PATINA

The artificial patina thus obtained was dried at room temperature, and its morphology was examined by SEM, and then EDS analyses were carried out on these layers. Micro-Raman spectra were recorded to identify the chemical nature of patina at different positions on the patina surface.

a. SEM Observations
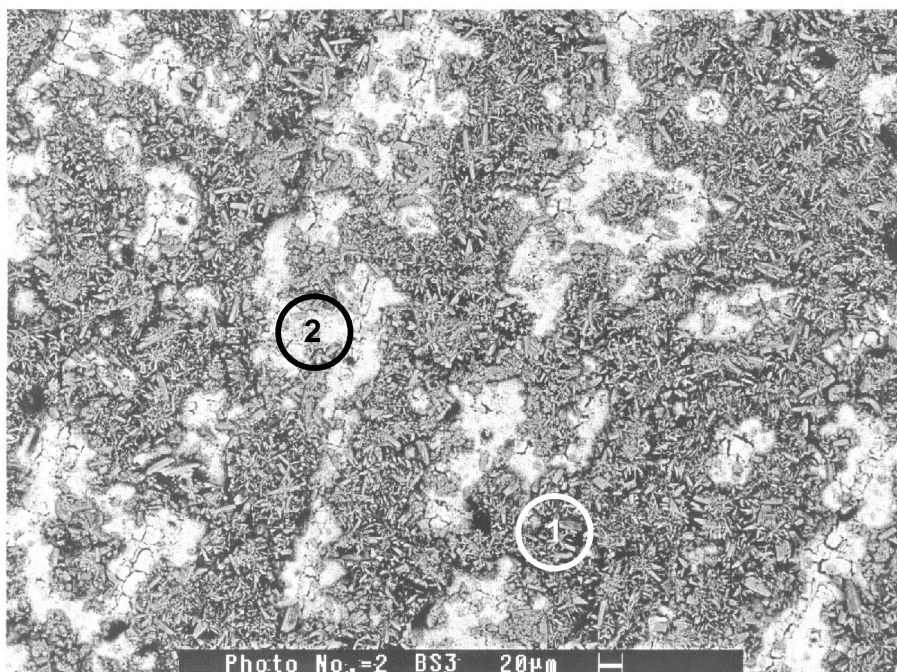
Figure 5.1: SEM image of the sulphate patina.

Fig. 5.1 is the SEM picture showing the surface morphology of the bronze covered by sulphate patina. It can be seen that this patina exhibits two different zones: a dark area covered with crystals in heaps of rod (Fig. 5.1, point 1) and a smooth white layer (Fig 5.1, point 2).

b. EDS Analyses

On these two types of layers, EDS analyses were carried out and the results are presented on Fig. 5.2 and in Table 5.1. The percentages presented here were normalized with respect to the total amount of elements analyzed.
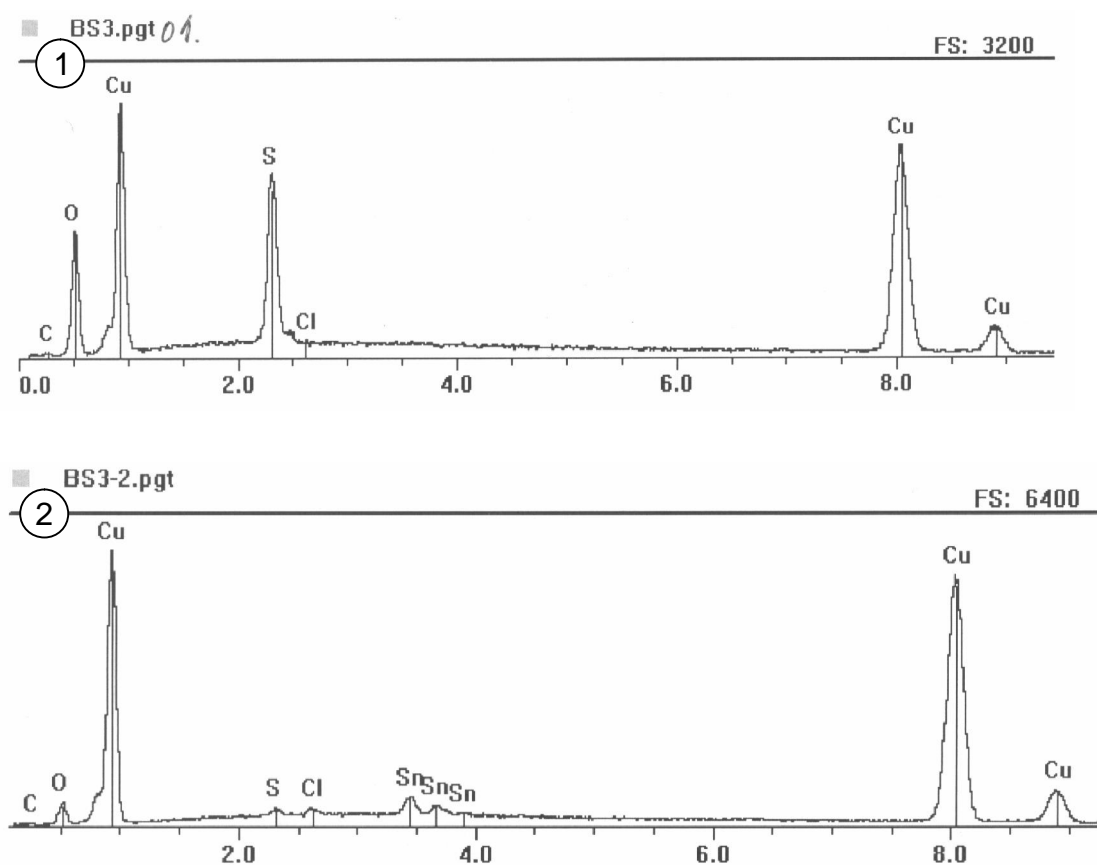
Figure 5.2: EDS analysis of the sulphate patina at the positions

marked 1 and 2 on the SEM image on Fig. 5.1.

Table 5.1: Elemental composition of the two zones marked in Fig. 5.1 on the sulphate patina.

at-%	Cu	O	S	Sn
1	23.0	72.6	4.4	0.0
2	70.5	27.7	0.5	1.3

Percentage normalized with analysed elements

The EDS results (Table 5.1-1) of the crystals in Fig. 5.1, point 1, show that they contain copper (23 at- %), oxygen (73 at-%) and sulphur (4.4 at-%). Presence of a sulphate compound is thus very likely.

The EDS results (Table 5.1-2) of the white surface in Fig. 5.1, point 2, show that this layer consists mainly of copper (70 at-%) and oxygen (27 at-%) with some tin (1.33 at-%). This would indicate that this flat white layer is composed mainly of copper-oxide with some traces of tin-oxide. The copper content is high for the mixture of Cu_2O or $Cu(OH)_2$ and SnO_2. The patina layer at this zone should be thin, since the EDS analyses concern the elemental content of about 1 µm thick, and then the substrate metal should be also detected.

c. Raman Spectroscopy

The obtained Raman spectrum that corresponds to the crystals in point 1 (Fig. 5.3-1) has three main signals: (a) in the highest frequency region (3700 to 3200 cm^{-1}) there are four bands and a shoulder which indicate the presence of OH groups; (b) a narrow and high intensity band at 974 cm^{-1}; which indicates the presence of SO_4^{2-}; and (c) bands due to the bending modes in the 510 to 370 cm^{-1} region. This spectra can be identified as brochantite, $Cu_4SO_4(OH)_6$. [132-134] The atomic composition of this compound for analysed elements (i. e. excluding hydrogen), Cu, O and S are respectively 27, 67 and 6.7 at-%. Therefore, there is a slight extra amount of oxygen, and H_2O is likely associated with brochantite on the patina

layer. The brochantite is monoclinic and actually may form, in addition to a prismatic form, acicular needle like crystals in agreement with SEM observation.
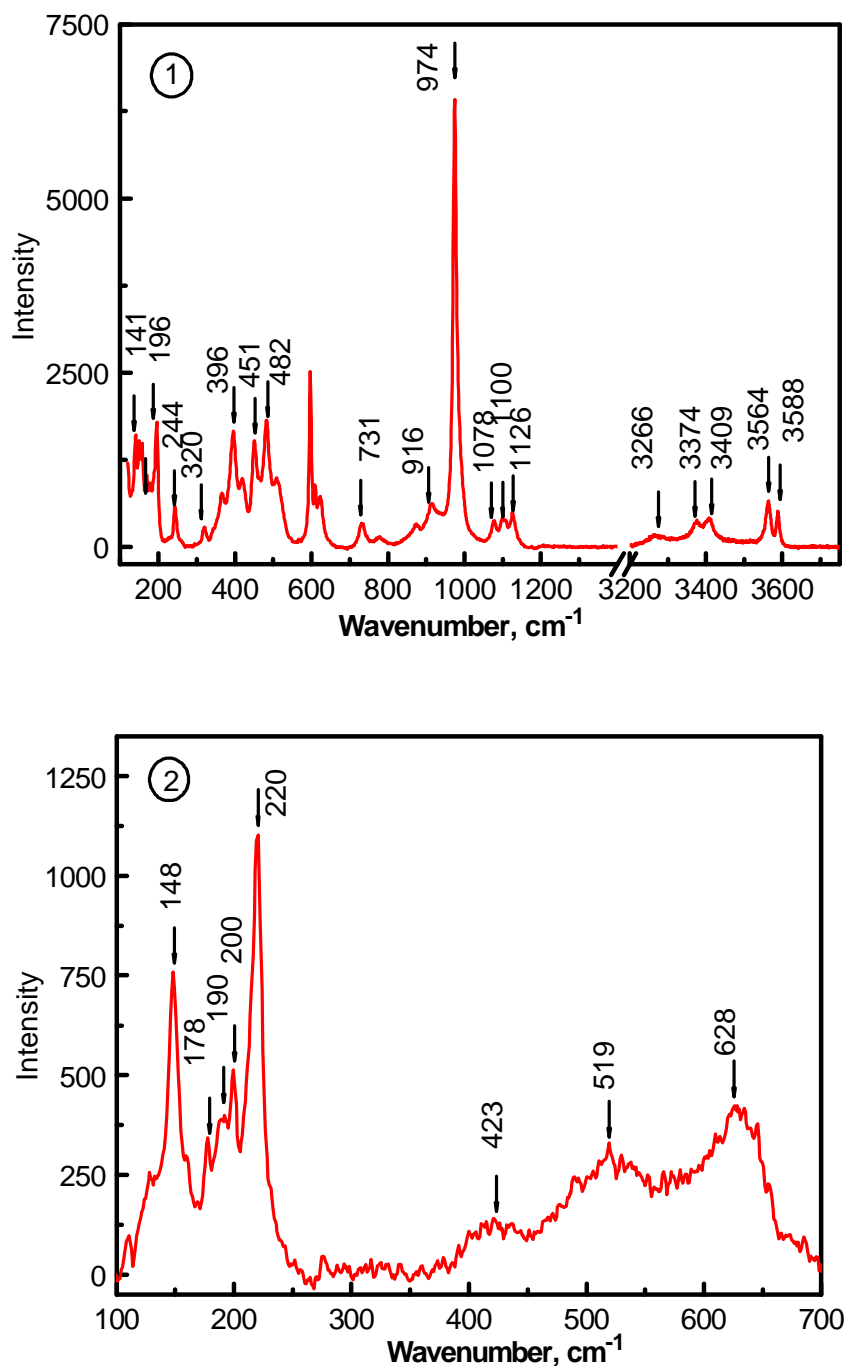
Figure 5.3: Raman spectra recorded on the sulphate patina.

The Raman spectrum corresponding to point 2 (Fig. 5.2-2) has two main groups: (a) two low frequency narrow bands at 148 cm^{-1} and 220 cm^{-1}; and (b) a broad feature in the

frequency range from 300 to 700 cm^{-1} consisting of three large bands at 423, 519 and 628 cm^{-1}. This spectrum can be identified as cuprite, Cu_2O. [135]

5.1.2. ELECTROCHEMICAL ANALYSIS OF THE SULPHATE PATINA

Electrochemical impedance spectra were collected at different immersion periods on the sulphate patina on two series of experiments, one in the solution without inhibitor (blank test solution) and another in the solution containing TMI. The bronze electrodes covered with patina were prepared several days before measurements.

a. Blank Test Solution

A sample of patina was immersed in the corrosion test solution without inhibitor. After one hour of immersion, EIS spectrum was collected each hour for the next 24 hours. Fig. 5.4 displays several impedance spectra obtained.
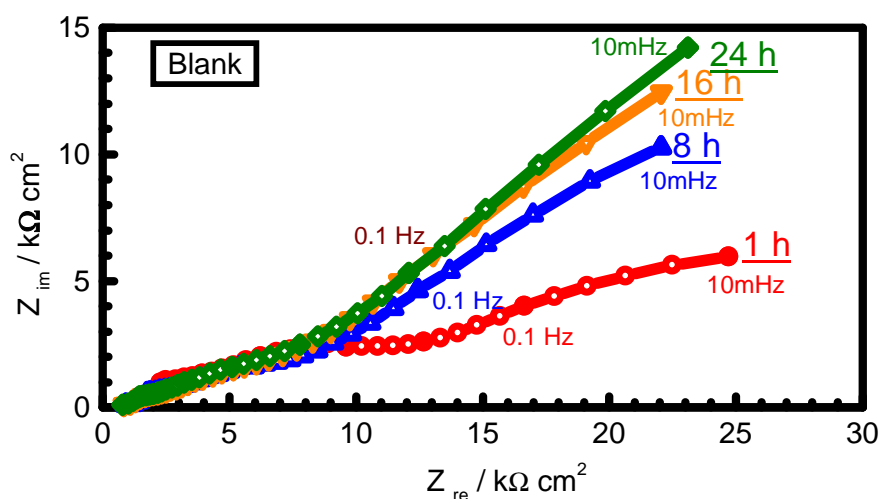
Figure 5.4: Electrochemical impedance spectra of the sulphate patina

in Na$_2$SO$_4$ / NaHCO$_3$ at pH 5 with different immersion time.

It can be seen that in absence of inhibitor the impedance modulus increases slightly with immersion period and the phase angle of the low frequency loop increases.

b. Inhibitor containing Solution

Although all samples were subjected to the same patina formation procedure, slight variations in patina composition of each sample may occur which may reflect in EIS spectra. In order to be able to compare uninhibited and inhibited samples, EIS spectra were also recorded prior to inhibitor application. Sample was immersed in the sulphate / carbonate solution and after one hour stabilization period an impedance spectrum named "Uninhibited" was collected. The sample was dipped out and dried in air. The sample was then dipped again in the corrosion test solution containing 5 mmol·dm^{-3} TMI. EIS spectra were collected every hour for the next 24 hours. Fig. 5.5 shows, as an example, several electrochemical impedance spectra obtained.
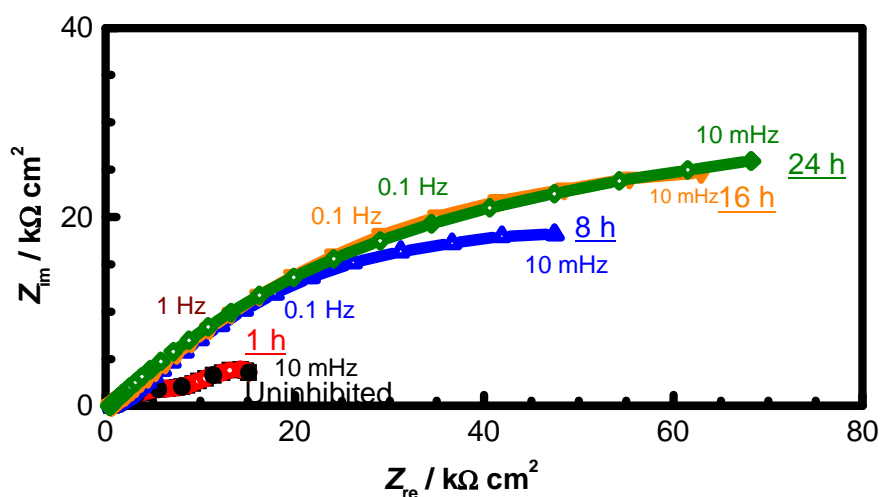
Figure 5.5: Electrochemical impedance spectra of the bronze covered by sulphate patina:

prior to experiments in uninhibited solution (Uninhibited)

and in the solution containing TMI with different immersion time.

In presence of TMI a marked increase of impedance modulus was observed after 8 hours of immersion, after which it grows slightly to stabilize at about 24 hour immersion.

In contrast to the impedance spectra observed with bare bronze, the equivalent circuit with two R-C circuits (Fig. 4.5) does not allow reproducing suitably the impedance spectra obtained, but three capacitive loops are necessary, though only two loops are clearly seen. This additional loop reveals itself at the high frequency side of the impedance diagram. Fig. 5.6 shows the equivalent electrical circuit used.
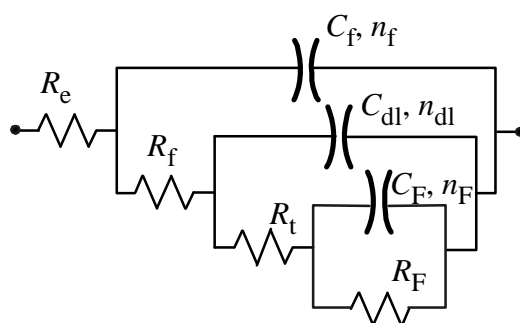
Figure 5.6: Equivalent circuit used for fitting EIS data.

Compared with the equivalent circuit used for the bare bronze specimens (Fig. 4.5), there is one additional parallel R - C couple. Thus, this circuit will be named 3RC. Since this behaviour appears in presence of the patina layer, the origin of this couple is postulated as allocatable to an insulating layer with ionic conduction:

R_f – Resistance representing ionic conduction through the surface film ($\Omega \cdot cm^2$);

C_f – Capacitance due to a dielectric property of the surface film ($F \cdot cm^{-2}$);

n_f – Coefficient representing a depressed feature of R_f - C_f circuit.

The physical origin of other elements is considered to be identical to the case of bare bronze.

Table 5.2 shows the results of the regression calculation of the impedance data obtained on the sulphate patina with the equivalent circuit illustrated.

Table 5.2: EIS data for the sulphate patina in sulphate / carbonate solution

with and without addition of TMI.

	Blank		No inh.	TMI		
t, hours	1	24	1	1	8	24
C_f, nF·cm^2	10	10	20	30	100	300
n_f	0.66	0.74	0.51	0.53	0.55	0.63
R_f, k·cm^2	2.8	1.2	2.0	1.4	1.4	1.4
C_d, µF·cm^{-2}	0.68	2.49	1.39	8.19	5.27	2.99
n_d	0.50	0.52	0.54	0.55	0.55	0.54
R_t, k·cm^2	9.3	6.6	6.2	6.5	7.9	26.2
C_F, µF·cm^{-2}	857	1821	589	65	23	32
n_F	0.50	0.54	0.53	0.54	0.51	0.54
R_F, k·cm^2	27.7	108.6	14.2	26.6	72.6	79.5

The comparison of the values of various elements determined by regression calculation, with respect to those of the bare bronze electrode, indicates clearly that this is the $R_f – C_f$ couple which appears for the patinated electrode, as postulated above. Thus, it can be ascertained that this contribution is closely related to the patina surface.

Values of C_f are between 10 and 300 nF·cm^2. For the uninhibited patina the C_f value does not change, which means that the thickness of this film stays the same during immersion in the solution. If the planar condenser model is assumed, then one can relate the capacitance C and the film thickness d will be linked by Eq. 3.30. Here, the dielectric constant will be close to 10 as for many minerals, and then as a thumb-rule, 10 nm thick layer gives 1 µF cm^{-2}. This thickness corresponding to the sulphate patina layer is too small compared with that estimated from SEM observation, but one may consider that this layer is rather porous with

coarse structure, and only very inner parts form a compact layer giving rise dielectric behaviour.

Sandberg et al. studied the patina runoff of old copper (exposed 200 years in north Europe). [136] They observed two layers, an inner cuprite layer exhibiting about 0.5 to 2.5 $\mu F \cdot cm^{-2}$ according to the marine atmosphere exposure time and outer, mainly brochantite patina layer with 10 to 30 $nF \cdot cm^{-2}$. These capacitance values agree well therefore to a patina layer for C_f. Besides, C_F values are also close to those reported by Sandberg et al.

When patina is dipped into the solution containing TMI, R_t, which decreases in the uninhibited solution, increases significantly. This means, in the light of theoretical approach presented earlier (§3.2.) that the redox process involving oxide layer was slowed down significantly. R_F values increase with immersion time in both blank and inhibitor containing solution, which means that in both cases the patina layer stabilizes with time. Corrosion products covering the electrode surface became more stable by the ageing effect. This can be explained by dissolution of the most reactive species in the electrolyte and by transformation of corrosion products into more stable compounds. As a result, the amount of the corrosion products involved in the redox process becomes smaller. Additionally when TMI is present in the solution, it adsorbs on the top of the oxide layer and reduces the cathodic reaction rate. It can be concluded that TMI protects the sulphate patina by slowing down the corrosion process and stabilizing the oxide layer.

5.2. CHLORIDE PATINA FORMED BY CHEMICAL PROCESS

Similarly to sulphate patina covering bronze specimens, the morphological and structural properties of the chloride patina were analysed by spectroscopic measurements. The corrosion properties were analysed by electrochemical impedance spectroscopy.

5.2.1. SPECTROSCOPIC MEASUREMENTS ON THE CHLORIDE PATINA

The next paragraphs concern the results relative to the chloride patina.

a. SEM Observation

Fig. 5.7 shows the SEM image of the bronze surface covered by patina formed chemically by applying NH_4Cl on a heated alloy coupon.
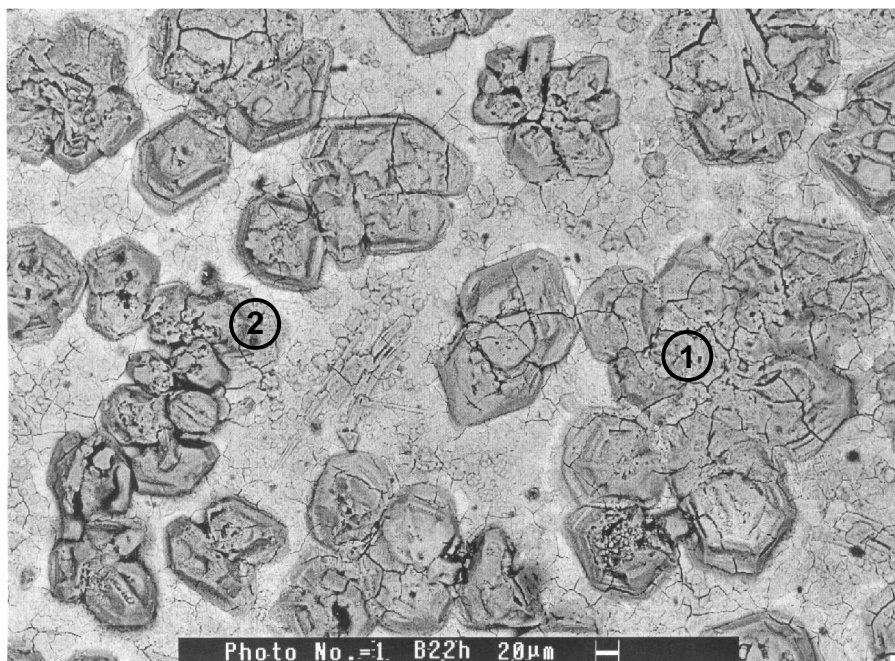
Figure 5.7: SEM image of the chloride patina.

As in the case of the sulphate patina, the bronze surface can be dinstinguished clearly into two areas: a layer formed by crystals (Fig. 5.7, point 1) and a smooth structured layer

(Fig 5.7, point 2). The crystals are much bigger than those observed on the sulphate patina, and seem to have pyramidal shape.

b. EDS Analyses

On these two types of layers, EDS analyses were carried out and the results are displayed on Fig. 5.8.
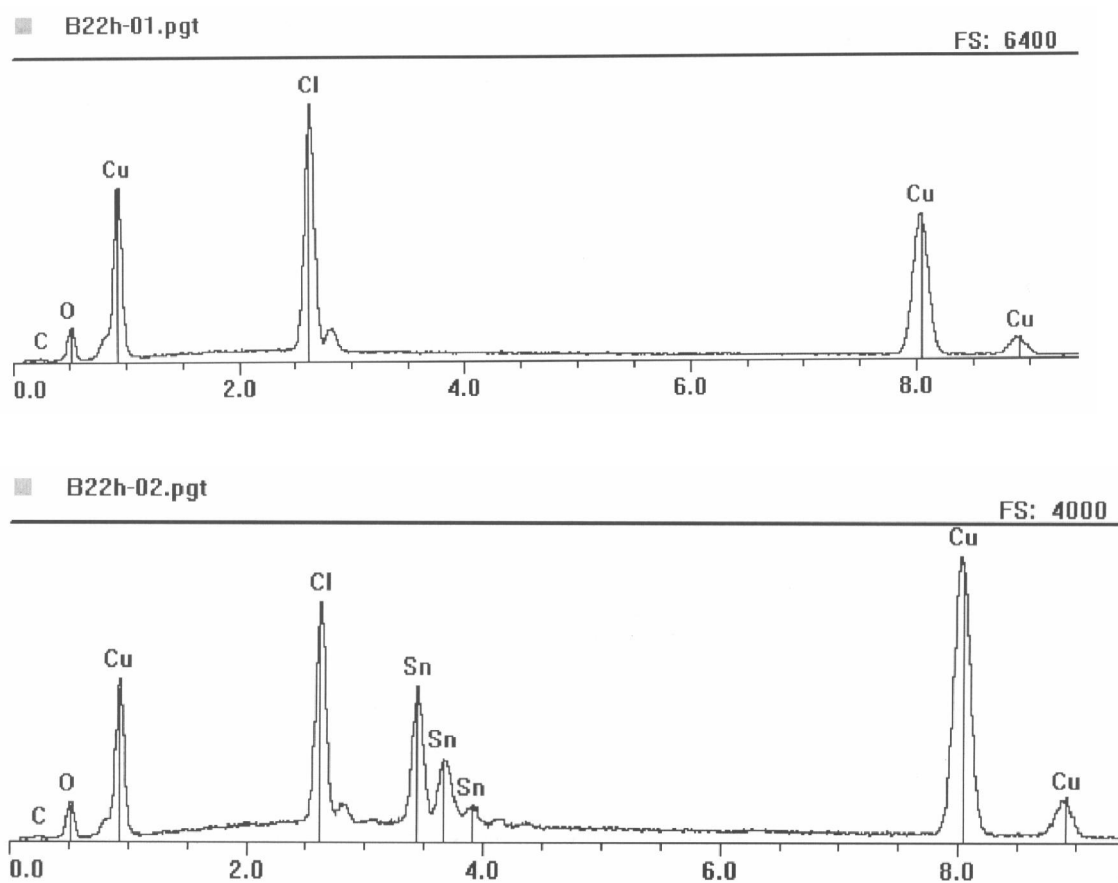
Figure 5.8: EDS analysis of the chloride patina in positions

marked on the SEM image on Fig. 5.7.

Table 5.3-1 summarizes quantitative analysis of EDS spectra. The crystal observed at point 1 contains copper (31 at-%), oxygen (51 at-%) and chloride (18 at-%). It appears that this is an oxy-chloride crystal.

The EDS results (Table 5.3-2) of the flat surface area, point 2, indicate that this layer consists mainly of copper (41 at-%), oxygen (42 at-%), chloride (11 at-%) and tin (5.5 at-%). Therefore, this flat surface may consist of copper-oxide and tin-oxides but also of certain amount of copper and tin chloride compounds.

Table 5.3: Elemental composition of the chloride patina

at different positions according to Fig. 5.7.

at-%	Cu	O	Cl	Sn
1	30.9	50.8	18.3	0.0
2	41.1	42.0	11.4	5.5

Percentage normalized with analysed elements

At point 2, the ratio of metallic element, Sn / (Cu+Sn) is 0.12 whereas the substrate bronze contains 0.033. Thus, there is an enrichment of Sn content. This phenomenon is due to the preferential dissolution of Cu, called also decuprification effect.

c. Raman Spectroscopy

Raman spectroscopy analyses were carried out to refine EDS analyses. The Raman spectrum obtained at point 1 (Fig. 5.7-1) has four main bands: (a) low frequency narrow band at 147 cm^{-1} assigned to OCuO bending modes; (b) intense band at 516 cm^{-1} assigned to CuO stretching vibrations; (c) three intense Raman bands at 971, 915 and 825 cm^{-1}; and (d) two bands at 3440 and 3349 cm^{-1}. This spectrum can be identified as the spectrum of atacamite, $Cu_2Cl(OH)_3$. [132, 137] The theoretical atomic percents of atacamite are as follows: 33 at-% Cu, 50 at-% O and 17 at-% Cl, corresponding well to the experimental data of EDS analysis. There is an additional band at 1049 cm^{-1} which could be assigned to nitrate, NO_3^-, coming

likely from the preparation of the patina. The crystal structure of atacamite is orthorhombic

and its crystal may have dipyramidal shape.
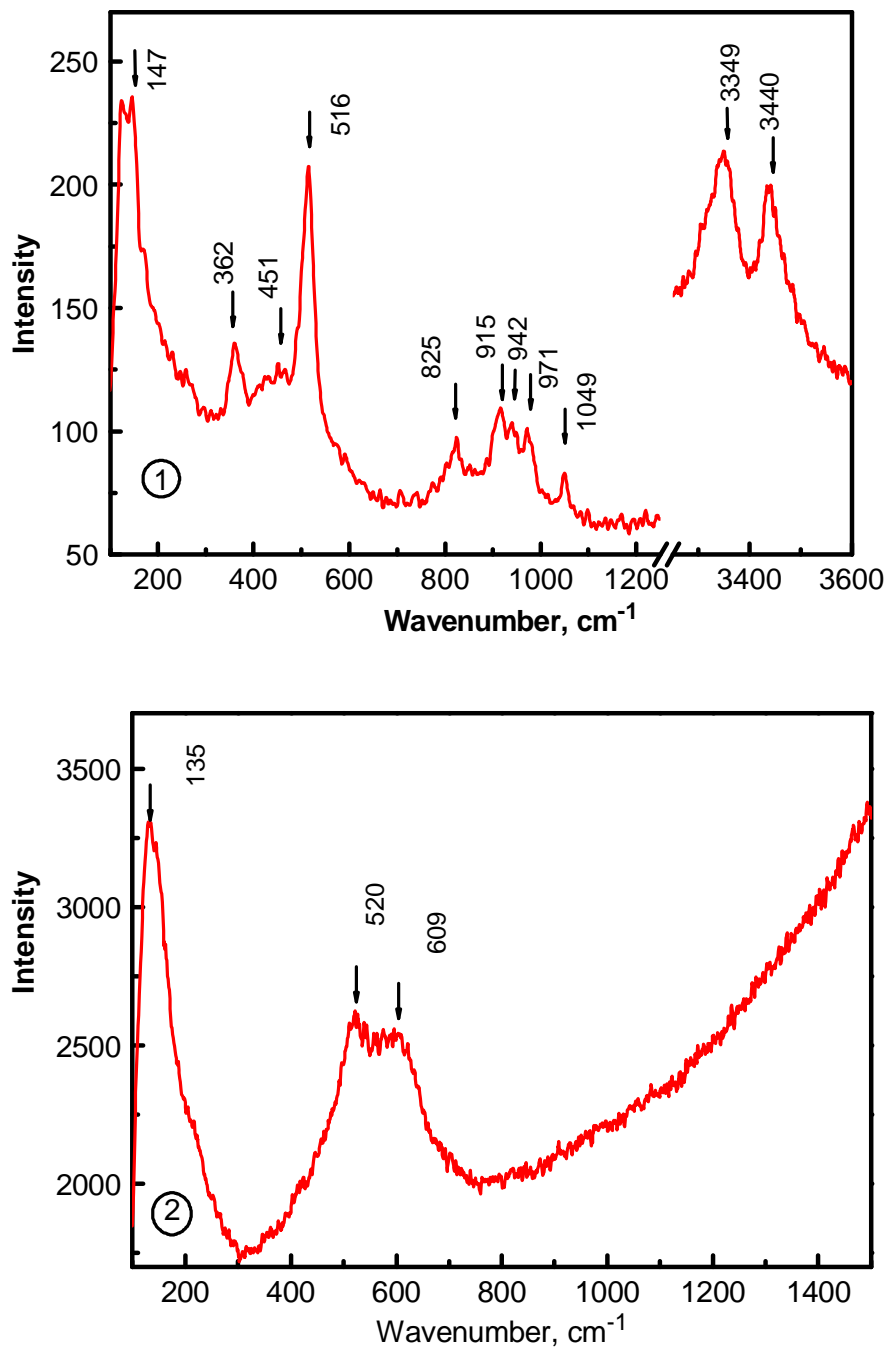
Figure 5.9: Raman spectra recorded on chloride patina

for two zones marked in Fig. 5.7.

The Raman spectrum corresponding to point 2 (Fig. 5.9-2) can be identified as a combination of amorphous Cu_2O, and SnO_2. When Cu_2O is finely divided or amorphous, only two or three broad bands are observed at about 420, 520 and 620 cm^{-1}. [135] When amorphous Cu_2O and SnO_2 are mixed together, several broad bands between 300 and 700 cm^{-1} are observed and it is impossible to separate these two compounds. [138]

Using the two metallic elements identified, and neglecting the chloride content, the theoretical elemental composition of this patina is 37 at-% Cu, 58 at-% O and 5 at-% Sn. It is very likely that this layer contains also some chloride salt in addition to the substrate copper and tin analysed by EDS. The increased content of tin content, compared with the substrate bronze, indicates a selective dissolution of copper similar to the bronze electrode covered by sulphate patina as stated earlier.

5.2.2. ELECTROCHEMICAL ANALYSIS OF THE CHLORIDE PATINA

Electrochemical impedance spectra were collected in different solutions, blank and inhibitor containing one, and at different immersion periods on the bronze electrode covered by chloride patina on two samples, prepared several days before the measurements.

a. Blank Test Solution

A sample of patinated bronze was immersed in the sulphate / carbonate test solution without inhibitor acidified to pH5 by addition of dilute sulphuric acid at room temperature. After 1 hour of immersion an EIS spectra were collected every hour for the next 24 hours. The results are presented in Fig. 5.10-a.
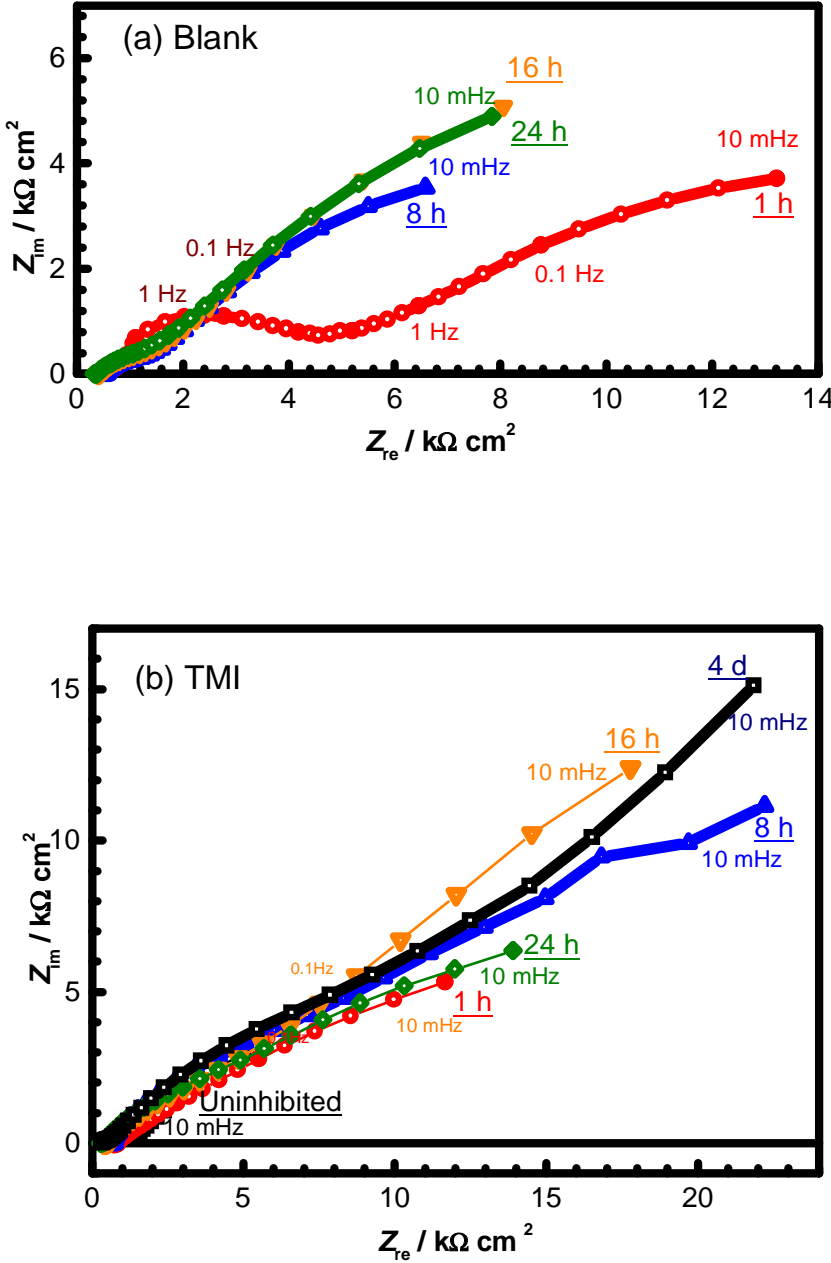
Figure 5.10: Electrochemical impedance spectra obtained on the chloride patina:

a) in blank solution and b) prior to experiments in uninhibited solution (Uninhibited)

and in the solution containing TMI for different immersion times.

b. Inhibitor containing solution

EIS spectrum was recorded prior to inhibitor addition. A sample was immersed in the sulphate / carbonate solution and after the one hour stabilization period an impedance spectrum named "Uninhibited" was collected. The sample was dipped out and dried in air. The same sample was then dipped again in the sulphate / carbonate solution, in this case containing 5 mmol·dm^{-3} TMI. EIS spectra were collected every hour for the next 24 hours. The results are displayed in Fig. 5.10-b.

It can be seen that in absence of TMI, the diameter of the impedance loop decreases with immersion time. In contrast, when TMI is present, even at 1 hour of immersion, a substantial increase in impedance modulus is evidenced, which further grows with immersion period. However, after reaching the maximum impedance loop after 8 hours, it decreases. An additional measurement was performed after 4 days immersion to discriminate if the protection is lost or if TMI remains protective to the bronze covered with the chloride patina. The impedance diagram of "4 days" shows clearly that the system was undergoing stabilization and TMI effectively protects the patinated bronze.

Table 5.4 shows the results of the regression calculation of the impedance data obtained on the chloride patina with 3RC equivalent circuit illustrated on Fig. 5.6.

Table 5.4. EIS data for the chloride patina in Na_2SO_4 / $NaHCO_3$

with and without addition of TMI.

	Blank		**No inh.**	**TMI**			
t, hours	**1**	**24**	**1**	**1**	**8**	**24**	**4×24**
C_f, µF·cm^2	0.04	0.67	0.06	2.22	0.95	0.20	0.11
n_f	0.65	0.55	0.75	0.54	0.50	0.53	0.67
R_f, k ·cm^2	4.0	0.2	0.2	0.5	0.5	0.1	0.3
C_d, µF·cm^2	19.6	2.8	4.4	24.8	27.8	21.5	58.6
n_d	0.64	0.61	0.54	0.52	0.55	0.61	0.56
R_t, k ·cm^2	2.5	1.0	0.7	4.7	36.9	7.3	19.7
C_F, µF·cm^2	1212	6179	3553	706	2654	809	1095
n_F	0.52	0.50	0.60	0.54	0.80	0.62	0.69
R_F, k ·cm^2	15.5	44.3	13.0	20.9	74.9	21.1	100.0

R_t decreases with immersion time when TMI is not present. In contrast, in presence of TMI, R_t increases markedly even after one hour of immersion, and then exhibits a maximum at 8 hours. After that it decreases up to 24 hours. However, after 4 days immersion in this inhibitor containing medium, R_t showed again a high value. This means that the redox process involving the surface cuprite layer and / or the cathodic reaction rate are significantly slowed down in presence of TMI, while in its absence these reaction rates increase with time. The R_F values grow with immersion time for both media, indicating that immersion leads to stabilization of the patina layer. In presence of TMI, R_F grows with time and reaches the highest value after four days. It can be concluded that TMI protects the bronze covered by chloride patina by slowing down the corrosion process. For both solutions, C_f values are similar to those observed with bronze specimens covered with sulphate patina, and R_f values

decrease slightly. TMI slows down the corrosion rate of the inner patina layer, as this is the case for the electrode covered by sulphate patina. C_F increases with immersion time indicating an accumulation of redox species, this behaviour is very different from the former case. The presence of chloride, even in a small content, may explain the difference observed on the oxide layer covering the bronze surface.

5.3. ELECTROCHEMICAL PATINA

The patina was synthesized in sulphate – carbonate solution by potentiostatic regulation on Cu-6Sn electrode. Its morphology and structural properties were analysed by spectroscopic measurements. The anticorrosion effect of TMI, PMI and BZI were examined by electrochemical impedance measurements.

5.3.1. SPECTROSCOPIC MEASUREMENTS ON THE ELECTROCHEMICAL PATINA

The electrochemical patina was dried at room temperature, and its morphology was examined by SEM, and then EDS analyses were carried out on these layers. Micro-Raman spectra were recorded to identify the structure of patina at different positions on the patina surface.

a. SEM Observations

Fig. 5.11 shows the SEM image of the bronze surface covered by electrochemically formed patina.
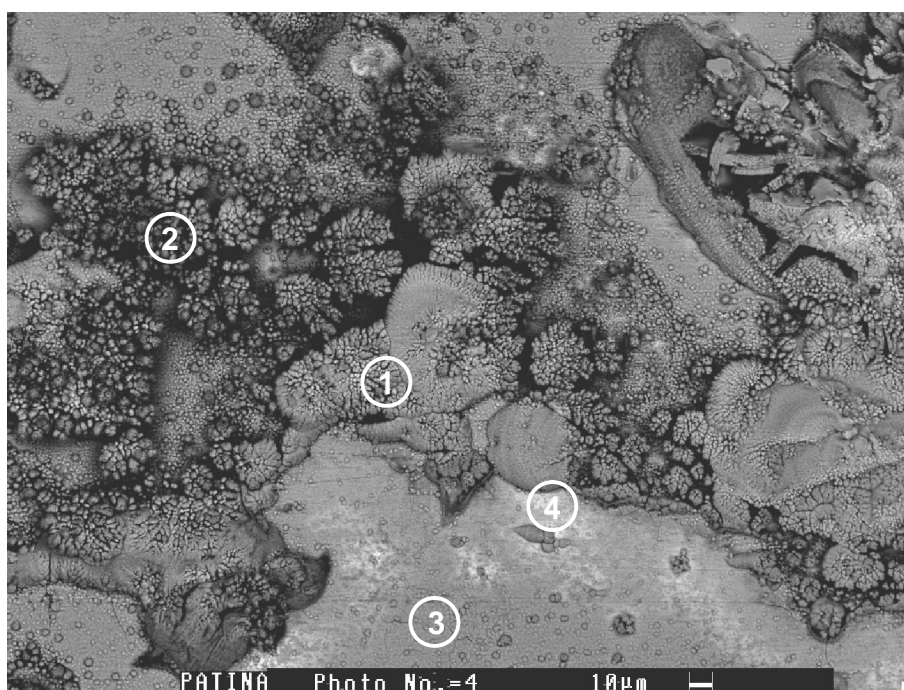
Figure 5.11: SEM image of the electrochemical patina.

This picture shows four morphologically different zones: two different features of crystals, (points 1 and 2) and two smooth zones with dark surface (point 3) and white surface (point 4). The crystals observed at points 1 and 2 are similar in shape, and consist of a heaping of small rounded shape.

b. EDS Analyses

EDS analyses were carried out on these four zones and they are presented on Fig. 5.12 and in Table 5.5. It is important to note that the carbon was not analyzed, as usual for EDS analyses.
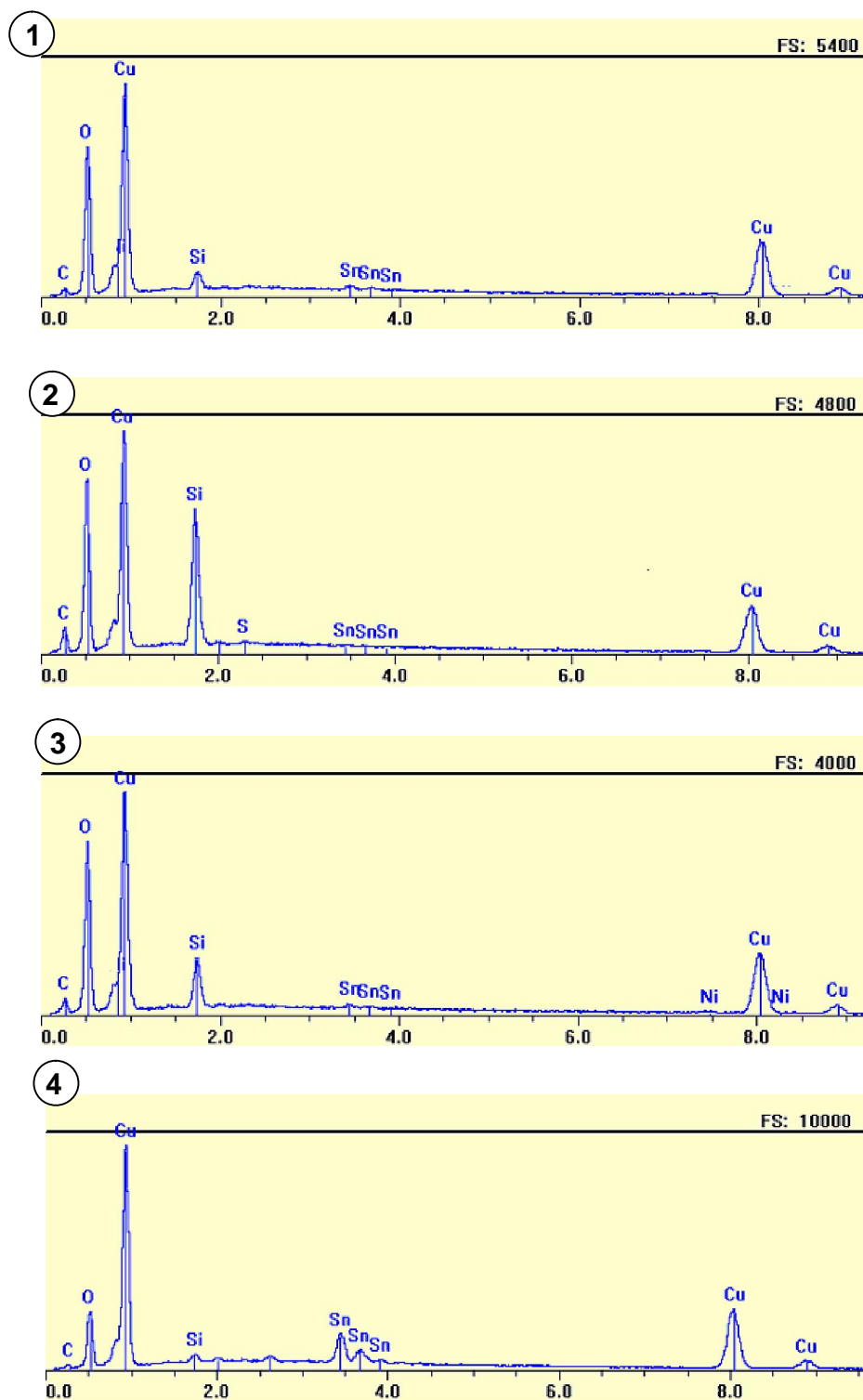
Figure 5.12: EDS analysis of the electrochemical patina in positions

marked on the SEM image on Fig. 5.11.

Table 5.5: Elemental composition in at-% of the bronze covered by electrochemical patina at different positions according to Fig. 5.11.

Points	Cu	O	S	Sn
1	28.3	71.5	0.2	0.0
2	34.3	65.5	0.0	0.1
3	34.9	64.9	0.0	0.2
4	52.0	43.8	0.0	4.2

Percentage normalized with analysed elements

Fig. 5.12 shows in some cases the presence of silicium. This is due to the contamination with the polishing paste. Because it is not relevant for our research it has been discarded for the quantitative analyses presented in Table 5.5.

The EDS results of the crystals in Fig. 5.11, point 1 (Table 5.5-1) show that they contain in atomic per cent, copper (28), oxygen (72) and sulphur (0.2), while the crystals at point 2 (Table 5.5-2), copper (34), oxygen (66) and tin (0.1) were detected. These results suggest that some kind of oxide is present. However, the oxygen content is high, therefore, considering the synthesis medium, the formation of a carbonate salt is very possible (note that the band corresponding to C is rather high, though quantitative analysis of this element is impossible.

The EDS results of the darker smooth layer, point 3 (Table 5.5-3) indicate that this zone contains copper (35), oxygen (65) and a small amount of tin (0.2), while the white smooth layer, point 4 (Table 5.5-4) contains copper (52), oxygen (44) and tin (4). The theoretical copper concentration calculated by supposing the surface species is a mixture of Cu_2O and SnO_2 and considering Cu and Sn are determined correctly, then the expected Cu content is 66 and 60 at-% respectively for the points 3 and 4. The experimental copper

concentration is thus markedly lower than those evaluated from the formation of anhydrous oxide. Consequently, the formation of Cu(OH) is quite possible which explains the presence of high amount of oxygen. At point 4, the Sn content for metallic elements Sn / (Cu+Sn) is 7.4 at-%, thus there is an enrichment of Sn at this area. The decuprification process is also detected as this was the case for the chloride patina.

c. Raman Spectroscopy

The Raman spectra corresponding to the crystal at point 1 is presented in Fig. 5.13-a. This spectrum allocates the crystal observed as malachite, $CuCO_3 \cdot Cu(OH)_2$. There was no spectrum that could confirm the presence of sulphate-crystals probably due, in one hand to the fact that the sulphate corrosion products were badly crystallized, and also its atomic content is very low since copper sulphate is soluble in aqueous medium. The theoretical atomic percentage of malachite, ignoring the presence of carbon is 29 and 71 at-% respectively for copper and oxygen, in a good agreement with the values given above. The crystal structure of malachite is monoclinic, and a similar crystals form was observed for the natural malachite minerals.

The Raman spectrum obtained at the smooth surface (point 3) is presented in Fig. 5.13-b. It exhibits some similar characteristics to spectra observed in Figure 5.9-2: (a) two low frequency narrow bands at 149 cm^{-1} and 216 cm^{-1}; and (b) a broad feature in the frequency range from 700 to 300 cm^{-1} consisting of three large bands at 431, 528 and 641 cm^{-1}. This spectrum indicates that this layer contains cuprite, Cu_2O. [139] The presence of a mixture of cuprite with SnO_2 cannot be discarded since the main bands belonging to SnO_2 and Cu_2O are located very close to each other.
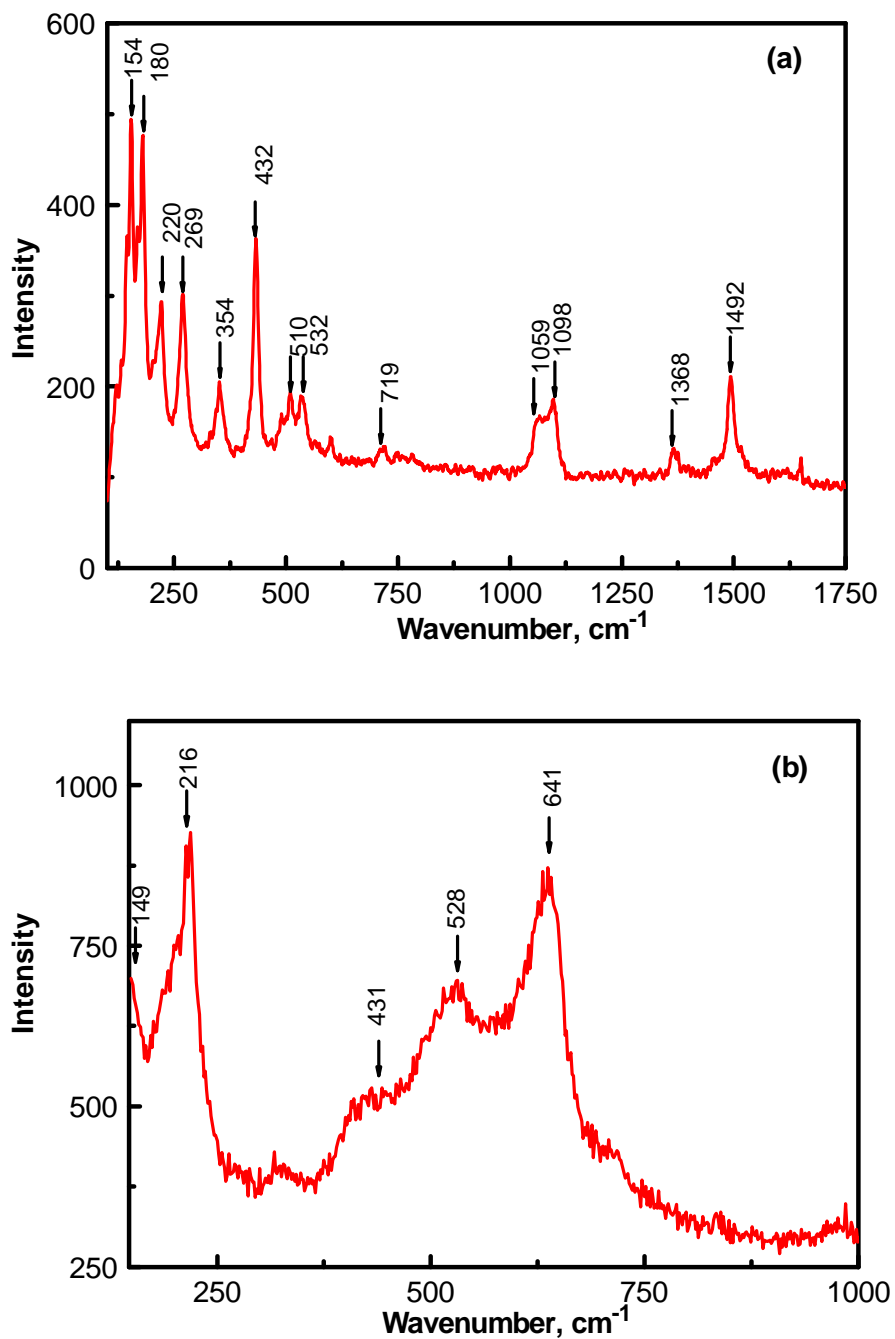
Figure 5.13: Raman spectra recorded on the bronze covered by electrochemical patina

at the positions 1 (diagram a) and 3 (diagram b) respectively

5.3.2. EIS MEASUREMENTS TO EXAMINE THE PROTECTIVE EFFECTIVENESS OF TMI

Electrochemical impedance spectra were collected with two samples in the corrosion test solution with or without TMI at different immersion periods.

a. Blank Test Solution

A bronze covered with the electrochemical patina was immersed in the corrosion test solution without inhibitor at pH5. After one hour of immersion EIS spectra were collected every hour for the next 24 hours. The Nyquist diagram of impedance spectra are presented in Fig. 5.14-a.

b. Inhibitor Containing Solution

An EIS spectrum was recorded prior to inhibitor application: the patinated bronze electrode was dipped into the sulphate / carbonate solution and after one hour stabilization period an impedance spectrum named "Uninhibited" was collected. The sample was dipped out and dried in air, then dipped again in the corrosion test solution containing 5 mmol·L^{-1} TMI. EIS measurements were carried out every hour for the next 24 hours. Fig. 5.14-b shows the electrochemical impedance spectra obtained in the solution containing by 5 mM TMI.

In absence of TMI, a rather well marked depressed capacitive loop can be seen in the high frequency domain followed by a highly depressed capacitive loop. In presence of inhibitor, the impedance behaviour remains capacitive, but no marked loop can be distinguished. It was found however that three capacitive loops are necessary to reproduce suitably the EIS spectra. Thus 3RC circuit was adopted for the regression calculation procedure.
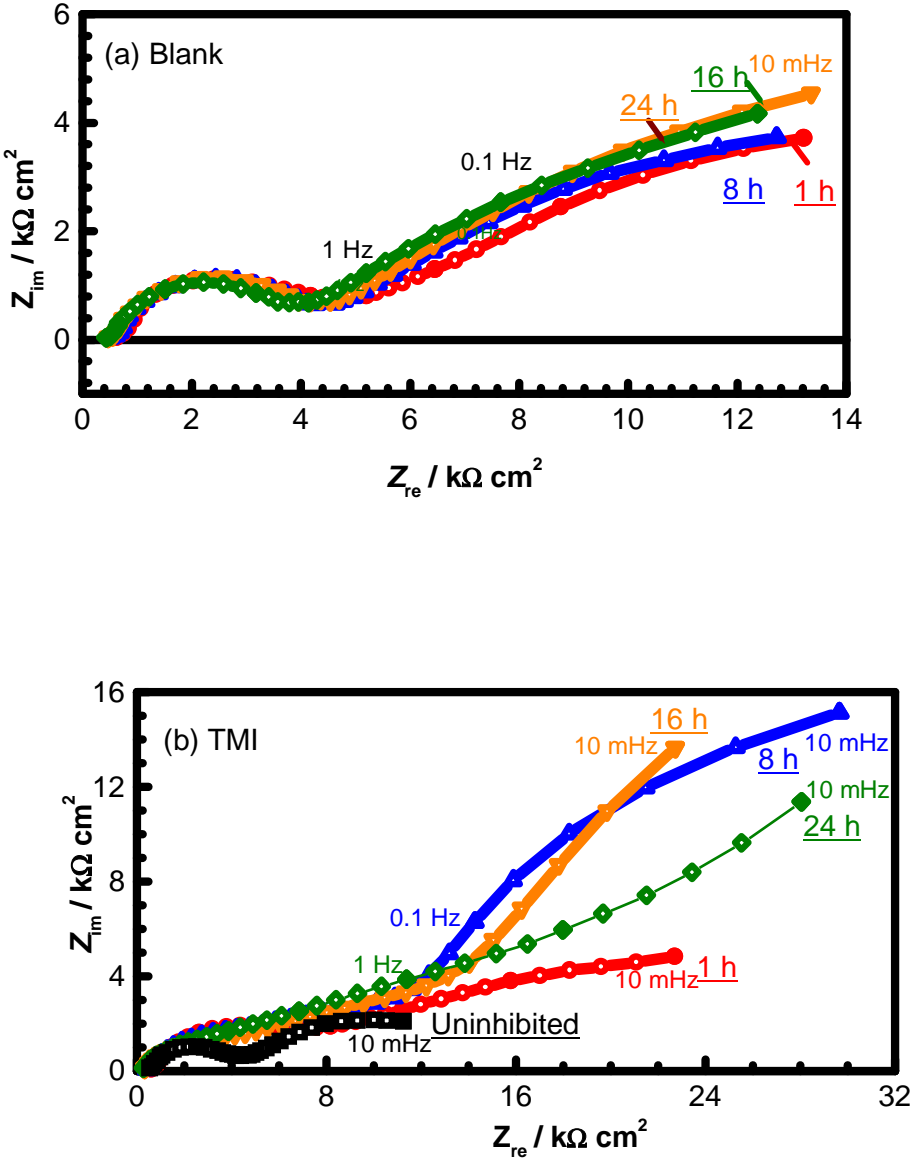
Figure 5.14: Electrochemical impedance spectra obtained on the electrochemical patina: a) in blank solution and b) prior to experiments in uninhibited solution (Uninhibited) and in the solution containing TMI for different immersion times.

Table 5.6 shows the results of the regression calculation of the impedance data obtained on the electrochemically patinated bronze according to 3RC circuit.

Table 5.6: EIS data for the electrochemical patina in Na₂SO₄ / NaHCO₃

with and without addition of TMI.

	Blank		No inh.	TMI		
t, hours	1	24	1	1	8	24
C_f, µF·cm²	0.02	0.09	0.01	0.03	0.25	0.16
n_f	0.77	0.74	0.96	0.80	0.56	0.50
R_f, kΩ·cm²	3.1	2.8	0.9	2.9	6.9	6.8
C_d, µF·cm²	4.77	6.49	0.07	0.21	16.94	23.42
n_d	0.55	0.57	0.61	0.67	0.60	0.50
R_t, kΩ·cm²	2.7	2.0	3.0	4.6	8.0	17.9
C_F, µF·cm²	795.3	855.7	397.1	141.0	298.3	1194
n_F	0.55	0.54	0.50	0.50	0.80	0.65
R_F, kΩ·cm²	14.2	16.3	9.9	19.5	43.2	54.1

To ascertain the protective effect of TMI for a longer period, the experiments were continued up to 8 days. The EIS spectra obtained are presented on Fig. 5.15.
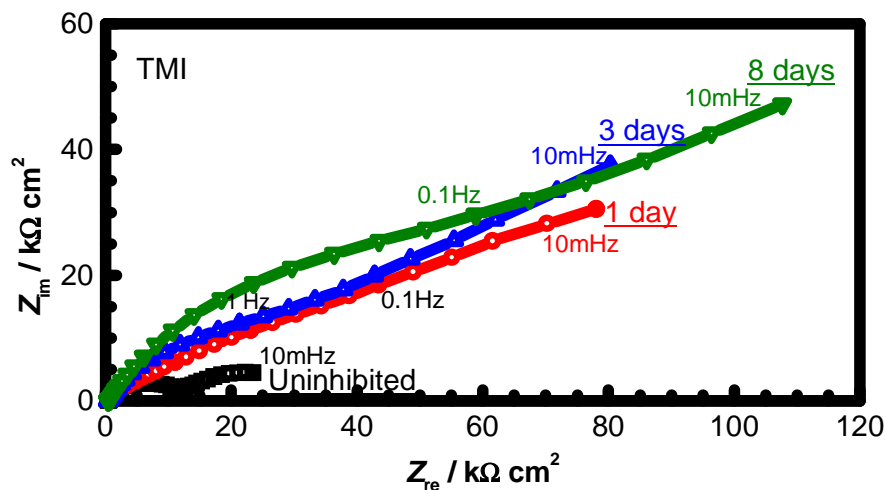
Figure 5.15: Electrochemical impedance spectra for the electrochemical patina in the

solution containing TMI with different immersion time.

The results of regression calculation with 3RC circuit are summarized in Table 5.7.

Table 5.7: EIS data for the electrochemical patina

in Na_2SO_4 / $NaHCO_3$ with and without addition of TMI.

No. of days	/	1	3	8
C_f, µF·cm^2	0.24	0.23	0.46	3.43
n_f	0.80	0.84	0.83	0.61
R_f, kΩ·cm^2	5.69	2.99	0.68	0.43
C_d, µF·cm^{-2}	1.10	0.10	0.11	4.13
n_d	0.86	0.50	0.51	0.67
R_t, kΩ·cm^2	4.6	51.1	70.0	78.9
C_F, mF·cm^{-2}	0.11	0.08	0.14	0.08
n_F	0.50	0.87	0.89	0.82
R_F, kΩ·cm^2	19.7	60.1	82.3	84.3

From the data presented in Tables 5.6 and 5.7, it can be seen that the value of C_f increases with immersion period, from 0.03 to 3.4 $\mu F \cdot cm^{-2}$. With the thumb's rule presented earlier, these values correspond to the film thickness changing from 300 to 3 nm. At the same time, R_f decreases from ca. 3 to 0.4 $k\Omega \cdot cm^2$, the resistivity of the surface film changes thus from 10^8 to 10^9 $\Omega \cdot cm$. The inner patina layer is thus to be considered as semi-conductor.

The charge transfer resistance, R_t, which was 3 $k\Omega \cdot cm^2$ before addition of 5 mM TMI increased to 4.6 $k\Omega \cdot cm^2$ after one hour of immersion and becomes as high as 80 $k\Omega \cdot cm^2$ after eight day immersion. The redox kinetics of surface oxide decrease significantly with the immersion time.

R_F increases significantly with immersion time, whereas C_F remains almost constant. The cathodic reaction taking place upon the electrode surface slows down with immersion time, that is, TMI hinders markedly the cathodic reaction rate. On bare bronze, it was observed on the Tafel plot (cf. Fig 4.9) that, for one hour immersion, TMI makes the cathodic reaction about 100 times smaller. The inhibiting effect of TMI to the cathodic reaction seems to be reinforced with the increase of immersion time. C_F remains almost constant, as stated above, therefore, the amount of copper oxide involving the redox process does not change significantly with immersion time, whilst R_t increases. The oxide film lost its reactivity with time in agreement with the hindering of the cathodic process.

5.3.3. EIS Measurements to examine the Protective Effectiveness of PMI

The influence of 10 $mmol \cdot dm^{-3}$ PMI with immersion time on the EIS spectra of the electrochemically patinated Cu-6Sn bronze, in 0.2 $g \cdot dm^{-3}$ Na_2SO_4 + 0.2 $g \cdot dm^{-3}$ $NaHCO_3$ at pH 5, is presented on Fig. 5.16.
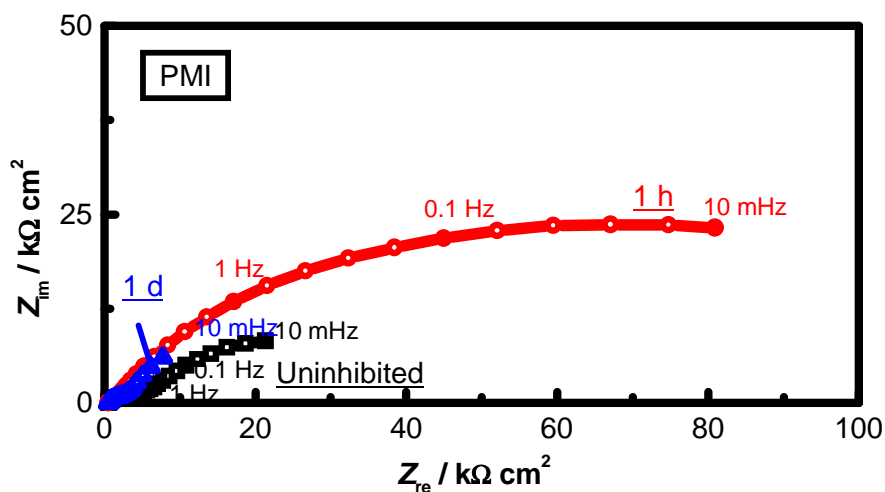
Figure 5.16: Electrochemical impedance spectra obtained on the electrochemical

patina in the solution containing PMI. No inhibitor refers an experiment

carried out without inhibitor on the same electrode.

Table 5.8 shows results of the regression calculation by a Simplex method with 3RC circuit.

C_f increases with immersion time indicating a thinning of the surface layer. In contrast, addition of PMI does not modify significantly the R_f value. Therefore, this molecule does not modify the barrier properties of the surface film.

Medium frequency circuit R_t-C_d corresponds to the charge transfer resistance and the double layer capacitance. R_t increases significantly in presence of PMI after one hour, therefore the redox process involved in $R_F - C_F$ couple slows down dramatically. In other words, PMI allows the stabilization of patina layer leading to the protection of the substrate bronze. Unlike after one hour, after one day R_F value decreases again, indicating that the inhibitor looses its protection ability. It is important to recall that PMI has no protective effect

towards the bare bronze electrode in pH5 solution. This corresponds to a small change of R_F after one hour immersion and its marked decrease after one day of immersion.

Table 5.8: EIS data for Cu-Sn covered by electrochemical patina

in Na₂SO₄ / NaHCO₃ with and without addition of PMI.

	No inh.	PMI	
t, hours	1	1	24
C_f, µF·cm^2	0.12	0.03	4.93
n_f	0.53	0.83	0.51
R_f, k ·cm^2	3.20	0.739	0.255
C_d, µF·cm^2	2.1	10.6	3.1
n_d	0.93	0.60	0.88
R_t, k ·cm^2	1.5	65.5	3.9
C_F, µF·cm^2	744	182	1154
n_F	0.50	0.57	0.90
R_F, k ·cm^2	41.3	54.9	16.4

5.3.4 EIS MEASUREMENTS TO EXAMINE THE PROTECTIVE EFFECTIVENESS OF BZI

The inhibiting effect of 5 mmol·dm^{-3} BZI with immersion time on the EIS spectra of the electrochemically patinated Cu-6Sn bronze, in the corrosion test solution is presented on Fig. 5.17.
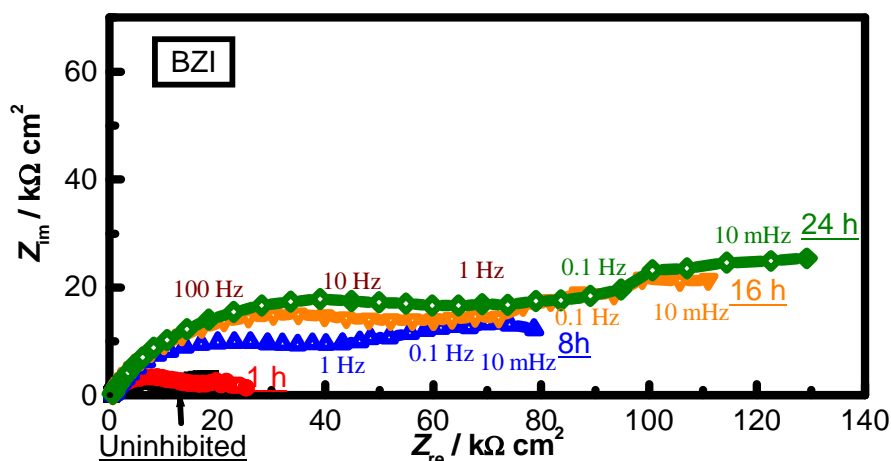
Figure 5.17: Electrochemical impedance spectra obtained on the bronze covered by electrochemical patina: prior to experiments in uninhibited solution (Uninhibited) and in the solution containing BZI for different immersion time.

It can be seen that in presence of BZI, the size of the impedance loop grows with time. It continues to increase even after 24 hours. The inhibitive effect improves with immersion time. By regression calculation on these spectra, let us examine what parameters will be more determining to this protective effect. Table 5.9 shows the results of the regression calculation of the impedance data with 3RC equivalent circuit.

Both R_f and C_f values decrease with immersion time in the solution containing BZI. That is, the surface layer becomes thicker but looses its barrier property. As for R_t, it increases with immersion time in presence of BZI. That is, this compound slows down the electrochemical processes taking place at the electrode surface. The same variation can be observed for R_F values which continuously grow with immersion time in the inhibited solution. BZI leads to the stabilization of patina with immersion time. It can be concluded that BZI protects Cu-6Sn bronze covered by electrochemical patina by stabilizing the oxide layer,

as well as by slowing down the rate of cathodic reaction leading to the improvement of the protective effect of BZI.

Table 5.9: EIS data of electrochemical patina in Na₂SO₄ / NaHCO₃ solution

with and without addition of BZI.

	No inh.	BZI	
t, hours	**1**	**8h**	**24**
C_f, µF·cm^2	0.04	0.06	0.01
n_f	0.71	0.67	0.86
R_f, k ·cm^2	3.0	2.8	1.3
C_d, µF·cm^2	0.51	2.18	0.09
n_d	0.55	0.54	0.51
R_t, k ·cm^2	8.2	24.8	73.0
C_F, µF·cm^2	501.4	121.3	73.5
n_F	0.55	0.54	0.54
R_F, k ·cm^2	11.7	45.5	95.9

5.4. PARTIAL CONCLUSIONS OF THE CHAPTER

Three types of patinas were prepared on the copper-tin binary alloy (Cu-6Sn) according to different patina formation procedures: chemical (*sulphate patina*), thermo-chemical (*chloride patina*) and electrochemical method (*electrochemical patina*). The morphology and the structure of these three patinas were examined by SEM, EDS and Raman spectroscopy. The results obtained with these experiments are consistent qualitatively as well as quantitatively.

The SEM pictures have shown that all three patinas consist of different zones: smooth parts and crystals. For all patinas, the smooth structure was identified by EDS and Raman spectroscopy to consist mainly of cuprite, Cu_2O. As for the crystals, the sulphate patina consist of brochantite, $Cu_4SO_4 \cdot (OH)_6$, the chloride patina of atacamite, $Cu_2Cl(OH)_3$, and the electrochemical patina of malachite, $CuCO_3 \cdot Cu(OH)_2$. The crystal shapes, observed by SEM, are in agreement with this identification. The EDS results have also shown that on the chloride and electrochemical patina an enrichment of tin, the decuprification process, takes place.

On all three patinas, the corrosion protection effectiveness of 4-methyl-1-*p*-tolylimidazole (TMI) was investigated by electrochemical impedance measurements. The obtained data were fitted with three parallel capacitance and resistance couples connected in ladder circuit. That is, compared with the electrical circuit used for the bare bronze electrode, an additional capacitive loop is necessary to reproduce suitably experimental EIS spectra. This additional loop reveals at the high frequency side of the impedance diagram, and is allocated to the barrier property of the patina layer.

The results of the EIS measurements have shown that TMI protects the bronze patinated by all three methods. It adsorbs on the top of the oxide layer of the sulphate patina, and reduces the cathodic reaction rate, which means that it slows down the corrosion process and stabilizes the oxide layer. On the chloride patina, TMI also slows down the corrosion rate of the inner patina layer, but in this case an accumulation of redox species takes place. For the electrochemical patina, TMI also hinders the cathodic corrosion rate. It can be concluded that in all three cases TMI acts by slowing down the cathodic corrosion rate.

Additionally, 4-methyl-1-phenylimidazole (PMI) and 1-H benzimidazole (BZI) were investigated as corrosion inhibitors for electrochemical patina. The results of the investigations concerning PMI have shown that this molecule allows the stabilization of the patina layer leading to the protection of the substrate bronze, but only for a short period. After one day, the inhibitor looses its protection ability. As in the case for bare bronze, PMI cannot be recommended as a corrosion inhibitor.

Unlike PMI, the investigations concerning BZI have shown that this molecule slows down the electrochemical process taking place at the electrode surface by stabilizing the oxide layer, as well as by slowing down the rate of the cathodic reaction.

6. CONCLUSIONS

The bronze statues, exposed in urban area, are damaged substantially by acid rain due to the direct effect of increasing air pollution. One of the mitigation methods to this problem is the use of a corrosion inhibitor. Therefore, three non-toxic inhibitors based on imidazole compounds were examined. As for the corrosion test medium, two solutions were used; a strongly acidic solution consisting of 0.2 g dm^{-3} Na$_2$SO$_4$ + 0.2 g dm^{-3} NaHCO$_3$, acidified to pH 3, that can be observed at the beginning of rain fall due to many pollutants accumulated at the bronze surface, and the same solution, in this case acidified to pH 5, corresponding to the typical acid rain. The absence of chloride in these test solutions is representative of urban area far from seaside.

The present dissertation was divided into four chapters in addition of the Introduction. Main statements presented in these chapters can be summarized as follows.

6.1 THEORETICAL APPROACH ON CORROSION OF BRONZE BY ACID RAIN

In Chapter 2, the physical and chemical properties of copper and its alloys are briefly described and their nomenclatures are given. At some examples of bronze statues of cultural heritage in Croatia that are presented for illustration, it can be seen that many of them are covered with dark to pale green patina. The chemical natures of patinas, as well as the minerals constituting bronze patina for different pollutant media are presented. This part is followed with the protective mechanism and the various classifications of inhibitors. Particular attention was paid for inhibitors applied on copper and copper alloys.

6.2 CORROSION MECHANISM AND EXPERIMENTAL CONDITIONS

In Chapter 3, the corrosion process taking place on copper in aqueous medium is examined. The reaction model involving Cu(I) intermediate species was proposed and its polarization curves and the electrode impedance are derived theoretically. It is concluded that the impedance spectrum has two capacitive loops; one for the double layer capacitance in parallel with the charge transfer process involving the redox reaction between Cu(0) and Cu(I), and the second loop, for the faradaic capacitance due to this redox process and the dissolution reaction of Cu(I) reaction intermediate.

This theoretical approach was followed by the presentation of three procedures employed in the present study for the artificial patina formation on Cu-6Sn binary bronze.

As for the experimental results, first the protective effects of three imidazoles (4-methyl-1-phenylimidazole, 4-methyl-1-*p*-tolylimidazole and 1-H benzimidazole) were examined on bare bronze in different concentrations. Then the patinated bronze was examined with the optimal inhibitor concentrations during 24 hours.

6.3. BARE BRONZE

The investigations performed in this work have revealed the effects of three non-toxic imidazole corrosion inhibitors on bare Cu-6Sn bronze in a Na_2SO_4 + $NaHCO_3$ solution simulating strongly (pH 3) and mildly (pH 5) acid rain:

4-methyl-1-phenylimidazole (PMI):

▪ The electrochemical investigations showed its good protective properties at pH 3, ~90 % inhibiting efficiency at the optimal concentration of 5 mmol·dm^{-3}, while at pH 5 they showed a low inhibitive effect. The results have suggested that at pH 5 PMI increases the

anodic reaction rate and that the cathodic reaction is mainly governed by the reduction of the dissolved oxygen under convective diffusion control.

⌗ The electrochemical impedance spectroscopy measurements at pH 3 have shown that PMI does not decrease the electrochemical reactivity of bronze, but rather inhibits the redox process involving the surface species. The whole surface species are not involved in the redox process, but very likely only cuprous compounds. The presence of PMI makes the reactivity of the bronze electrode surface more homogeneous.

4-methyl-1-p-tolylimidazole (TMI):

⌗ Electrochemical investigations have shown that the optimal concentration of TMI is 5 mmol·dm^{-3} at both pH values. An excess of TMI however accelerates the corrosion rate, at pH 5, and at the concentration 10 mmol·dm^{-3} z is negative. This increase is essentially due to the increase of the cathodic current. One of the possibilities of this side-effect will be the reduction of TMI molecules rather than desorption of TMI from the bronze surface since the anodic current densities remain stable. It was also observed that TMI is a cathodic inhibitor, with an effect similar to the corrosion kinetics of PMI at pH 3.

⌗ The impedance spectroscopy measurements have again confirmed the results obtained by the *dc* measurements. At pH 3 TMI adsorbs likely at active sites making the surface distribution of the reaction rate homogeneous. At pH 5 TMI has no marked inhibiting effect towards the redox process preceding the dissolution step of the reaction intermediate. The electrode surface becomes rough and certainly the corrosion products make the ionic strength at the vicinity of the electrode surface higher. The reduction reaction of TMI may take place at particular reaction sites. The protection of bronze statues exposed in urban area by this inhibitor is particular and needs meticulous

monitoring of the inhibitor concentration, as at lower and higher inhibitor concentrations, the corrosion rate may be higher than in the uninhibited solution.

1-H benzimidazole (BZI):

- The investigations have shown that BZI is a mixed inhibitor, with an optimal concentration of 5 mmol·dm^{-3} at pH 3, while at pH 5 even only 0.1 mmol·dm^{-3} is sufficient to obtain marked inhibiting effect (above 90%).

- The impedance spectroscopy measurements have shown at pH5 that the surface coverage by BZI may modify deeply the double layer structure. This high adsorption effect is really reflected by good inhibiting efficiency, *z*, observed for the coupling pH 5 solution – BZI even at very low inhibitor concentrations. An efficient inhibitive effect towards the redox process taking place at the electrode surface was also observed.

- Benzimidazole exhibits the best protection properties among the studied corrosion inhibitors, as well for the inhibitive efficiency that is maintained for an excess addition to the corrosive medium. However, after long immersion (over 1 month), its surface colour changes into a brown-reddish colour. Therefore, this inhibitor cannot be applied at present time to protect statues covered by green patina and exposed in urban area.

The results on all three inhibitors at both pH values have shown that the interaction between the inhibitors and the bronze surface is spontaneous physisoption by attractive force.

Three corrosion evaluation methods (Tafel extrapolation, linear polarization, and electrochemical impedance spectroscopy) exhibited coherent results.

6.4. PATINATED BRONZE

To investigate a possible protection of different types of patinas three kinds of patinas were produced on a Cu-6Sn bronze: two chemical patinas: (1) a sulphate patina synthesized in the $CuSO_4 \cdot 5H_2O$ solution and (2) a chloride patina formulated in the NH_4Cl solution; and a kind of (3) electrochemical patina, developed in this dissertation, formed in the Na_2SO_4 / $NaHCO_3$ solution. The structure and morphology of all patinas were examined by SEM, EDS and Raman spectroscopy. The results have shown that the sulphate patina consists of a smooth structure of cuprite, Cu_2O, and a crystalline layer of brochantite, $Cu_4SO_4 \cdot (OH)_6$. The chloride patina consists of a smooth structure that is a combination of amorphous Cu_2O, and SnO_2, and a crystalline layer of atacamite, $Cu_2Cl(OH)_3$. The electrochemical patina consists of a smooth structure of cuprite, Cu_2O, and tin-oxide, SnO_2, and a crystalline layer of malachite, $CuCO_3 \cdot Cu(OH)_2$, and a type of copper-sulphate compound that could not be identified precisely, probably due to its amorphous structure.

The corrosion properties of all patinas were examined by electrochemical impedance spectroscopy in a solution of Na_2SO_4 and $NaHCO_3$ at pH5 which simulates an urban environment. In the same solution a non-toxic corrosion inhibitor 4-methyl-1-*p*-tolylimidazole was added to examine it for possible protection of patina. The EIS results collected every hour during 24 hours showed that the inhibitor, adsorbed on patina from the aqueous solution, improves the stability of all three kinds of patinas and can be recommended for protection of works of art.

The protective properties of 4-methyl-1-phenylimidazole (PMI) and 1-H benzimidazole (BZI) were also examined on the electrochemical patina. The results have shown again that BZI protects the patina, while PMI does not.

7. LITERATURE

1. Filipović, S. Lipanović: *Basic and Anorganic Chemistry*, Part II, VIII issue, Školska knjiga, Zagreb, 1991.

2. Mining-technology.com, Net Resources International, 2010: http://www.mining-technology.com/.

3. United Nations Conference on Trade and Development: *The UNCTD Handbook of Statistics 2009*: http://www.unctad.org/.

4. P. R. Roberge: *Handbook of Corrosion Engineering*, McGraw-Hill, New York, 2000.

5. World Centre for Materials Joining Technology, UK, 2009: http://www.twi.co.uk/content/jk23.html.

6. E. Stupnišek-Lisac, K. Tadić, H. Otmačić, H. Takenouti: *Electrochem. Soc. Trans.* **9/2** (2007) 31.

7. D. P. Fitzgerald, J. Nairn, A. Atrens: *Corr. Sci.* **40** (1998) 2029.

8. K. P. FitzGerald, J. Nairn, G. Skennerton, A. Atrens: *Corr. Sci.* **48** (2006) 2480.

9. K. Borsheim, Bronze Patina Process, 2004: www.borsheimarts.com/patina.htm.

10. B. Rosales, R. Vera, G. Moriena: *Corr. Sci.* **41** (1999) 625.

11. K. Rahmouni, S. Joiret, L. Robiola, A. Srhiri, H. Takenouti, V. Vivier: *Bulg. Chem. Commun.* **37** (2005) 26.

12. D. de la Fuente, J. Simancas, M. Morcillo: *Corr. Sci.* **50** (2008) 268

13. G. P. Cicileo, M. A. Crespo, B. M. Rosales: *Corr. Sci.* **46** (2004) 929.

14. T. E. Graedel, K. Nassau, J. P.Franey: *Corr. Sci.* **27** (1987) 639.

15. J. P. Franey, M.E. Davis: *Corr. Sci.* **27** (1987) 659.

16. K. Nassau, P.K. Gallager, A.E. Miller, T.E. Graedel: *Corr. Sci.* **27** (1987) 669.

17. R. L. Opila: *Corr. Sci.:* **27** (1987) 685.

18. J. Muller, C. Mc Crory-Joy: *Corr. Sci.* **27** (1987) 695.

19. T.E. Graedel: *Corr. Sci.* **27** (1987) 721.

20. K. Nassau, A. E. Miller, T. E. Graedel: *Corr. Sci.* **27** (1987) 703.

21. H. Strandberg: *Atmosph. Environ.* **32** (1998) 3511.

22. L. Robbiola, J.-M.Blengino, C. Fiaud: *Corr. Sci.* **40** (1998) 2083.

23. P. Dillmann,G. Beranger, P. Piccardo, H Matthiessen: *Corrosion of metallic heritage artefacts, Investigation, conservation and prediction for long-term behaviour*, EFC publications (EFC48), Woodhead Pub. Cambridge (GB), 2007.

24. R. Hughes, M. Rowe: *The colouring bronzing and patination of metals* Thames & Hudson, London (GB), 1991.

25. K. Rahmouni, H. Takenouti, N. Hajjaji, A. Srhiri, L. Robbiola: *Electrochim. Acta* **54/22** (2009) 5206.

26. K. Marušić, H. Otmačić Ćurković, H. Takenouti, A. D. Mance, E. Stupnišek-Lisac: *Chem. Biochem. Eng. Quart.* **21/1** (2007) 71.

27. K. Marušić, H. Otmačić-Ćurković, Š. Horvat-Kurbegović, H. Takenouti, E. Stupnišek-Lisac: *Electrochim. Acta*, **54** (2009) 7106.

28. L. Muresan, S. Varvara, E. Stupnišek-Lisac, H. Otmačić, K. Marušić, Š. Horvat Kurbegović, L. Robbiola, K. Rahmouni, H. Takenouti: *Electrochim. Acta*, **52/27** (2007) 7770.

29. J. M. Cronyn, *The Elements of Archaeological Conservation*, Routledge, London and New York, 1990, p. 213.

30. R. Baboian, *NACE Corrosion Engineer's Reference Book*, NACE International, Houston, 2002.

31. J. D. Nairn, S. G. Skennerton, A. Atrens: *J. Mat. Sci.*, **38** (2003) 995.

32. T.E. Graedel, K. Nassau, J.P. Franey: *Corr. Sci.* **27** (1987) 639-657.

33. The mineral and locality database, Jolyon Ralph and Ida Chau, 1993: http://mindat.org/.

34. Theo Kloprogge - Vibrational Spectroscopy and Photo Atlas of Minerals, Queensland University of Minerals, 2003: http://www.mineralatlas.com/.

35. Mineralogy Database, 1997-2009: http://webmineral.com/.

36. Crystal Classics, 2007-2009: http://www.crystalclassics.co.uk/.

37. M. Pourbaix: *Atlas of electrochemical equilibrium in aqueous solution*, Pergamon Press, New York, 1966.

38. P. A. Schweitzer: *Atmospheric Degradation and Corrosion Control Corrosion*, Marcel Dekker, New York, 1999.

39. Trabanelli: *Corrosion Mechanisms*, Marcel Dekker, New York, 1987.

40. Š. Horvat-Kurbegović: *Numismatic News* **1/47** (1994) 165.

41. Š. Horvat-Kurbegović: *Proceedings of the 1st International Numismatical Congress in Croatia, INNC-95,* 1996, p. 47.

42. The Social Learning Group: *Learning to Manage Global Environmental Risks*, MIT Press, London, 2001.

43. Gerry Best: *Environmental Pollution Studies*, Liverpool University Press, Liverpool, 1999.

44. P. Elvingson, C. Agren: *Attacking air pollution – Critical loads, airborne nitrogen, ozone precursors*, Report from the fourth international NGO strategy seminar on air pollution. The Swedish NGO Secretariat on Acid Rain, Göteborg, Sweden, 1996.

45. Republic of Croatia - Central Bureau of Statistics, 2006:

http://www.dzs.hr/Hrv_Eng/ljetopis/2008/PDF/01-bind.pdf.

46. H. E. Townsend: *Outdoor Atmospheric Corrosion*, ASTM, Philadelphia, 2002.

47. I. L. Rosenfield: *Corrosion Inhibitors*, McGraw-Hill, New York, 1981.

48. P. A. Schweitzer: *Corrosion Engineering Handbook, Corrosion of Linings and Coatings, Cathodic and Inhibitor Protection and Corrosion Monitoring*, Marcel Dekker, New York, 1989.

49. W. J. Lorenz, F. Mansfeld: *International Conference on Corrosion Inhibition*, National Association of Corrosion Engineers, Dallas, 1983.

50. Y. I. Kuznetsov: *Organic Inhibitors for Corrosion of Metals*, Plenum Press, New York, 1996.

51. T. P. Hoar, R. P. Khera: *Proceedings of the 1st European Symposium on Corrosion Inhibitors*, Ann. Univ. Ferrara, N.S., Sez. V, Suppl. 3 (1961) 73.

52. V. S. Sastri, E. Ghali, M. Elboujdaini: *Corrosion Prevention and Protection Practical Solutions*, John Wiley & Sons, London, 2007.

53. S. Papavinasam: *Corrosion Inhibitors*, in R. Winston Revie (ed.): *Uhlig's Corrosion Handbook*, John Willey and Sons Inc. USA, 2000, p. 1089.

54. A. D. Merzer, *Corrosion Inhibition: Principles and Practice* in L. L. Shreir (ed.): *Corrosion*, Butterworth, London, 1976.

55. G. Trabanelli: *Corrosion Inhibitors* in: F. Mansfeld (ed.), *Corrosion Mechanisms*, Marcel Dekker, New York, 1987.

56. W. J. Lorenz, F. Mansfeld, *Electrochim Acta* **31** (1986) 467.

57. E. Stupnišek-Lisac: *Corrosion and Protection of construction materials*, FKIT, Zagreb, 2007.

58. C. Fiaud, *Corrosion Inhibitors*, The Institute of Materials, European Federation of Corrosion, 1994.

59. M. M. Antonijević, M. B. Petrović: *Intern. J. Electrochem. Sci.* **3** (2008) 1.

60. E. Samiento-Bustos, J. G. González Rodriguez, J. Uruchurtu, G. Dominguez-Patiño, V. M. Salinas-Bravo: *Corr. Sci.*, **50**/8 (2008) 2296.

61. R. Naderi, M. Mahdavian, M. M. Attar: *Electrochim. Acta*, **54**/27 (2009) 6892.

62. A. Igual Muñoz, J. García Antón, J. L. Guiñón and V. Pérez Herranz: *Electrochim. Acta*, **50**/4 (2004) 957.

63. J.G. Thomas: *Mechanism of Corrosion Prevention by Inhibitors*, in L. L. Shreir (ed.): *Corrosion*, Butterworth, London, 1976.

64. A. P. Brynza, N. A. Kormshchikova: *Poroshkovaya Met.*, **5**/8 (1966) 606.

65. Amy Forsgen: *Corrosion Control through Organic Coatings*, Taylor & Francis Group, Boca Raton, 2006.

66. T. Rossel: *Werkstoffe u. Korrosion*, **20** (1969) 854.

67. E. M. Sherif, S.-M. Park, *Electrochim. Acta* **51** (2006) 4665.

68. K. E. Salah, M. Keddam, K. Rahmouni, A. Srhiri, H. Takenouti: *Electrochim. Acta* **49** (2004) 2771.

69. E. Stupnišek-Lisac, A. Brnada, A. D. Mance: *Corr. Sci.* **42** (2000) 243.

70. G. Moretti, F. Guidi: *Corr. Sci.* **44** (2002) 1995.

71. E. Stupnišek-Lisac, D. Kasunić, J. Vorkapić-Furač; *Corrosion* **51** (1995) 767.

72. E. Stupnišek-Lisac, V. Cinotti, D. Reichenbach: *J. Appl. Electrochem.* **29** (1999) 117.

73. E. Stupnišek-Lisac, A. Lončarić-Božić, I. Cafuk: *Corrosion* **54** (1998) 713.

74. E. Stupnišek-Lisac, A. Gazivoda, M. Madžarac: *Electrochim. Acta* **47** (2002) 4189.

75. R. Gašparac, C. R. Martin, E. Stupnišek-Lisac: *J. Electrochem. Soc.* **147** (2000) 548.

76. H. Otmačić, E. Stupnišek-Lisac: *Electrochim. Acta* **48** (2003) 985.

77. H. Otmačić, J. Telegdi, K. Papp, E. Stupnišek-Lisac: *J. Appl. Electrochem.* **34** (2004) 545.

78. G. Xue, J. Ding, P. Wu, G. Ji: *J. Electroanal. Chem.* **270** (1989) 163.

79. R. Babić, M. Metikoš-Huković, M. Lončar: *Electrochim. Acta* **44** (1999) 2413.

80. X. R. Ye, X. Q. Xin, J. J. Zhu, Z. L. Xue: *Appl. Surf. Sci.* **135** (1998) 307.

81. W. Qafsaoui, C. Blanc, N. Pebere, H. Takenouti, A. Srhiri, G. Mankowski: *Electrochim. Acta* **47** (2002) 4339.

82. F. Zucchi, G. Trabanelli, M. Fonsati: *Corr. Sci.* **38** (1996) 2019.

83. Gy. Vastag, E. Szőcs, A. Shaban, I. Bertóti, K. Popov-Pergal, E. Kálmán: *Solid State Ionics* **87** (2001) 141.

84. D. Kuron, H-J. Rother, R. Holm, S. Storp: *Werkstoffe u. Korrosion* **37** (1986) 83.

85. A. G. Brolo, M. L. A. Temperini, S. M. L. Agostinho: *Electrochim. Acta* **44** (1998) 559.

86. Da-quan Zhang, Li-xin Gao, Guo-ding Zhou, *Corr. Sci.* **46** (2004) 3031.

87. P. Yu, D.-M. Liao Y.-B. Luo, Z.-G. Chen, *Corrosion* **59** (2003) 314.

88. R. Subramanian, V. Lakshminarayanan: *Corr. Sci.* **44** (2002) 535.

89. R. B. Faltermeier: *Stud. in Conserv.* **44** (1998) 121.

90. V. Brusić, M. A. Frisch, B. N. Eldridge, F. P. Novak, B. M. Rush, G. S. Frankel, *J. Electrochem. Soc.* **138** (1991) 2253.

91. N. I. Sax: *Dangerous Properties of Industrial Materials*, Reinhold Publishing Corp., New York, 1957.

92. D. A. Pillard, J. S. Cornel, D. L. Dufresne, M. T. Hernandez: *Water Research* **35** (2001) 557.

93. Woo-Jin Lee: *Mat. Sci. Eng.* **A348** (2003) 217.

94. H. Otmačić Ćurković, E. Stupnišek-Lisac, H. Takenouti: *Corr. Sci.* **52**/2 (2010) 398.

95. H. Otmačić Ćurković, E. Stupnišek-Lisac, H. Takenouti: *Corr. Sci.* **51** (2009) 2342.

96. H. Otmačić-Ćurković: "*Inhibiting action of imidazole derivatives on metal corrosion*", PhD thesis, University of Zagreb, 2007.

97. L. D. Hanke: *Handbook of Analytical Methods for Materials*, Material Evaluation and Engineering Inc., USA, 2001: http://www.mee-inc.com/hamm300d.pdf (13.02.2007) .

98. C. Cantafio: *Scanning Electron Microscope Usage and Analysis of Metal Fatigue in Mead Silver Paperclips*, 1998: http://antoine.frostburg.edu/engin/sem/index.html (20.02.2007.).

99. C. V. Raman: *Ind. J. Phys.* **2** (1928) 387.

100. D. David, R. Caplain, A Hugot Le Goff: *Méthode usuelles de carctérisations des surfaces*, Eyrolles, Paris, 1998.

101. P. A. Christensen, A. Hamnett: *Techniques and Mechanisms in Electrochemistry*, Chapman & Hall Inc., New York, 1994.

102. D. Landolt: *Introduction to Surface Reactions: Electrochemical Basis of Corrosion*, in P. Marcus, J. Oudar (ed.): *Corrosion Mechanisms in Theory and Practice*, Marcel Dekker, New York, 1995.

103. Southampton Electrochemistry Group: *Instrumental Methods in Electrochemistry*, Ellis Horwood, London, 1990.

104. J. O'M. Bockris, A. K. N. Reddy, M. Gamboa-Aldeco: *Modern Electrochemistry Vol. 2A, Fundamentals of Electrodics*, Kluwer Academic/Plenum Publisher, New York, 2000.

105. M. Stern, A. L. Geary: *J.Electrochem. Soc.* **104** (1957) 56.

106. F. Mansfeld: *Corrosion* **29** (1973) 397.

107. C. Wagner, W. Traud: *Electrochem. Soc.* **44** (1938) 391.

108. PAR, *Application Note AC-1, Basics of Electrochemical Impedance Spectroscopy.*

109. D. C. Silverman: *Primer on the AC Impedance Technique*, in R. Baboian (ed.): *Electrochemical Techniques for Corrosion Engineering*, NACE, USA 1986, p. 73.

110. F. Mansfeld: *Corrosion* **36** (1981) 301.

111. D. D. Macdonald: *Electrochim. Acta* **51** (2006) 1376.

112. J. R. Macdonald: *Impedance Spectroscopy, Emphasizing Solid Materials and Systems*, John Wiley & Sons, USA, 1987.

113. C. Gabrielli: *Identification of Electrochemical Processes by Frequency Response Analysis*, Solartron Instruments, Universite Pierre et Marie Curie, Paris, 1980.

114. D. C. Silverman: *Practical Corrosion Prediction Using electrochemical Techniques* in R. Winston Revie (ed.): *Uhlig's Corrosion Handbook*, John Willey and Sons Inc. USA, 2000.

115. I. Epelboin, C. Gabrielli, M. Keddam, H. Takenouti: *Electrochemical Corrosion Testing*, ASTM STP 727, 1981, p. 150.

116. C. Gabrielli, M. Keddam, H. Takenouti: "*Kramers-Kronig transformation in relation to the interface regulating device*" in "*Electrochemical impedance: Analysis and interpretation*" 140-153, J.R. Scully, D.C. Silvermann, and M. W. Kendig, editors, A.S.T.M., STP 1188, 1994.

117. E. Warburg: *Uber des Verhalten Sogenannter Unpolarisierbarer Elektroden gegen Wechselstrom*, Ann. Phys. Chem., 67 (1989) p. 493, Op cit., E. Barsoukov, J. R. Macdonald: *Impedance Spectroscopy, Theory, Experiment, and Applications, 2nd edition*, p. 54, John Wiley and Son, New York.

118. A. J. Bard, L. R. Faulkner: *Electrochemical Methods, Fundamentals and Applications*, John Wiley & Sons, Inc., New York, 1980.

119. H. Takenouti, Manual of Ariane – simplex regression calculation software, unpublished, LISE – UPR 15 of CNRS (1995) France.

120. I. Zpelboin, M. Keddam: *J. Electrochem. Soc.*, **117** (1970) 1052.

121. M. Keddam, O.R. Mattos, H. Takenouti: *J. Electrochem. Soc.*, **128**, (1981) 257.

122. M. Keddam, O.R. Mattos, H. Takenouti: *J. Electrochem. Soc.*, **128** (1981) 266.

123. I. Epelboin, C. Gabrielli, M. Keddam, H. Takenouti: *A-C impedance measurements applied to corrosion studies and corrosion rate determination*, in *Electrochemical Corrosion Testing*, F. Mansfeld and U. Bertocci, editors, STP 727, 150-192. American Society for Testing and Materials, Philadelphia (Pa), 1981.

124. A. J. Bard, L. R. Faulkner: "*Electrochemical methods : Fundamentals and Applications*", John Wiley and Sons, pp. 854 – 855, New York, 2001.

125. Library 4 Science, UK, 2000-2008:

http://www.chromatographyonline.org/topics/freundlidh/adsorption/isotherm.html.

126. M. Lebrini, F. Bentiss, H. Vezin, M. Lagrenee: *Corr. Sci.* **48** (2006) 1279.

127. D. Zhang, Q. Cai, X. He, L. Gao, G. S. Kim: *Corr. Sci.* **51/10** (2009) 2349.

128. K. Bhrara and G. Singh: *Appl. Surf. Sci.* **253** (2006) 846.

129. R. Rosliza, W. B. Wan Nik: *Curr. Appl. Phys.* **10** (2010) 221.

130. ASTM G1-03 (2003) Standard Practice for Preparing, Cleaning, and Evaluating Corrosion Test Specimens.

131. A. Yurt, G. Bereket, A. Kivrak, A. Balaban, B. Erk: *J. Appl. Electrochem.* **35** (2005) 1025.

132. V. Hayez, V. Costa, J. Guillaume, H. Terryna, A. Hubina: *Analyst* **130** (2005) 550.

133. P. Makreski, G. Jovanovski, S. Dimitrovska: *Vibr. Spectr.* **39** (2005) 229.

134. M. Schmidt, H.D. Lutz: *Phys. Chem. Min.* **20** (1993) 27.

135. G. Niaura, *Electrochim. Acta* **45** (2000) 3507.

136. J. Sandberg, I. Odnevall Wallinder, C. Leygraf, N. Le Bozec: *Corr. Sci.* **48** (2006) 4316.

137. R. L. Frost, *Spectrochim. Acta*, Part A **59** (2003) 1195.

138. M. C. Bernard, S. Joiret: *Electrochim. Acta* **54** (2009) 5199.

139. L. Robbiola, R. Portier: *J. Cultural Heritage* **7** (2006) 1.

8. LIST OF SYMBOLS

a	Activity
A	Surface area, cm^2
b_a, b_c	Tafel slopes, $V \cdot dec^{-1}$
B_a, B_c	Anodic and Cathodic Tafel constant, V^{-1}
B	Stern-Geary coefficient, V
c	Concentration, $mol \cdot dm^{-3}$
C	Capacitance, $F \cdot cm^{-2}$
d	Thickness of layer, nm
E	Potential, V
f	Frequency, Hz
F	Faraday constant, 96485 $A \cdot s \cdot mol^{-1}$
ΔG	Gibbs energy, $kJ \cdot mol^{-1}$
I	Current, A
j	Imaginary unit, $\sqrt{-1}$
j	Current density, $A \cdot cm^{-2}$
K, K'	Adsorption equilibrium constant, $dm^3 \cdot mol^{-1}$
K_1, K_{-1}, K_2	Reaction rate
K	Ion strength, $mol \cdot cm^{-1}$
L	Inductance, H
M	Atomic mass, $g \cdot mol^{-1}$
n	Number of exchanged electrons
n	Cole-Cole coefficient
N	Number of samples
N_A	Number of analysed samples

R   Gas constant, 8.314 $J \cdot K^{-1} \cdot mol^{-1}$

R Resistance, $\Omega \cdot cm^2$

RR_A Analysed amount of samples, %

T Temperature, K

t Time, s

v Corrosion rate, $g \cdot cm^{-2} \cdot s^{-1}$

X Independent variable

Y Dependent variable

Z Impedance, Ω or $\Omega \cdot cm^2$

z Inhibiting efficiency, %

Greek letters

δ Thickness of layer, nm

ε Permittivity, $F \cdot cm$

η Overpotential, V

θ Fractional surface coverage, %

κ^{-1} Debye length in electrolyte, nm

λ Wave length, nm

μ Electrochemical potential, $J \cdot mol^{-1}$

σ Warburg coefficient, $\Omega \cdot s^{-0.5}$

τ Time constant

φ Phase shift, rad

ω Frequency, $rad \cdot s^{-1}$

Curriculum vitae

Katarina Marušić (nee Tadić) was born in Zagreb, Croatia, on May 27. 1980. She attended elementary school and gymnasium in Zagreb, Salt Lake City in Utah, USA and Göttingen in Germany. She graduated from Faculty of Chemical Engineering and Technology, University of Zagreb, Croatia

During her studies she received an Award from the Chancellor of the University of Zagreb for her student scientific work. She obtained a scholarship for student practical work, which she did in Poland on the Department of Instrumental Analysis, Technological faculty, University of Szczecin. She obtained her B. Sc. diploma in 2004.

Since 2005 she has been employed at the Faculty of Chemical Engineering and Technology, Department of Electrochemistry as a research assistant. During that time she has completed postgraduate studies in the field of chemical engineering.

She is fluent in English and German, and is able to use French and Spanish.

She has participated in three international scientific projects and has published six papers in CC scientific journals and six in other scientific journals. She has participated at six international and three national scientific congresses

She is married and a mother of two children.

Scientific papers in CC journals:

1. Marušić, Katarina; Otmačić, Helena; Landek, Darko; Cajner, Franjo; Stupnišek-Lisac, Ema; Modification of carbon steel surface by the Tenifer® process of nitrocarburizing and post-oxidation. // *Surface & Coatings Technology* **201** (2006) 3415-3421.

2. Telegdi, Judit; Otmačić Ćurković, Helena; Marušić, Katarina; Al-Taher, F; Stupnišek-Lisac, Ema; Kálmán, Erika; Inhibition of Copper Corrosion by self Assembled Amphiphiles. // *Chemical and Biochemical Engineering Quarterly* **21** (2007) 1, 77-82.

3. Muresan, Liana; Varvara, Simona; Stupnišek-Lisac, Ema; Otmačić, Helena; Marušić, Katarina; Horvat Kurbegović, Šefka; Robbiola, Luc; Rahmouni, Kamal; Takenouti, Hisasi; Protection of bronze covered with patina by innoxious organic substances. // *Electrochimica Acta* **52** (2007) 27, 7770-7779.

4. Marušić, Katarina; Otmačić Ćurković, Helena; Takenouti, Hisasi; Mance, Ana Dunja; Stupnišek-Lisac, Ema; Corrosion Protection of Synthetic Bronze Patina. // *Chemical and Biochemical Engeenering Quartely* **21** (2007) 1, 71-76.

5. Otmačić Ćurković, Helena; Marušić, Katarina; Stupnišek-Lisac, Ema; Telegdi, Judit; Electrochemical and AFM Study of Corrosion Inhibition with Respect to Application Method. // *Chemical and biochemical engeenering quartely* **23** (2009) 1, 61-66.

6. Marušić, Katarina; Otmačić-Ćurković, Helena; Horvat-Kurbegović, Šefka; Takenouti, Hisasi; Stupnišek-Lisac, Ema, Comparative studies of chemical and electrochemical preparation of artificial bronze patinas and their protection by corrosion inhibitor. // *Electrochimica Acta* **54** (2009) 27, 7106-7113.

Scientific papers in proceedings of international congresses with reviews:

1. Otmačić Ćurković, Helena; Marušić, Katarina; Stupnišek-Lisac, Ema; Copper Corrosion Inhibition in Sulphate Media. // *Proceedings Eurocorr 2007*, Dechema, 2007, 1-7.

2. Milohanović, Ivana; Šimunec, Tomislav; Otmačić Ćurković, Helena; Marušić, Katarina; Stupnišek-Lisac, Ema; Copper Protection under Flow Conditions. // *Corrosion and Material Protection*, Prag : SVUOM, 2007, 1-7.

3. Otmačić Ćurković, Helena; Marušić, Katarina; Stupnišek-Lisac, Ema; Bronze Protection in Simulated Acid Rain. // *17th International Corrosion Congress, Proceedings* / Narasi Sridhar (ur.), Las Vegas : NACE International, 2008, 1-7.

Scientific papers in proceedings of domestic congresses with reviews:

1. Tadić, Katarina; Otmačić, Helena; Cajner, Franjo; Landek, Darko; Takenouti, Hisasi; Stupnišek-Lisac, Ema; Korozijska otpornost modificiranih metalnih površina. // *KORMAT 2006, 17. Savjetovanje o zaštiti materijala i industrijskom finišu* / Rajhenbah, Darko (ur.), Zagreb : Hrvatsko društvo za zaštitu materijala, 2006, 87-94.

2. Otmačić Ćurković, Helena; Marušić, Katarina; Stupnišek-Lisac, Ema; Zaštita brončanih skulptura u uvjetima urbane atmosfere. // *Zbornik radova 18. Savjetovanja o zaštiti materijala i industrijskom finišu, KORMAT 2008* / Esih, Ivan (ur.), Zagreb : Društvo za zaštitu materijala, 2008, 138-144.

Scientific papers in other journals:

1. Stupnišek-Lisac, Ema; Otmačić, Helena; Marušić, Katarina; Mance, Ana Dunja; Takenouti, Hisasi; Corrosion Protection of Bronze Patina by New Non-toxic Organic Inhibitors. **//** Electrochemical Society Transactions 9 (2007) 2, 31-42.

Abstracts in congress proceedings:

1. Stupnišek-Lisac, Ema; Tadić, Katarina; Otmačić, Helena; Takenouti, Hisasi; Corrosion Protection of Bronze Patina by New Non-Toxic Organic Inhibitors. // *Meeting Abstracts, 209th ECS Meeting*, Denver, Colorado, SAD, 2006, 312.

2. Muresan, Liana; Varvara, Simona; Stupnišek-Lisac, Ema; Otmačić, Helena; Marušić, Katarina; Horvat Kurbegović, Šefka; Robbiola, Luc; Rahmouni, Kamal; Takenouti, Hisasi; Protection of bronze covered with patina by innoxious organic substances. // *Abstracts EMCR 2006*, Dourdan, Francuska, 2006, 150.

3. Marušić, Katarina; Stupnišek-Lisac, Ema, Formiranje, ispitivanje i zaštita umjetne patine na bronci. // *XX. Hrvatski skup kemičara i kemijskih inženjera, knjiga sažetaka* / Vasić-Rački, Đurđa (ur.), Zagreb: HDKI, 2007, 278.

4. Otmačić Ćurković, Helena; Marušić, Katarina; Stupnišek-Lisac, Ema; Telegdi, Judit, Electrochemical and AFM study of corrosion inhibition with respect to application method. // *Book of Abstracts, First Regional Symposium on Electrochemistry of South East Europe*, Zagreb: Hrvatsko društvo kemijskih inženjera, 2008, 70-71.

5. Otmačić Ćurković, Helena; Marušić, Katarina; Stupnišek-Lisac, Ema; Takenouti, Hisasi; EIS study of copper corrosion inhibition on RDE. // *The 59th Annual Meeting of the International Society of Electrochemistry*, 2008.

6. Otmačić Ćurković, Helena; Marušić, Katarina; Stupnišek-Lisac, Ema; Zaštita patinirane i čiste bronce ekološki prihvatljivim inhibitorima korozije. // *12. Seminar Arhivi, knjižnice, muzeji*, 2008.

7. Marušić, Katarina; Otmačić Ćurković, Helena; Stupnišek-Lisac, Ema; Takenouti, Hisasi; Protection of bronze patina by an environment friendly corrosion inhibitor. // *Book of Abstracts 6th Spring Meeting of the International Society of Electrochemistry*, 2008, 255.

8. Otmačić Ćurković, Helena; Marušić, Katarina; Stupnišek-Lisac, Ema; Zaštita patinirane i čiste bronce ekološki prihvatljivim inhibitorima korozije. // *1. Susret sekcije restauratora i preparatora HMD-a* / Slađana Latinović (ur.), Zagreb : Arheološki muzej, 2009.

Congress abstract in other journals:

1. Otmačić Ćurković, Helena; Marušić, Katarina; Prtenjak, Andreja; Škrobica, Ana; Stupnišek-Lisac, Ema; The inhibiting effect of 1-phenyl-4-methyl imidazole on bronze // *Meeting Abstracts 212th ECS Meeting*, The Electrochemical Society, 2007, 831.